THE SOLIDIFICATION OF SOME METAL/NON-METAL EUTECTICS

H.A.H. Steen M.A.

St. John's College

A thesis submitted for the degree of Doctor of Philosophy in the University of Oxford

Department of Metallurgy

Michaelmas term 1973

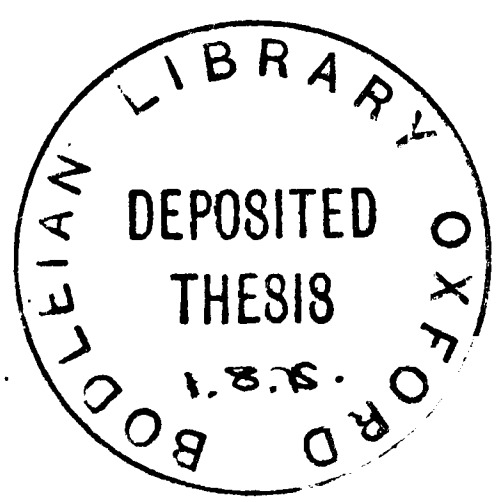

ACKNOWLEDGEMENTS

I should like to thank the staff of the Department of Metallurgy for their assistance in this work. I am particularly grateful to Dr. A. Hellawell for his continued help and encouragement, to Professor P.B. Hirsch for providing laboratory facilities, and to Mr. M.J. Cox for technical assistance.

I am indebted to the Science Research Council and to the British Cast Iron Research Association for financial support.

Abstract

An attempt has been made in this thesis to elucidate the effects of growth velocity, temperature gradient and impurity additions on the structure of the aluminium-silicon eutectic, and in particular on the transition from an (unmodified) flaky to a (modified) fibrous morphology.

Samples of pure eutectic alloy have been unidirectionally solidified over a range of growth rates and at two temperature gradients, and specimens examined by optical, transmission electron and scanning electron microscopy in order to characterise the flake to fibre transition. It has been found that the transition occurs over a range of growth rates, with increasing temperature gradient favouring the fibrous morphology. Transmission electron microscopy has confirmed the presence of twins in the flake silicon, but twins have not been observed in the fibrous silicon, although this is not considered to be conclusive evidence that twins were not present. Measurements have been made of the growth undercooling as a function of velocity for the flaky silicon, and it has been found that the flake silicon eutectic can be grown at undercoolings of 15°C and over.

In order to compare the effects of different modifying elements, ingots of pure alloy have been doped with various impurity elements and thermally analysed, after which the microstructures have been examined using optical and scanning electron microscopy. It has been found that sodium, potassium and strontium modify the eutectic while other group II and the group V elements are ineffective. Comparison of growth undercoolings has showed that the modified eutectic grows at undercoolings of 3°C and over, the undercooling under given conditions

increasing in the order strontium, potassium, sodium. Lithium has been found to produce an anomalous microstructure. Phosphorous has been found to refine the primary silicon, and crystallographic particles inside the primary crystals have been shown by microprobe analysis to contain phosphorous and aluminium.

A hot stage has been designed and constructed in which experiments using eutectic droplets melted onto silicon single crystal substrates have been carried out. Measurements have been made of undercoolings for nucleation of eutectic on silicon showing that silicon does not nucleate the eutectic. The droplets have been found by X-ray analysis to be polycrystalline, so no epitaxial relationship has been found for eutectic aluminium and primary silicon. Growth layers formed by cooling modified and unmodified droplets from above the eutectic temperature have been compared, and it has been concluded that these layers had been formed by layer growth of the $\{111\}$ silicon substrate. Twinned primary silicon crystals have been observed projecting upwards from the growth layer and it has been concluded that growth using twin plane re-entrant edges is more kinetically favourable than $\{111\}$ layer growth. The principle of temperature gradient zone melting has been used to compare the migration rates of modified and unmodified droplets across a silicon single crystal substrate in an applied temperature gradient. It has been found that modification by strontium reduces the migration rate.

Finally, it has been proposed that morphological transitions in this system depend on the difference between the kinetic undercoolings of the aluminium and silicon phases, and that they do not occur at fixed total undercoolings.

Contents

I Introduction

Alloys of aluminium with 5% to 25% by weight of silicon, together with cast irons are the only eutectic alloys which have so far found extensive commercial application as structural materials. Their practical viability is due to a combination of their good casting characteristics, low density, high resistance to corrosion and good mechanical properties. The alloy is an example of a composite material grown in situ, with the stiff but brittle silicon phase reinforcing the more ductile aluminium. Thus the mechanical properties depend primarily on the nature and scale of distribution of the silicon phase, and work on this alloy is concerned principally with correlating these factors with the conditions under which the alloy is solidified and with the alloy composition. In this connection it has been found that very small concentrations of sodium produce a great refinement in the dispersion of the two phases, accompanied by a considerable improvement in mechanical properties, and the fact that this refinement can be obtained over a wide range of casting conditions gives the alloy its commercial importance.

Some previous work has been done on this system, the results of which were presented for a part II thesis (32). In this work, the mechanical properties corresponding to different eutectic silicon morphologies were investigated, the range of compositions over which primary free alloy could be grown for a set of growth rates was determined, and the freezing rate for fixed temperature gradient at which the morphology of the eutectic silicon phase changed from coarse flakes to fine fibres in the pure alloy was measured.

The aim of the current work was to investigate further the

conditions of temperature gradient and growth rate under which the refinement occurs, and to compare the effects of small concentrations of various impurity elements on the eutectic structure. In addition it was hoped to carry out some more definitive experiments on the growth of silicon into solutions in aluminium, with and without the presence of impurity elements.

II Theoretical considerations

1) The eutectic reaction

According to the Phase rule, a system of three phases and two components has one degree of freedom, so that at constant pressure, the three phases can coexist only at one temperature and with fixed compositions. Thus the invariant equilibrium is represented on the binary phase diagram by the eutectic isotherm, the ends of which coincide with the compositions of the solid phases, with the liquid phase having an intermediate composition. At the eutectic isotherm the reversible eutectic reaction occurs

$$L \rightleftharpoons \alpha + \beta$$

Where L is the liquid phase, and α and β the solid phases.

2) Principles of eutectic solidification

The eutectic reaction proceeds, like the solidification of a pure metal, by a process of nucleation and growth. Since two phases, of different composition from the liquid, are formed, the reaction is incongruent, and both phases must nucleate for growth to occur. It is normally assumed that one phase nucleates first, probably on a heterogeneous site in the liquid, causing a solute build up nearby which offers a site for nucleation of the second phase. Once the nuclei have been formed, solidification can proceed, with the growth rate being controlled by the rate of heat extraction from the system.

Under equilibrium conditions, the reaction would occur at the eutectic temperature, but with a finite cooling rate the liquid must be undercooled below the eutectic temperature to provide the free energy for the formation of nuclei of the two phases. In addition an undercooling is needed to provide the driving force for the solid phases to grow at a finite rate, and this under-

cooling for growth has three components.

$$\Delta T = \Delta T_C + \Delta T_B + \Delta T_K$$

Where ΔT_B is the undercooling needed to provide the energy of the α - β phase boundaries, and can alternatively be considered as the undercooling due to the curvature of the solid-liquid front. ΔT_K is the kinetic undercooling, due to the nucleation barrier to deposition of atoms from the liquid onto the solid.

ΔT_C is the constitutional undercooling, which is due to the build up of solute in the liquid ahead of the growing solid phase.

Clearly if the interphase spacing is increased, the area of interphase boundary per unit volume, and hence ΔT_B, decreases, while the mean solute diffusion distance and hence ΔT_C, increases. According to Tiller (1) the optimum spacing is that which allows maximum growth rate at a given undercooling, or which gives a minimum undercooling at a given growth rate. This condition was rationalised as being equivalent to minimising the rate of production of entropy during solidification. This minimum also implies that $\frac{d\,\Delta T}{d\,\lambda}_B = \frac{-d\,\Delta T}{d\,\lambda}_C$, where λ is the interphase spacing, and this is perhaps a more meaningful stability criterion.

Hence there is a mutual dependence between growth rate, scale of dispersion and undercooling.

3) Classification of eutectics

An historical review of the attempts to classify the various eutectic structures is given by Day (2). Currently the most satisfactory classification is considered to be that due to Hunt and Jackson (3). According to the scheme of Jackson (4), solid phases are divided into faceting and non-faceting types depending on whether the equilibrium structures of low index crystallographic faces are atomically smooth or rough. He shows that crystals of phases with a high entropy of fusion assume a faceted shape, while

those of phases with a low entropy of fusion are generally isotropic. Generally metals have low and non-metals high entropies of fusion, but this quantity depends for a given phase on the temperature and composition of the melt from which the phase is growing. Thus decreasing growth temperature gives increasing entropy of fusion, and growth from a (disordered) liquid solution of a phase is associated with a larger entropy change than growth from liquid of the same composition as the growing phase. There is a significant nucleation barrier to the deposition of new layers of atoms on a smooth interface, so that faceted materials grow with a high kinetic undercooling, while that for non-faceted materials is negligible in comparison.

On this basis Hunt and Jackson (3) classify eutectics according to their component phases as faceted/faceted, faceted/non-faceted, and non-faceted/non-faceted. Depending on the eutectic system and the solidification conditions, eutectic growth may occur in three ways.

1) The two phases may grow independently with long diffusion distances.

2) They may grow by repeated nucleation and growth of one or both phases, although this would require large undercoolings or an improbably high density of heterogeneous nucleation sites in the liquid.

3) The two phases may grow in a coupled manner with relatively short diffusion distances. This coupled growth may be either steady state, when a constant diffusion distance is maintained, or non steady-state when the diffusion distance fluctuates.

They considered the possible growth modes for different types of eutectic.

(a) Non-faceted/non-faceted eutectics

These may grow in a coupled manner at a steady-state diffusion front, forming alternate lamellae of α and β phase or rods of one phase embedded in a matrix of the other, depending on the volume proportions of the phases. Experimentally the relationship between lamellar spacing λ and growth rate V has been found (5, 6) to be $\lambda^2 V$ = constant, and Tiller (1) and Jackson and Chalmers (7) have derived this equation theoretically.

(b) Faceted/faceted eutectics

At low growth rates these grow independently with a non-isothermal solid-liquid interface, while at very high rates the undercooling ahead of the interface may be sufficiently high to allow a repeated nucleation and growth mechanism, giving a spherulitic structure (8). Otherwise the structure is likely to be similar to that of faceted/non-faceted eutectics since as one phase advances the other fills in the resulting gaps.

(c) Faceted/non-faceted eutectics

At very low freezing rates these may grow independently but at normal rates they grow at a duplex front which is steady state at lower rates but which breaks down to a non-isothermal front at high rates, with a fluctuating diffusion distance. All these growth modes are found in the aluminium-silicon system.

Because of the high kinetic undercooling necessary, the faceted phase must grow either at a higher total undercooling (i.e. behind the non faceting phase) or at the same total undercooling but with a lower solute undercooling (i.e. projecting in front of the non-faceting phase so that solute rejection is efficient). It is possible for this kinetic undercooling to be reduced by the presence of defects such as screw dislocations (9) or t n re-entrant grooves (10) on the growing surface, but on

the other hand a further local undercooling will be needed to form these defects. It is a matter of some uncertainty as to whether the defects are present due to growth accidents, or whether they are necessary for growth to be able to proceed.

The growth direction of faceted materials is crystallographic, depending on the orientation of the slowest growing (most close packed) faces, and is not necessarily the imposed growth direction. For this reason an optimum diffusion distance cannot be maintained, and growth is non-steady state unless the faceted phase is so oriented that it can grow normal to the solid-liquid front.

A phase growing in a faceted manner must be convex in two dimensions towards the liquid, as otherwise steps forming preferential sites for the growth of new layers will always be present, and the interface will become rough - Hume and Mullin (11).

Both cast irons and aluminium silicon alloys are examples of a faceting/non-faceting system.

4) <u>The coupled region</u>

The coupled region of a given eutectic system is the range of compositions and conditions of temperature gradient and growth rate over which no primary phases are formed during solidification. Under equilibrium conditions the occurrence, composition and proportions of primary and eutectic can be predicted directly from the phase diagram. Experimentally it has been found that coupled growth may occur over a range of compositions, depending on the growth conditions. Thus when the growth rate V is large relative to the temperature gradient G, the eutectic range increases with V (32) while when G is large relative to V the range decreases with increasing V, the extent of the coupled region being proportional to G/V (13).

According to Hunt and Jackson (14) the condition for a primary phase to be present in a specimen freezing at a given rate is that the primary should grow at a higher temperature than, that is in front of the short range diffusion typical of a eutectic. Thus in order to determine the conditions under which coupled growth will occur, we must consider the growth temperatures of the primary and eutectic, and the effect on these temperatures of variables such as composition, temperature gradient, growth rate, and possible kinetic restrictions on the growth of one of the phases.

We consider first the growth temperature of a primary phase. The total undercooling ΔT_D of a primary dendrite can be divided into contributions from solute undercooling ΔT_C, the curvature undercooling ΔT_B, and the kinetic undercooling ΔT_K.

$$\Delta T_D = \Delta T_C + \Delta T_B + \Delta T_K$$

The solute undercooling can be subdivided into an undercooling due to the average solute build up ahead of the interface and one due to lateral solute rejection at the tip of the growing dendrite. The effect of the average solute build up can be derived as follows - see fig. 1 and fig. 2 -

C_o is the average liquid composition.

C_α is the composition of primary being deposited.

C_I is the liquid composition at the dendrite tip.

$\frac{dc}{dx}$ is the composition gradient in the liquid at the interface.

G is the imposed temperature gradient.

m is the primary liquidus slope.

V is the growth velocity.

At the tip, the imposed temperature gradient is equal to the temperature transform of the composition gradient for equilibrium conditions, i.e. $G' = \frac{mdc}{dx}$

Mass balance requires $V(C_I - C_o) = D\frac{dc}{dx}$

Combining these: $m(C_I - C_o) = \frac{GD}{V}$

or $T_o - T_I = \frac{GD}{V}$

i.e. $\Delta T = \frac{GD}{V}$

Burden (49) has shown that the undercooling due to lateral solute rejection at the dendrite tip is directly proportional to V and r, the radius of curvature of the tip. The curvature undercooling is given by $\Delta T_B = \frac{2\gamma}{r\Delta S}$ where γ is the solid-liquid surface energy, and ΔS the entropy of fusion.

$$\Delta T_D = \frac{GD}{V} + AVr + \frac{2\gamma}{r\Delta S} + \Delta T_K$$

Since r is not known, an assumption is made that at constant velocity, the value of r is that for which the undercooling is a minimum, in other words the condition is that $\frac{\partial(\Delta T_D)}{\partial r} = 0$, and if ΔT_K is neglected compared to the other contributions this is equivalent to $\frac{\partial(\Delta T_B)}{\partial r} = -\frac{\partial(\Delta T_C)}{\partial r}$

Using this condition, r is proportional to $\frac{1}{\sqrt{V}}$

$$\Delta T_D = \frac{GD}{V} + B\sqrt{V} + \Delta T_K$$

where B is a constant.

If T_D is the actual dendrite growth temperature, the condition for coupled growth is that $T_D < T_e$, where T_e is the actual eutectic growth temperature.

$$T_e = T_E - \Delta T_E$$

where ΔT_E is the eutectic undercooling and T_E the equilibrium eutectic temperature.

Thus the limits of the coupled region are defined by

$$T_D = T_e$$

Fig (3) shows T_D and T_e plotted against V for a given composition and imposed temperature gradients G, and G_2, $G_1 < G_2$. It can be seen that between V_3 and V_1 and V_3 and V_2

primary and eutectic grow, while outside these limits primary is suppressed. Fig (3) neglects the kinetic undercooling of the primary and the eutectic undercooling, which is satisfactory for non-faceted/non-faceted eutectics, but for a faceted/non-faceted system such as aluminium-silicon ΔT_K and ΔT_E are not negligible at high growth rates as both terms increase with V. Thus while fig (3) still describes the situation for aluminium-silicon at low V and high G, at high V the situation is described on the different sides of the eutectic composition by figs (4, 5). T_{Si} and T_{Al} are the liquidus(or extrapolated liquidus) temperatures for the given composition. Because of the importance of the kinetic undercooling at high rates, the growth temperature of primary silicon decreases more rapidly with undercooling than that of the eutectic, which in turn decreases more rapidly than that of primary aluminium. The result is a coupled region - fig 6 - which is assymetrical at high growth rates.

From the condition derived above for the limits of the coupled region, we can derive an expression for the range of compositions on the α rich side of the eutectic over which coupled growth occurs.

$$T_D = T_e$$

$$\therefore T_o - T_E = \Delta T_D - \Delta T_E$$

$$\therefore m(C_o - C_E) = \Delta T_D - \Delta T_E$$

$$\therefore \Delta C_\alpha = \frac{1}{m}\left[\frac{GD}{V} + B\sqrt{v} + \Delta T_K - \Delta T_E\right]$$

[Both ΔT_K and ΔT_E are functions of v]

The above treatment (p 9–10) is due to J. D Hunt (59)

Fig 1

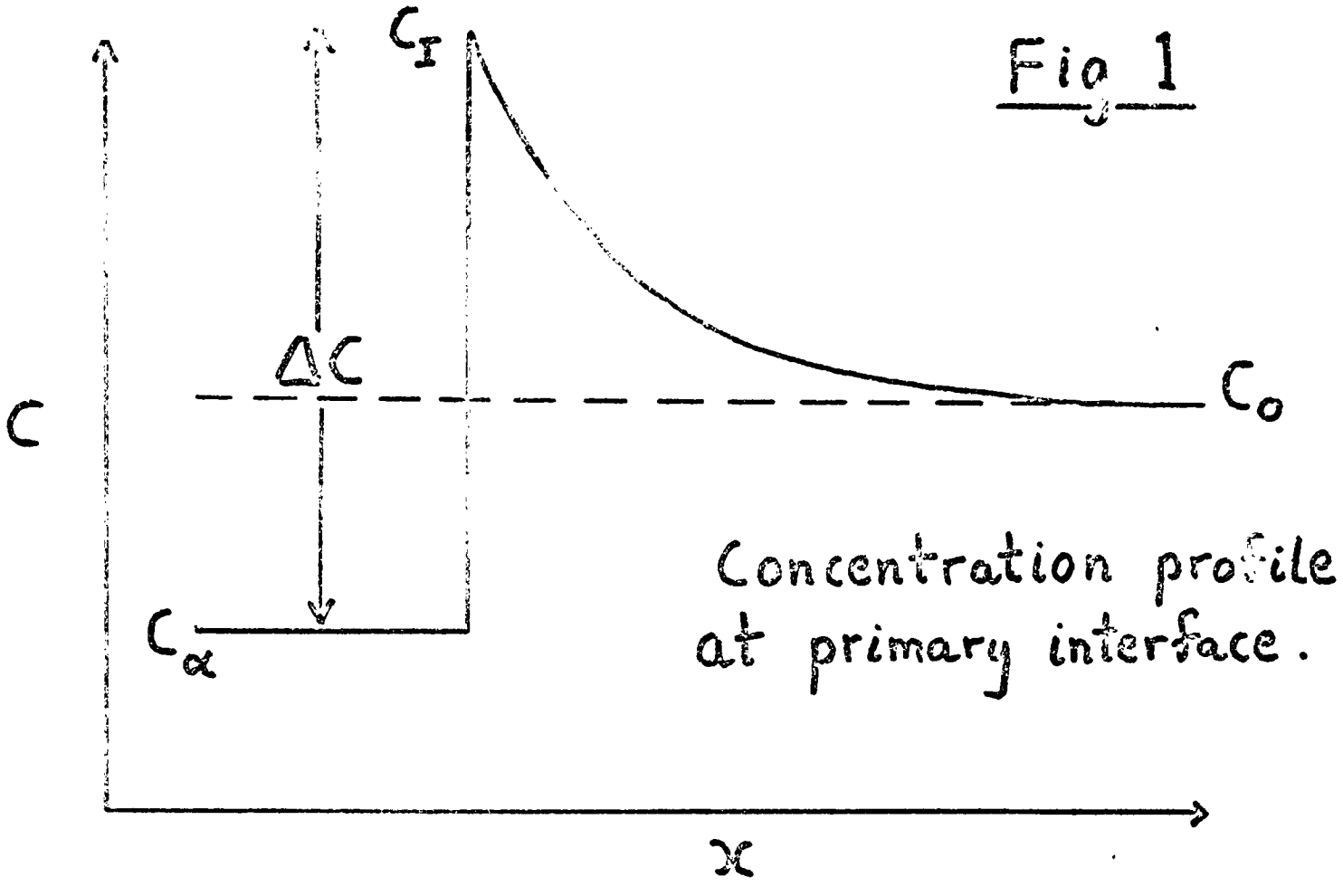

Concentration profile at primary interface.

Fig 2

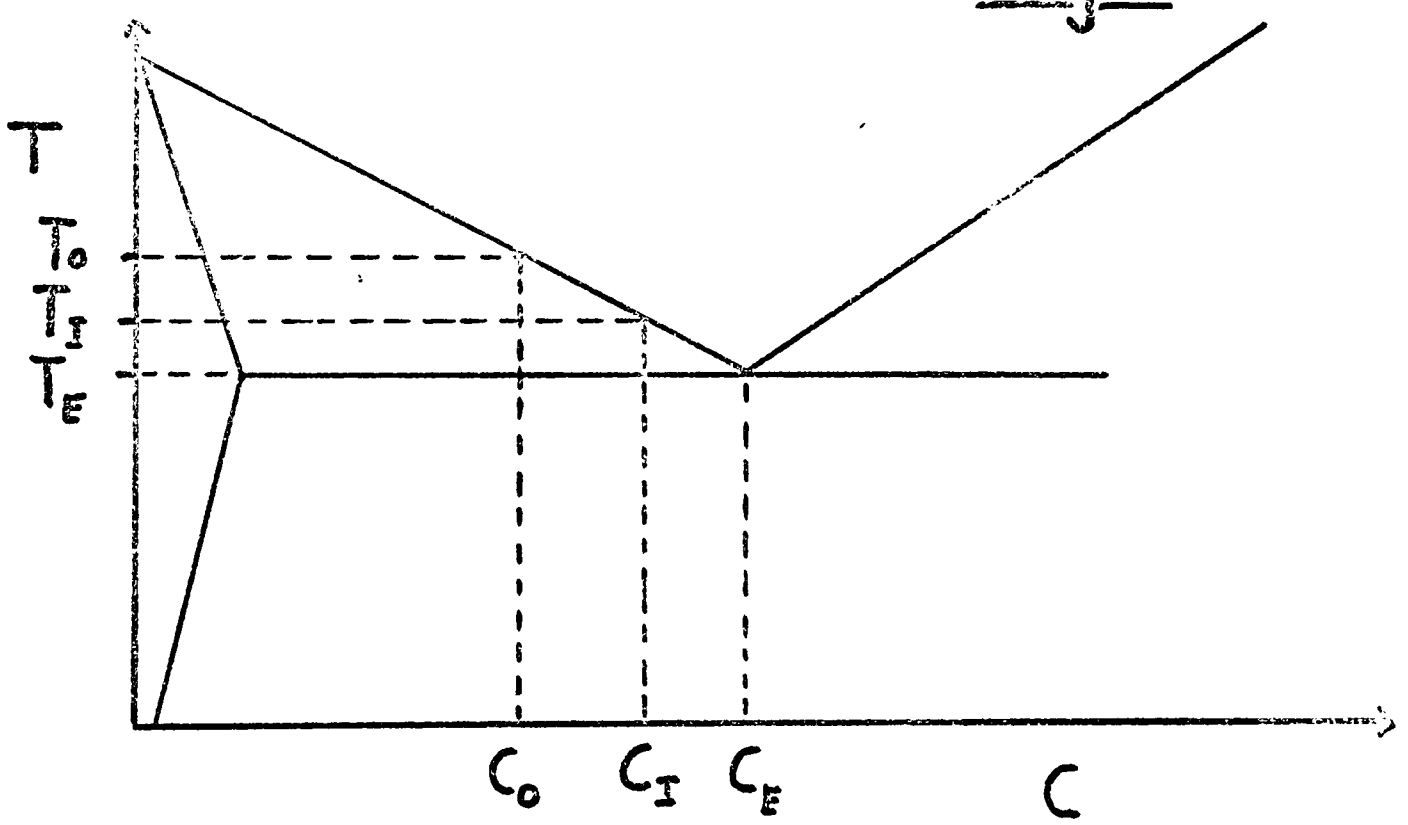

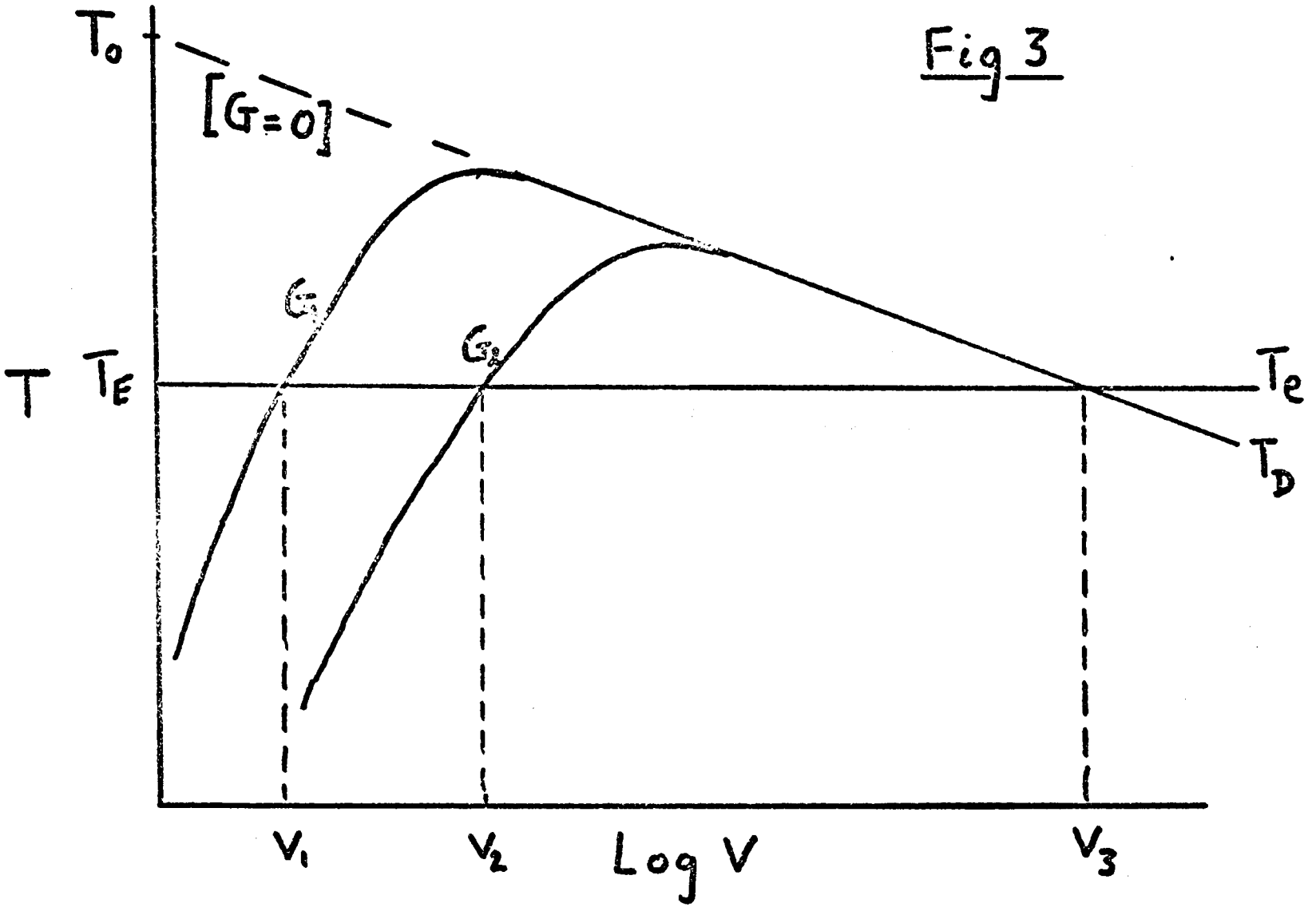

Fig 3

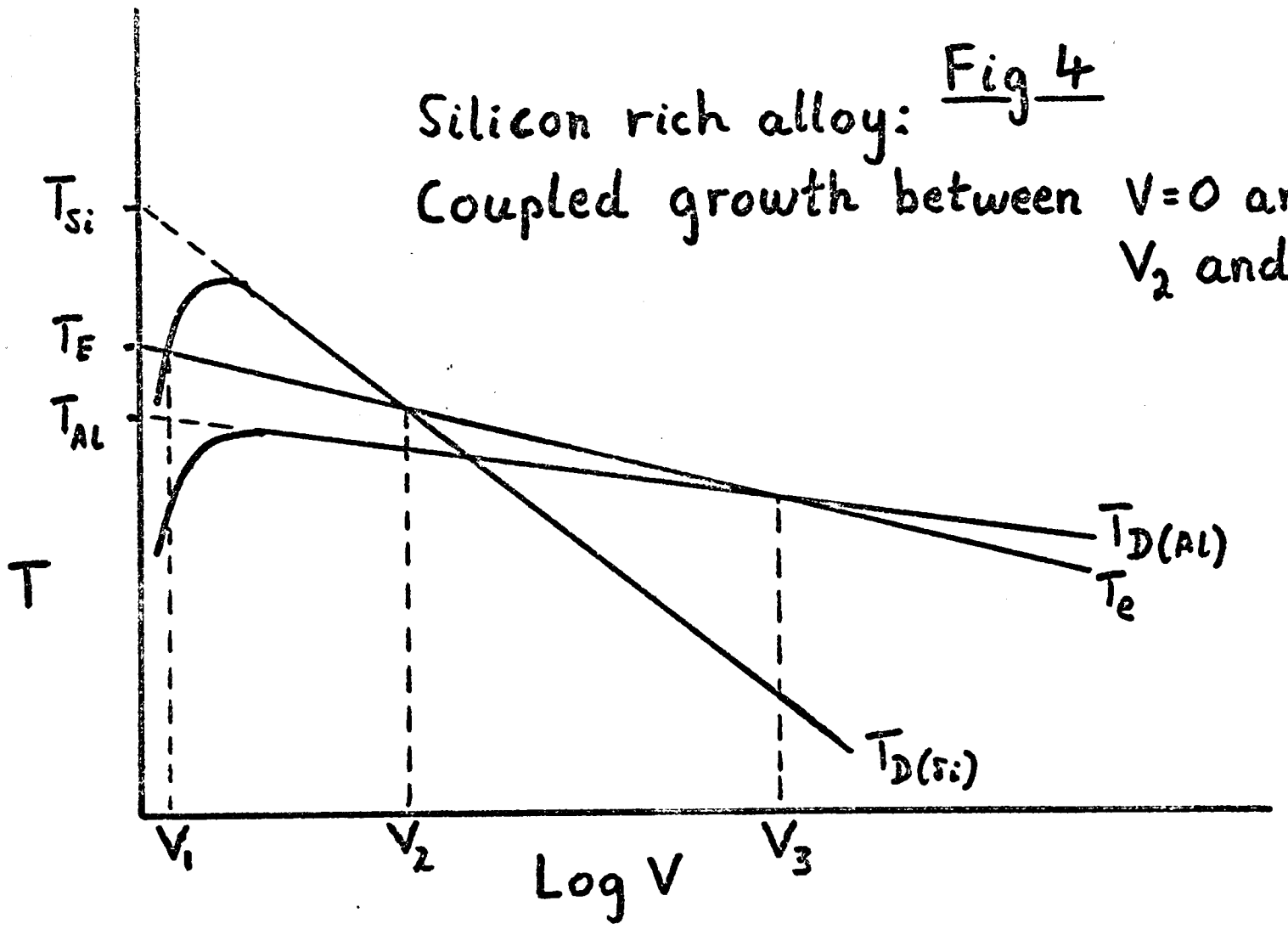

Fig 4

Silicon rich alloy:
Coupled growth between V=0 and V_1
V_2 and V_3

Fig 5

Aluminium rich alloy:
Coupled growth between V=0 and V_1

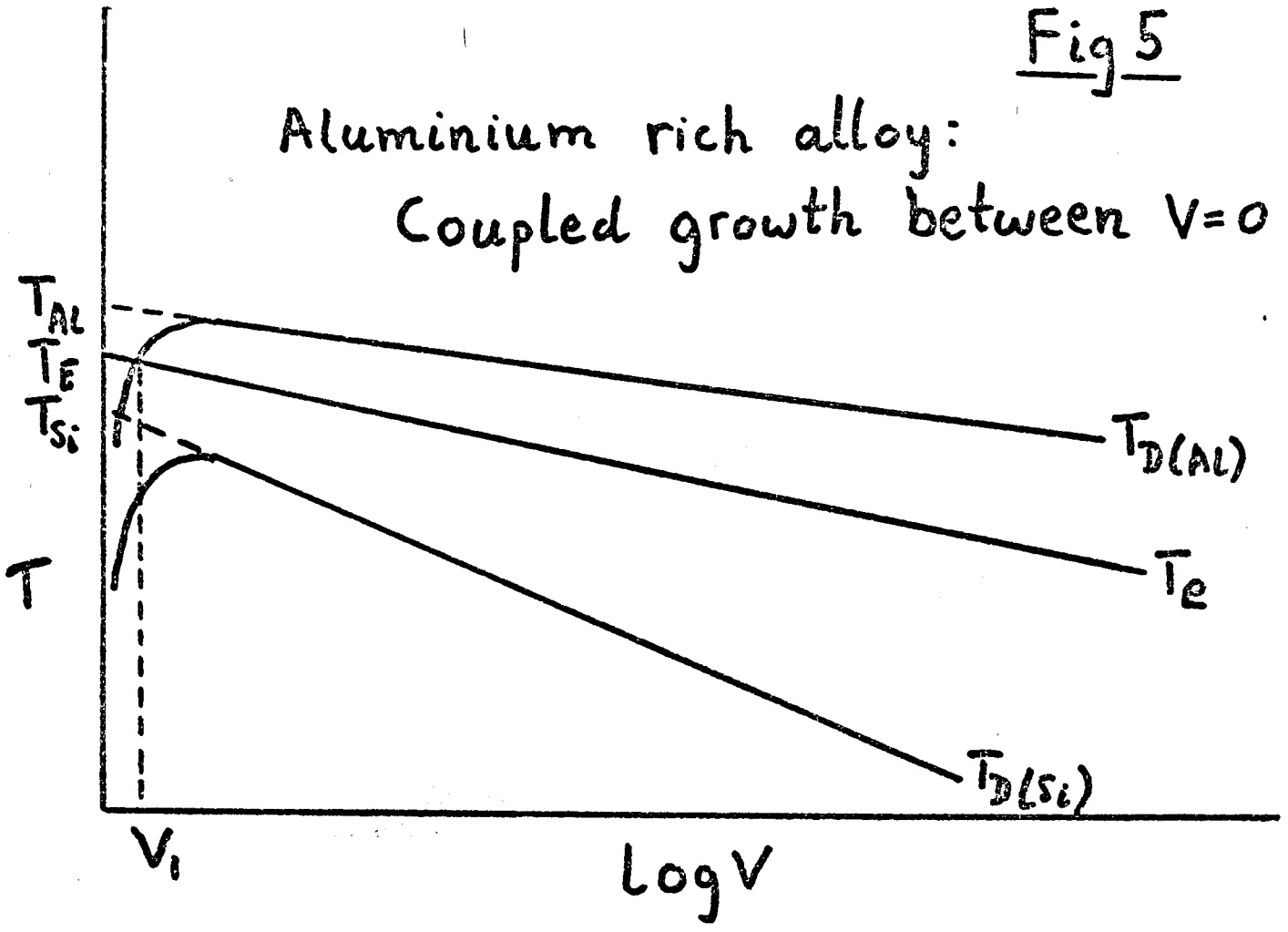

Fig 6

Coupled region on Al-Si phase diagram (Schematic)

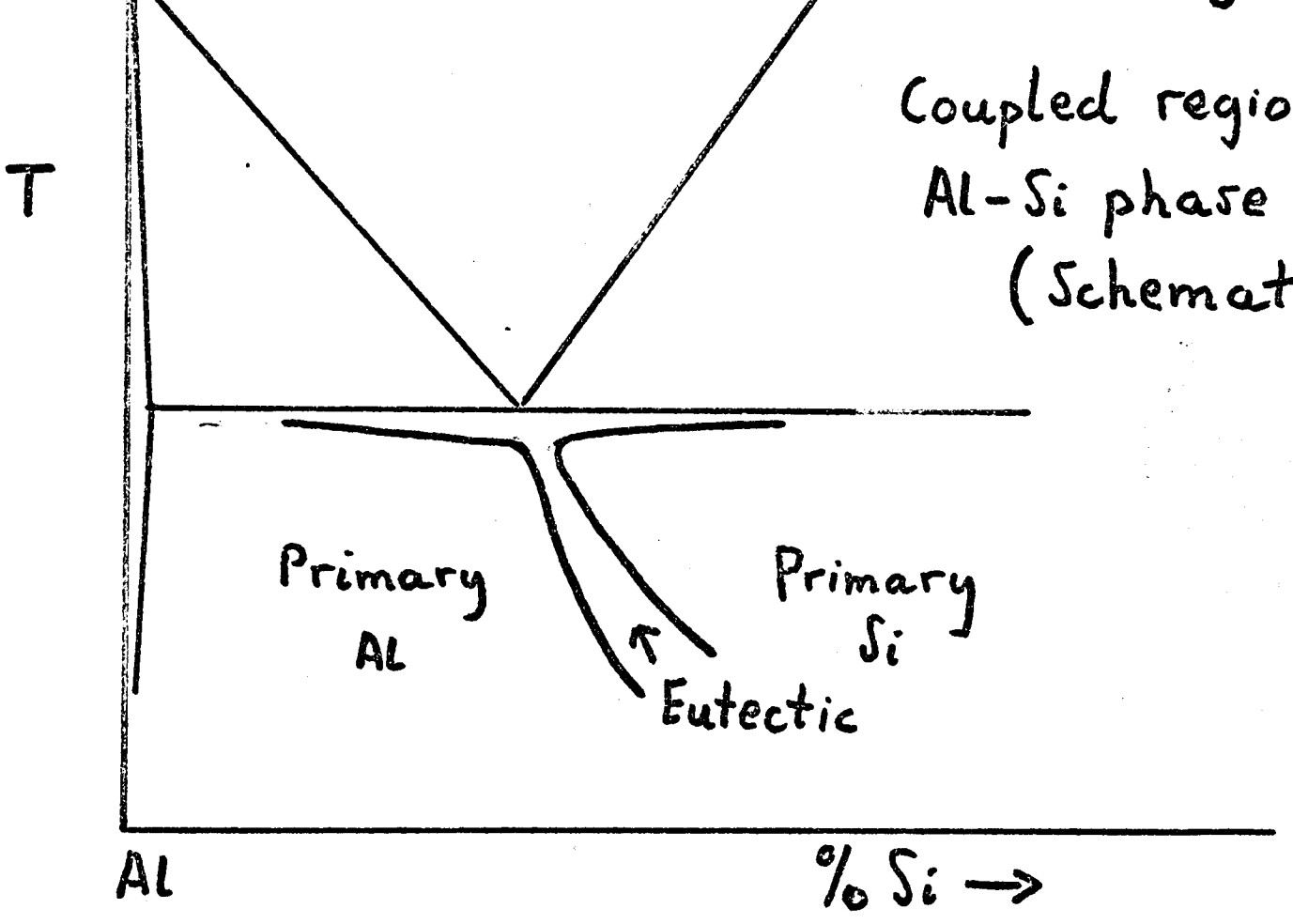

III Previous work on the aluminium-silicon system

1) The phase diagram - fig 7 -.

Gwyer and Phillips (15) determined the aluminium and silicon liquidus lines by thermal analysis and extended these to a eutectic point at 11.7 wt% silicon and 577°C. However their alloys contained up to 0.3 wt% of iron and with purer materials Willey (16) using a method of hot filtration at 578°C on alloys containing 9 to 19 wt%Si obtained filtrates of 12.5 wt%Si, and this is currently accepted as the eutectic composition.

The mean liquidus slopes are given by Hansen (17) and by the supplement by Elliott (18) to be:

Aluminium	6.5°C per wt%
Silicon	9.5°C per wt%

The same sources give the solid solubilities at the eutectic temperature to be:

Aluminium in silicon	10^{-2} wt%
Silicon in aluminium	1.59 wt%

2) Introduction

The commercial importance of this alloy is due to the discovery by Pacz (19) that the addition of a small quantity of sodium fluoride to the molten alloy before casting resulted in a considerable refinement of the scale and distribution of the eutectic silicon phase, accompanied by a great improvement in mechanical properties. Consequently much of the early work was done on the modified alloy. In order to understand the mechanism of modification, however, it is necessary first to determine what structures can be produced in the pure (unmodified) alloy.

3) The unmodified eutectic microstructure

Gayler (20) showed that, using relatively pure materials, sand cast alloys gave a microstructure of elongated silicon particles (flakes) in an aluminium matrix, while chill casting produced an effect similar to that of modification, the silicon phase appearing as isolated globules (in a two-dimensional section) in the aluminium matrix. She found that chill cast alloys froze up to 12°C below the equilibrium eutectic point, with the apparent eutectic composition moving to higher silicon contents.

Straumanis and Brakss (21) discovered that the silicon phase had no preferred orientation, while the $\langle 100 \rangle$ aluminium preferred orientation they found was not confirmed, and is thought to have been due to the presence of primary aluminium dendrites in their specimens. This lead investigators to assume that the silicon particles, which appeared isolated on optical micrographs, were not interconnected, so that each particle was thought to have been separately nucleated, and a number of theories describing the mechanisms by which this could occur were put forward.

Thall and Chalmers (22) suggested that the rate of advance of the eutectic interface depended on heat flow considerations, such that the interface of a phase with high thermal conductivity and low heat of fusion, (here aluminium), should advance faster than that of a phase with low thermal conductivity and a large heat of fusion (silicon). Then while at low growth rates the silicon may be interconnected, at higher rates the aluminium tends to overgrow the silicon so that repeated nucleation of the silicon phase becomes necessary for growth to proceed.

Tiller (1) explained the eutectic structure by proposing that neither phase could nucleate the other, so that the second phase nucleated heterogeneously in the liquid, producing an array of randomly oriented, non-interconnected crystals. Plumb and Lewis (23) put forward a similar theory, postulating that the two phases nucleated alternately in a cyclic freezing pattern.

Meussner (24) and Ghosh and Kondic (25) inferred from optical micrographs that the 'flaky' silicon eutectic was probably interconnected. They showed silicon flakes of similar orientation on both sides of aluminium dendrites and this was taken to imply some continuity in the structure. Meussner showed that the primary silicon was heavily twinned, and inferred that the eutectic was as well. He emphasised the controlling effect the silicon phase has on the eutectic morphology, showing that the silicon phase nucleates readily and grows rapidly into a branched plate structure, while aluminium nucleates on these plates and grows to fill in the gaps in the silicon. Hence the aluminium shows no preferred orientation.

Hogan et al (55) have shown by anodising the flake eutectic that the aluminium grain size is very small, being of the same order as the interflake spacing. They argue that since the silicon phase leads, diffusion is too slow to prevent a build up of silicon at the aluminium front. This build up of solute slows the growth of the aluminium phase, and nucleation of new aluminium grains takes place ahead of the interface. The 'trapped' silicon is assumed to nucleate and grow on the {111} flake faces. It should be pointed out, however, that the anodising technique is sensitive to very small differences in orientation, so it may have been that subgrains rather than grains were being examined.

Chadwick (26) pointed out that the silicon phase grows crystallographically, and not necessarily perpendicular to the growth front, inferring that repeated nucleation is necessary to maintain even an approximately constant spacing. He also reported (7) that extraction showed the eutectic silicon to be not interconnected.

Bell and Winegard (28), on the other hand, also extracted the silicon phase, but found it to be continuous within one grain. The continuity of the silicon was confirmed by Day and Hellawell (29) using scanning electron microscopy of the deeply etched eutectic.

Day (30), (2), pointed out that the eutectic morphology depends on temperature gradient as well as growth rate, and directionally solidified the pure eutectic over a wide range of gradients and rates, classifying the silicon morphologies as follows - see fig (8) -

In region A the two phases grow independently with a diffusion distance of about 1 mm.

In region B the silicon phase grows as rods with a <100> fibre texture, aligned in the growth direction. Growth occurs at a more or less steady state front by short range diffusion. With decreasing G/V, irregular side plates appear on the rods.

In region C the silicon occurs as irregular, interconnected plates with a (111) habit which are heavily twinned, this accounting for the absence of a preferred orientation. Growth is by a fluctuating short range diffusion process, the silicon projecting ahead of the aluminium so that it grows at a lower solute undercooling, and a kinetic undercooling which while high, is lower than it would be if there were no twins in the silicon.

There is a further transition in structure in region C at a

growth rate of about 1 mm/S, above which the silicon grows as interconnected fibres. This fibrous structure was shown by scanning electron microscopy of deep etched specimens to be interconnected, and similar to the structure produced by sodium modification. Day and Hellawell assumed that, like the flakes, the fibres were heavily twinned.

They explained the various structural transitions in terms of the possible silicon growth mechanisms: In the absence of defects, growth rate and undercooling are related, according to Rosenberg and Winegard (31), by

$$V_1 = K_1 \Delta T^n \quad \text{where } n \sim 2$$

An activation energy is necessary for the formation of twins, so that the growth velocity of twinned silicon will vary exponentially with the undercooling.

$$V_2 = K_2 \exp(K_3 \Delta T)$$

Then in region B the twin free material grows at a lower undercooling at a given rate, while in region C the twinned material grows at the lower undercooling.

The transition to interconnected fibres occurs at a high growth rate, where the silicon drops behind the aluminium front to find higher undercoolings in order to continue growing in a coupled manner. They suggest that the silicon is then growing at 'holes' in the aluminium front.

Steen (32) investigated the flake-fibre transition, and from optical and scanning electron micrographs inferred that it occurred at about 0.4 mm/S, although a plot of hardness against growth rate indicated a structural change at about 1 mm/S. He also confirmed the existence of an assymetrical coupled region and charted it as a function of composition and growth rate. Gigliotti and Colligan (33) similarly found an assymetric coupled region,

plotting composition against growth temperature, for the pure alloy, while modification with sodium caused coupled growth to occur at smaller undercoolings for a given composition, increasing the assymetry of the coupled region.

Hillert and Lange (34) carried out unidirectional solidification at high rates and observed a continuous change of the plate-like structure to a fibrous structure with growth rates of 10^{-4} mm/S to 3 mm/S under a temperature gradient of 30°C/mm. Hillert et al (35) propose that the random orientation of the plate like silicon in a eutectic colony is due not to multiple twinning but to a gradual change in orientation of the plates as in the similar white cast iron system. Growth of the flake eutectic is still considered, however, to occur by a twin plane re-entrant mechanism. In contradiction to Day and Hellawell they infer from the regularity of the fibrous eutectic that it is not multiply twinned, and argue that its growth may not depend on a T.P.R.E. mechanism.

4) Nucleation of the unmodified eutectic

Nucleation behaviour in a number of binary alloys was investigated by Sundquist and Mondolfo (36) who found that the effective nucleating phase was the one with the higher entropy of fusion, here silicon. Similar experiments by Crosley and Mondolfo (37), using eutectic droplets on a silicon substrate, however, showed that while aluminium nucleated the eutectic at 5-7°C undercooling, silicon was not an effective nucleant for the eutectic. Meussner (24) observed eutectic silicon crystals attached to primary silicon, while Hillert et al (35) found twin planes in primary silicon crystals to be parallel to nearby silicon flakes, and both these observations imply that primary silicon does nucleate the eutectic.

5) Modifying elements

As mentioned above, the commercial importance of this alloy arises from the discovery by Pacz (19) that a small addition of an alkaline fluoride greatly improved the mechanical properties, changing the eutectic silicon from an irregular coarse form to a very finely dispersed form similar to that obtained by rapidly quenching the alloy.

It was soon found that a number of other elements produced a similar effect on the microstructure. Edwards, Frary and Churchill (38) took out a patent covering the use of the alkaline earths and their hydroxides. Kim and Heine (39) added an assortment of elements at varying concentrations and differing temperatures of addition, using commercial purity alloys. They assessed the effect of each element in terms of whether or not coarse polyhedral silicon was present and what proportion of the microstructure appeared 'modified'. Their criterion for deciding whether or not a structure was modified was not defined, but was taken to be a refinement of the microstructure of the eutectic. They found sodium to be fully effective, with the other alkali metals somewhat less potent modifiers and lithium ineffective. Cadmium, arsenic, selenium and calcium all produced a small proportion of modified microstructure. Generally a higher temperature of addition produced more modification, and since the alloys were cast a minute after adding the modifier, this was probably because a higher temperature for addition allowed more time for the modifier to be dissolved in the alloy.

Davies and West (41), using the pure alloy, investigated the modifying effects of a number of elements, finding that chloride/fluoride fluxes were effective modifiers for potassium, rubidium, caesium and sodium, but not for lithium. 0.2 wt% of lithium or

bismuth produced some modification, but magnesium, cadmium and lead were found to be ineffective.

A number of workers - Gurtler (40), Crosley and Mondolfo (37) and Kim and Heine (39) have found that in hypereutectic alloys, the primary silicon can be considerably refined by the addition of small quantities of phosphorous, as little as 0.00015% being reported to be effective. With the addition of more phosphorous, the morphology of the eutectic is also altered, being changed from interconnected colonies of flakes (termed lamellar by Gurtler) to apparently randomly oriented, rather coarser crystals, (the structure termed granular by Gurtler).

6) Effects of modification - summary -

The majority of work on the effects of modification has been done using sodium modified alloys, and in as much as other modifying elements (excepting phosphorous) also produce a structual refinement, it is assumed that these effects are common to other modifying elements.

a) Mechanical properties are improved, ductility, tensile strength and hardness all being increased (22), (32).

b) Correspondingly there is a change in the microstructure in that the eutectic silicon particles appear smaller and more rounded in an optical micrograph, while scanning electron microscopy reveals the silicon to have changed from interconnected plates to branched fibres.

c) Thermal analysis has shown (20), (23) that the freezing point is lowered, while the melting point remains unchanged.

d) The eutectic composition moves towards higher silicon concentrations (20).

e) The viscosity of the liquid alloy is increased, while the surface tension and diffusion rate are decreased (23), (41), (42).

f) Rapid freezing produces a microstructure morphologically the same as but rather finer than that produced by modification.

7) Thermal analyses

Thermal analysis with relatively pure alloys was first carried out by Thall and Chalmers (22). They found using cooling rates between 15 and 90°C/min that the normal eutectic solidified 1 to 2°C below the heating arrest, while the modified eutectic undercooled by 6 to 9°C. Modification did not affect the solidification temperature of the primary phases, although the primary silicon arrest was unclear, probably because of variable undercooling of the primary silicon before it solidified. Their cooling curves did not show any recalescence.

Plumb and Lewis (23) found a recalescence of 1-2°C on all their curves. They showed that the unmodified eutectic undercooled by 1-2°C, while the modified eutectic arrest was 8-9°C below the equilibrium eutectic point. They found that alloys containing less than the saturation value of sodium undercooled less. Thus 0.006%Na gave an undercooling of 6°C and 0.016%Na one of 9°C.

Crosley and Mondolfo (37) observed a 2-3°C recalescence preceeding solidification of the unmodified eutectic at 'negligible' undercooling. Primary Aluminium undercooled 5-7°C below the liquidus, while primary silicon gave no clear arrest. Modification did not affect the primary arrests, but the eutectic arrest was depressed 10-12°C below equilibrium. Like Plumb and Lewis they found that sodium concentrations below the saturation value gave smaller undercoolings.

Gigliotti and Colligan (33) contended that while the scale of dispersion of the silicon phase was cooling and hence growth rate dependent, the morphology was not, depending only on the presence

or absence of a modifying element. They reported that at a cooling rate of $4\frac{1}{2}^{o}C/S$ gave a fine plate eutectic growing at an undercooling of $13^{o}C$, while a rate of $1^{o}C/S$ gave a coarse plate structure at an undercooling of $3^{o}C$. A modified alloy cooled at $1/5^{o}C/S$ gave a fine fibrous eutectic and an undercooling of $13^{o}C$, while a similar alloy cooled very slowly gave a coarser but still fibrous eutectic with a $3^{o}C$ undercooling. However these results can be interpreted as showing that the flake to fibre transition takes place at greater undercoolings (more than $13^{o}C$) in the pure alloy than in the sodium doped alloy (less than $3^{o}C$).

Gurtler (40) investigated the freezing temperatures of phosphorous bearing and pure alloys, both with and without sodium. He found the eutectic arrest in phosphorous modified alloys was about $2^{o}C$ below equilibrium at cooling rates between $\frac{1}{2}^{o}C/S$ to $4^{o}C/S$ while when sodium was added the growth undercooling increased from about $3^{o}C$ to $8^{o}C$ over these rates. He reported that sodium modification of the pure alloy did not significantly affect the undercooling for a given cooling rate, the undercooling increasing from about $3^{o}C$ at $\frac{1}{2}^{o}C/S$ to $16^{o}C$ at $4\frac{1}{2}^{o}C/S$.

Because cooling rates and not growth rates are specified in these experiments, the different results cannot be compared directly. It can be concluded though that at low growth rates the pure eutectic grows at about $2^{o}C$ undercooling, increased by modification to between $4^{o}C$ and $9^{o}C$. At high rates the undercooling for growth of the flake eutectic inreases rapidly, up to over $15^{o}C$ and modification does not significantly change this undercooling.

8) Mechanical properties

The majority of work done on the mechanical properties of aluminium silicon eutectics has used commercial alloys, and Thall and Chalmers (22) quote the following values for tensile strength,

elongation and Brinell hardness of the commerical alloy.

Alloy		Tensile strength lb/in^2	Elongation %	Brinell hardness
Normal	Sand	18000	2	50
Modified	Cast	28000	1.3	58
Normal	Chill	28000	3.6	63
Modified	Cast	32000	8	72

Steen (32) carried out some tensile tests on chill cast and slowly directionally frozen specimens of the pure alloy, and reported U.T.S. values 10-20% higher than those given by Thall and Chalmers. This was attributed to the absence of the brittle Al_3Fe compound in the pure material. Considerable variation was found in % elongation, and this was also generally greater than in the commercial alloys. It was shown that in the flake eutectic, fracture occurs by the propagation of cracks along the {111} cleavage planes, and since these were the planes of faceted flakes in which the twin planes were also {111}, growth of cracks could occur very easily. In the fibrous eutectic these paths for easy crack propagation were no longer available, so mechanical properties were greatly improved.

9) Theories of modification

The earliest theories of modification postulated that the modifying element in some way affected the aluminium-silicon phase diagram.

Guillet's 'true flux' theory (43) suggested that the modifying element acted to remove impurities such as alumina and silica by reduction, but the fact that unmodified structures existed in high purity alloys disproved this theory.

Jeffries (44) proposed that the modified alloy was metastable, but X-ray diffraction showed that the phases in both

modified and unmodified alloys were identical.

Ransley and Neufeld (45) suggested that the modified alloy was a ternary eutectic, but the fact that the melting point of the alloy was not depressed by modification showed that the equilibrium state of the alloy was unaltered.

More recent theories deal with the effect of the modifying element on either the nucleation or the growth of the eutectic phase. Since it has been shown that the modified silicon eutectic is continuous (29) and that fully modified directionally frozen specimens may be produced (35), it is clear that pure nucleation theories are unsatisfactory. Other early theories, however, while still assuming a repeated nucleation and growth mechanism, postulate that the modifier affects the growth part of the process, and these theories are still relevant to a continuous growth model.

The nucleation theories proposed that the modifying element was adsorbed onto heterogeneous nucleation sites in the liquid alloy, so that nucleation then took place at a greater undercooling. The ways in which this increased undercooling caused smaller silicon particles to be produced were explained variously: Spengler (46) thought that the density of successful nucleation centres increased with undercooling. Plumb and Lewis (23) proposed that the lower diffusion rate at lower temperatures meant that individual particles could not grow so large. Tiller (1) hypothesised that the increase in local growth rate caused a local solute build up, producing a solute undercooling which outweighed the nucleation undercooling. Thus growth of each particle rapidly stops and a smaller particle size results. Kim and Heine (39) postulated that the modifier forms compounds with silicon, depressing the nucleation of the silicon phase. Thus the modifier must be added at a temperature which is sufficiently

high to allow compound formation.

Growth theories generally consider that the presence of a modifying element somehow retards the growth of the silicon phase, so that while in non-modified alloys the silicon plates lead, in modified eutectics the silicon lags behind the aluminium.

Thall and Chalmers (22) proposed a mechanism similar to that involved in their account of the formation of the chill cast eutectic. Here the sodium acts to lower the surface tension between the solid aluminium and silicon phases, increasing the interfacial angle and tending to cause overgrowth of the silicon by aluminium. This theory was proposed assuming spherical silicon particles in the modified alloy, but partial overgrowth by this mechanism would give a refined but continuous structure which is consistent with what is now known about the morphology of modified silicon.

Edwards and Archer (46) considered that sodium formed a 'colloidal mist' just above the eutectic temperature which obstructed growth of the eutectic, causing supercooling and hence more nucleation, giving a finer eutectic. Archer and Kempf (47) proposed a similar mechanism with the modifier being adsorbed onto the growing silicon faces.

Davies and West (41) discussed the mechanisms of restricted growth. They concluded that the reduced diffusion rate of silicon did not cause the change in scale of dispersion observed, since the modification effect was not dependent on cooling rate. They carried out experiments on bimetallic interfaces which showed that sodium lowers the surface tension of the liquid eutectic and may alter the solid/solid surface energies. However with sodium present they found no dihederal angles at grain boundaries and inferred that Thall and Chalmers' mechanical obstruction model was inoperative.

They favoured the adsorbtion model as being compatible with their observations, in particular with the fact that a slowly cooled bimetallic specimen gave a thick silicon growth layer which the presence of sodium reduced to a thin, discontinuous one. Thus up to a saturation concentration of sodium, silicon growth is increasingly retarded until a maximum effect is acheived when the fastest growing faces are slowed to the growth rate of the slowest. Favourable sites for the nucleation of fresh layers are poisoned, so that two-dimensional nucleation becomes necessary and growth takes place at a high undercooling while the melting temperature remains unchanged. The growth of primary silicon but not that of primary aluminium is poisoned, so the eutectic will apparently move towards higher silicon contents.

They found that with excess sodium present a compound of the type NaALSi was formed which reciprocally acted as a nucleating agent with silicon. Thus with excess sodium a sodium rich layer is built up ahead of the interface and eventually NaALSi is formed, nucleating large silicon crystals. This was their explanation of the overmodification bands found in alloys with excess sodium.

These ideas were supported by autoradiographic studies done by Plumb and Lewis (23) to determine the distribution of sodium in the modified alloy. They found that sodium was preferentially adsorbed on silicon and that at concentrations above 0.012% the sodium segregated to a sodium rich constituent.

Day and Hellawell (30) suggested that sodium is adsorbed on T.P.R.E. sites in the flake eutectic, thus poisoning growth and increasing the undercooling, leading to more frequent overgrowth by aluminium and more frequent twin formation. They found that the $\langle 100 \rangle$ growth form found at low rates was not affected by sodium, inferring that this was because it did not depend on

T.P.R.E. sites for growth.

There is some dispute about what is the growth orientation of the fibrous modified eutectic. Gigliotti and Colligan (33) observed grooves along the axes of long fibres which were well aligned with the growth direction. These grooves which were observed under the scanning electron microscope were interpreted as twin traces and it was concluded that growth occurred by a T.P.R.E. mechanism, so that the axes of these fibres could not be $\langle 100 \rangle$. Hillert et al (35) argue that the modified eutectic is not twinned, and that modification takes place either because $\{100\}$ facets grow and stop the T.P.R.E. mechanism functioning, or because the twin planes are poisoned by sodium. They cited the apparent regularity of the modified structure on optical micrographs as indicating that the silicon was not multiply twinned. Fibres were observed with side plates at 90° angles round them, and the similarity between this and the rod like morphology found at very low growth rates was held to support a $\langle 100 \rangle$ growth direction for the fibres, the side plates having a $\{100\}$ habit.

10) Primary silicon

Work has been done on the effect of modifying elements on the morphology of primary silicon in order to elucidate the mechanism of modification.

Hillert et al (35) have examined the growth of primary silicon, both unmodified and in the presence of increasing concentrations of sodium. In the absence of sodium equiaxed and hexagonal plate-like crystals, both containing parallel twins, were observed. They concluded from the presence of equiaxed crystals that the T.P.R.E. mechanism was no more effective than a growth mode involving the nucleation of many new atomic layers

on advancing facets in these crystals. They suggest that the hexagonal plate crystals contained many closely spaced twins in bands parallel to the flat sides, so that these crystals did grow preferentially by a T.P.R.E. mechanism.

With the addition of increasing concentrations of sodium, {100} facets became more prominent, indicating that these were then the slowest growing. Here growth was thought to be layer nucleation limited. At very high sodium contents, other facets developed, and eventually spherical silicon crystals were produced.

Day (27) showed that with a concentration of 0.5% sodium, these spherical crystals contained non-radial {111} twin boundaries, but that with the addition of still more sodium, spherulitic crystals could be produced with an increased density of now radial twins. He inferred that the effect of sodium was to increase the {111} twin density by poisoning those twins already present, as he had previously proposed for eutectic silicon.

Thus it is not clear whether the effect of modification on primary silicon is to favour the development of {100} facets or to produce a greatly increased density of twins.

11) Overmodification

As mentioned earlier the overmodification bands produced by excess sodium concentrations have been attributed by Davies and West (41) to the formation of an AlSiNa compound.

Hillert et al (35) directionally solidified some specimens with excess sodium, obtaining overmodification bands at rates below a critical value. The eutectic between the bands was much finer than that found in normally modified specimens grown at the same rate, indicating that the eutectic was growing faster than the

applied rate and the bands corresponding much slower. It was found that the bands did not always contain coarse silicon particles, and crystals of AlSiNa were not detected in the over-modification bands, so it was concluded that the theory of Davies and West (41) which depended on AlNaSi particles nucleating large silicon crystals was incorrect.

Hillert et al quote some work by Wamich and Winterager showing that the temperature inside an overmodified alloy could fluctuate by as much as 10°C during directional freezing, with the same periodicity as the bands, implying that bands form when the front reaches a critical temperature. They suggest that this occurs when the growth rate is slowed to a sufficient extent to allow a critical quantity of sodium to be adsorbed. Then a cooperative effect leads to a rapid drop in growth rate and increase in adsorbtion. Correspondingly there is a critical undercooling above which there is a cooperative effect between decrease in adsorbtion and increase in growth rate. Considering fig (9). T_S and T_R are the critical temperatures for band formation and rapid growth. If a specimen is solidified at rate V_1 and is growing initially in the slow mode, the undercooling increases down the slow mode curve until T_R is reached and growth changes to the rapid mode. Then growth velocity decreases towards the applied freezing rate, but first reaches T_S when growth changes abruptly into the slow mode, and a cyclic process is followed. At velocities above V_2 a stable rapid growth mode is established as the corresponding growth temperature lies below T_S. It is proposed that decreasing the sodium content can be represented by moving the curves for the two growth modes closer together, and the critical temperature levels nearer to the eutectic.

Fig 7

The aluminium-silicon phase diagram

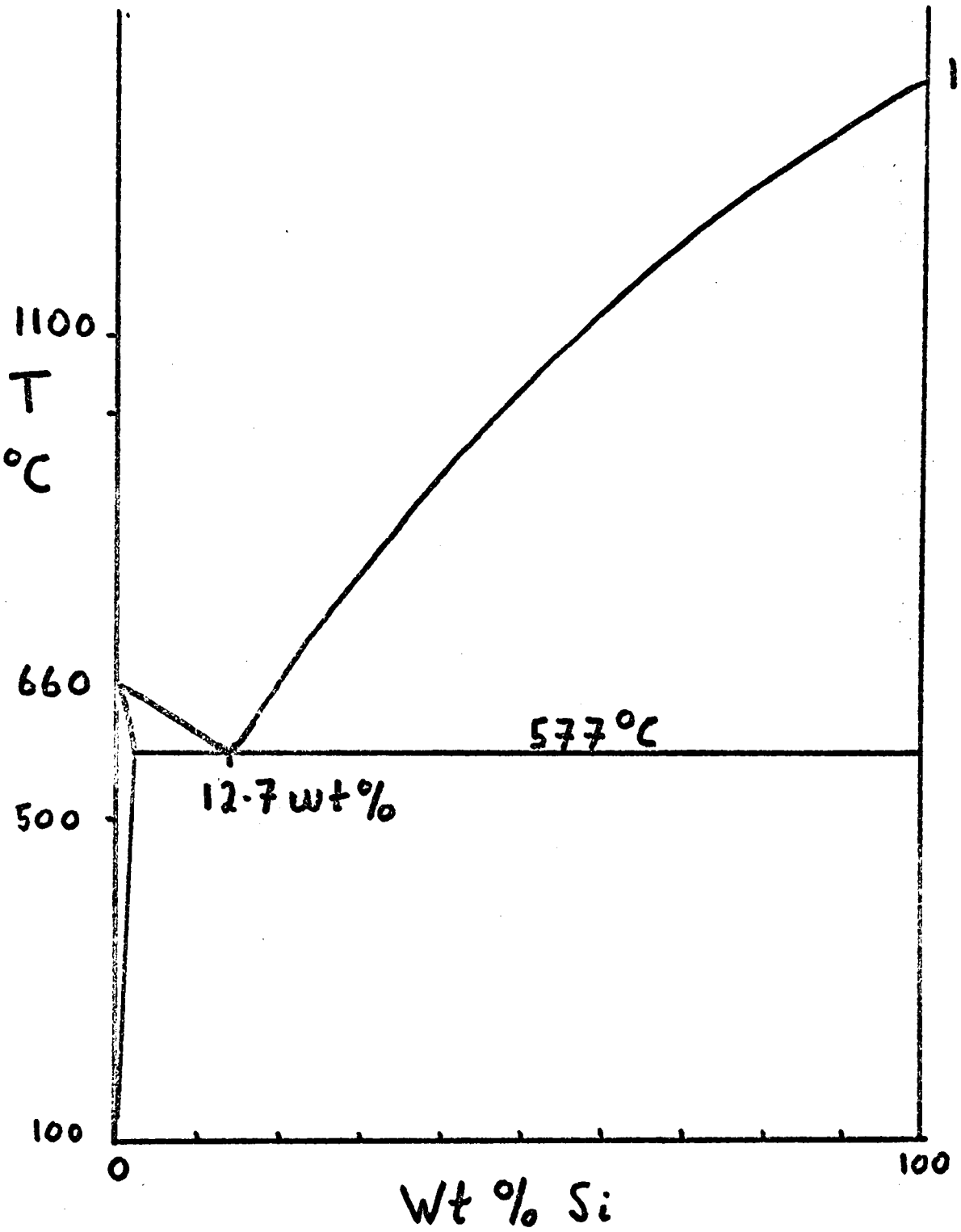

Fig 8

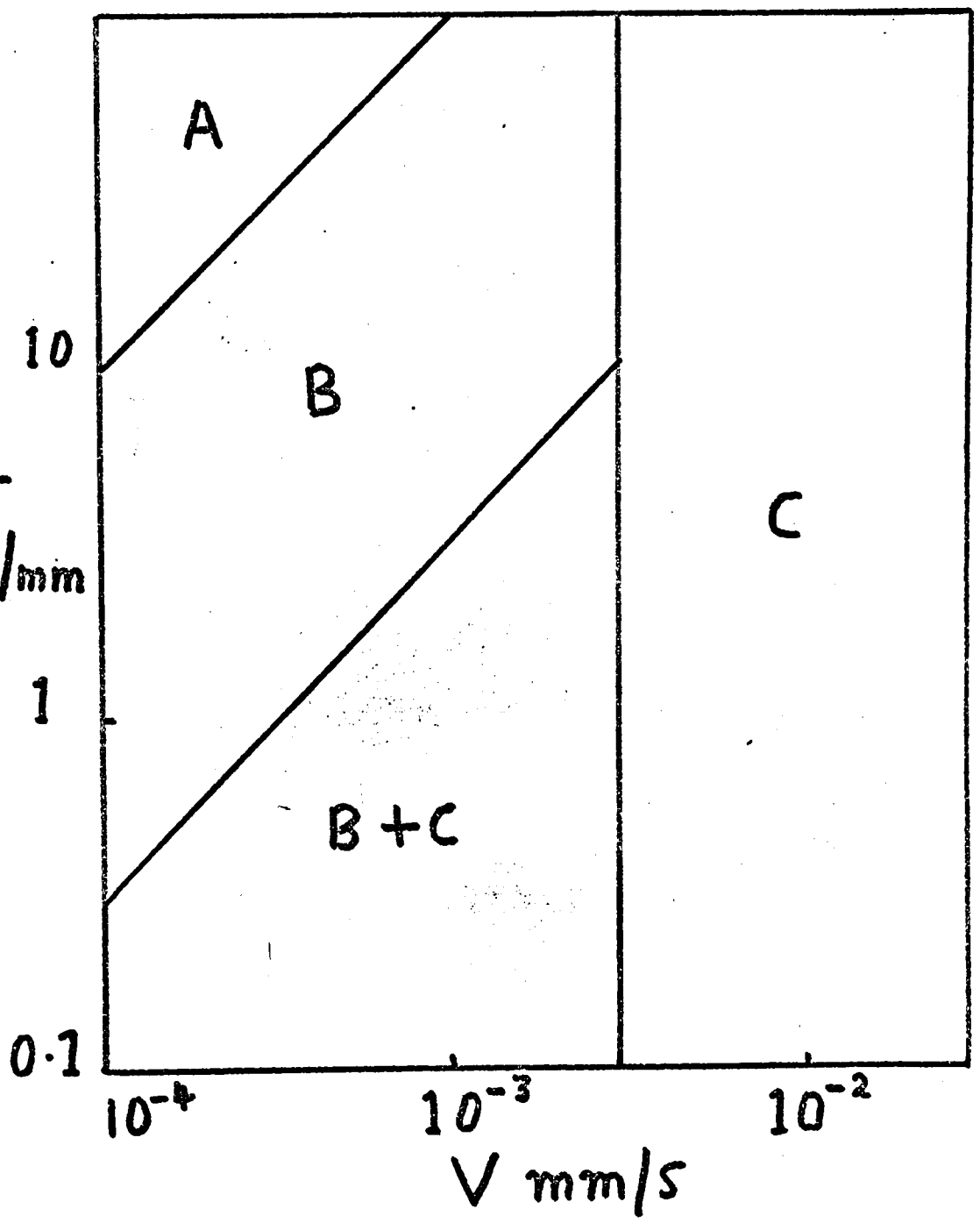

Fig 9

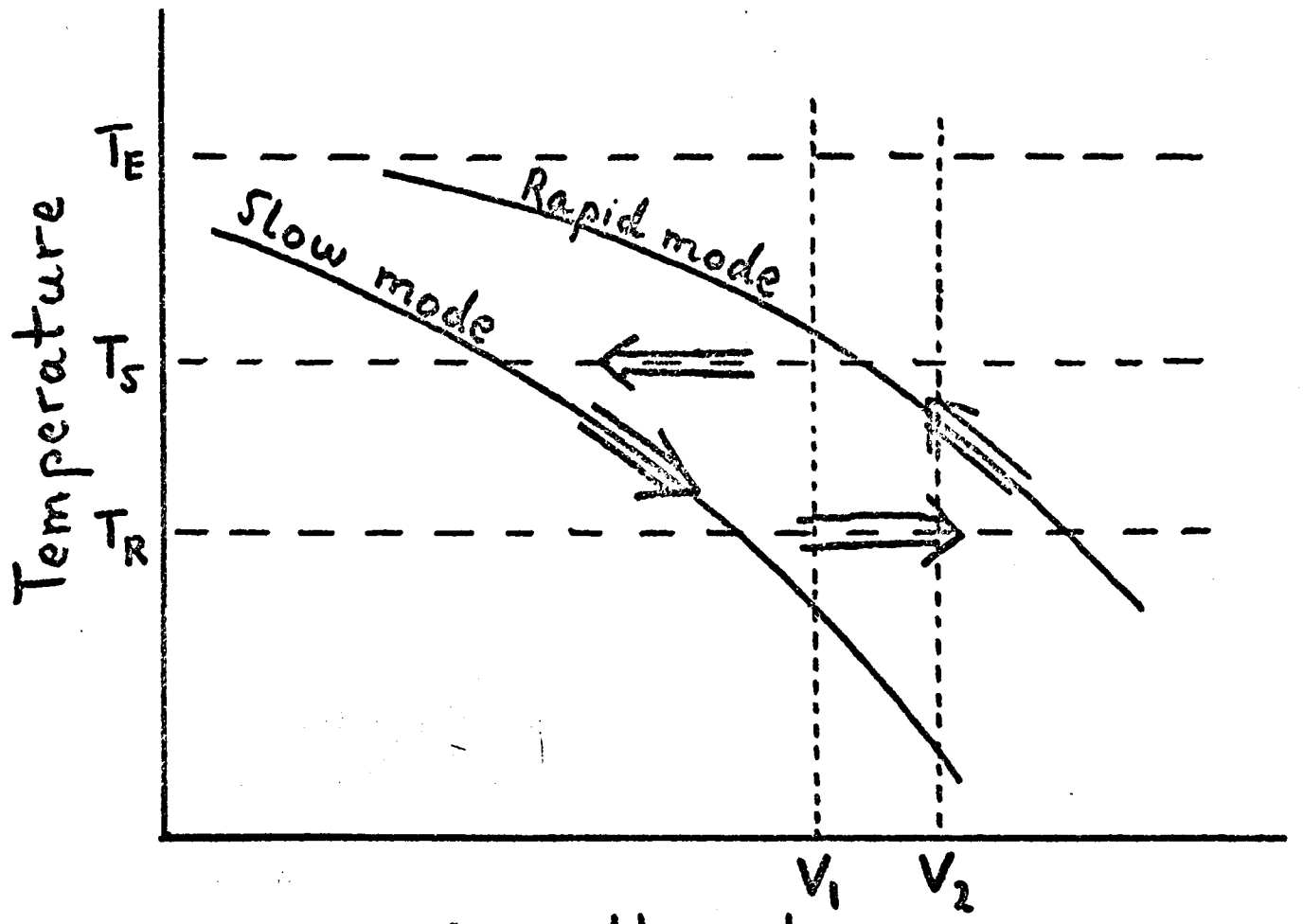

IV Introduction to the experimental work

From the literature survey it can be seen that the solidification of aluminium-silicon eutectics is still not fully understood, and a number of points of contention emerge:

a) It is not clear whether the growth of silicon is dependent on twins, or whether their presence is incidental. In particular there is disagreement as to whether or not the fibrous eutectic is heavily twinned.

b) The orientation of the fibrous eutectic silicon has not been determined directly.

c) A large number of elements are claimed to modify the eutectic. It is not clear whether the effects of all these elements on the eutectic morphology, scale of dispersion and growth undercooling are the same.

d) No direct measurements have been made of growth undercooling as a function of growth rate.

e) It is not clear whether or not primary silicon nucleates the eutectic.

In previous work done on this system by the author and presented as a part II thesis, samples of unmodified alloy were directionally solidified over a range of rates and with varying silicon concentrations in order to determine conditions for coupled growth at those rates, and find out over what range of rates the eutectic morphology changed from flaky to fibrous. This transition was characterised, using one temperature gradient, by optical and scanning electron microscopy. The scanning pictures obtained were rather unclear, so it was decided to reasses the transition using some clearer scanning electron micrographs, and to characterise the transition at a higher temperature gradient in order to find out whether the growth

velocities over which the transition occurred depended on applied temperature gradient.

In order to find out whether twins were present in the fibrous silicon, the extracted silicon phase was examined using transmission electron microscopy.

Measurements were made of undercooling against growth rate using samples directionally frozen at rates near to the flake-fibre transition rate.

To compare the effects of different modifying elements, ingots of pure alloy were doped with various impurities and thermally analysed after which the microstructures were examined using optical and scanning electron microscopy.

A hot stage was designed and constructed in which experiments using eutectic droplets melted onto a silicon single crystal substrate were carried out:

a) Measurements were made of undercoolings for nucleation of eutectic on silicon.

b) Growth layers formed by cooling modified and unmodified droplets at various rates from above the eutectic temperature on the substrate were compared.

c) The principle of temperature gradient zone melting was used to compare the migration rates of modified and unmodified eutectic droplets across a silicon substrate in an applied temperature gradient.

It was hoped from (b) and (c) to draw some conclusions about the kinetics of silicon growth from solution.

V Directional solidification experiments

1) Alloy preparation

The alloys used were prepared from high purity elements supplied with the following analyses:

A.I.A.G. Super Raffinal aluminium, Si 1 p.p.m., Fe 2.2 p.p.m. Cu 1 p.p.m.

J.M. Czochralski silicon - Al 1 p.p.m., Mg 1 p.p.m.

Accurately weighed amounts of aluminium and silicon were melted in an alumina crucible, using radio frequency induction heating, to produce alloys of eutectic and hypereutectic composition. Melting was carried out under argon at a pressure of about half an atmosphere and the melts were homogenised by maintaining the alloys at about 1000°C for approximately one hour.

2) Sample preparation

For these experiments it was necessary to fill recrystallised alumina tubes, sealed at one end, with alloy. This was acheived using the apparatus illustrated in fig (10). An alumina crucible containing the alloy was placed in a stainless steel rig which held a number of tubes vertically so that their open ends rested on the surface of the alloy. The rig was placed in a silica tube in a resistance furnace. The tube was evacuated and the alloy melted, after which the vacuum was broken so that air pressure forced molten alloy up the alumina tubes, which were then removed from the rig and allowed to cool.

In order to measure undercoolings, it was necessary to have a thermocouple sheath surrounded by eutectic alloy inside the recrystallised alumina tube. The sheath used was a fine, thin walled alumina tube of dimensions 1 mm o.d. and 0.6 mm i.d. Some of this size tubing was cut to the same lengths as the alumina tube

which was to be loaded. The sheath was sealed at both ends in an oxy-coal gas flame and inserted into the alumina tube which was loaded with alloy as described above. After removal from the rig, the loaded tube was allowed to cool and then a length of about 10 mm was cut from its base to reveal the open end of the thermocouple sheath.

3) Directional solidification apparatus

Once loaded into alumina tubes, alloy samples were directionally solidified using the apparatus illustrated in fig (11). This consisted of a jacket through which water flowed to keep the apparatus cool. Inside this, a column of water could be maintained at a given level by a constant head apparatus. The water inside the jacket was shielded from radiation from the furnace by a copper nose cone, through a hole in which the sample could freely pass. Alternatively the constant head could be dispensed with and the nose cone replaced by a copper toroid in which the specimen tube had a sliding fit. The bottom of the water jacket was sealed by a P.T.F.E. plug, through which a tube with a screw thread on its outside passed. The sample tube was held in the end of a rod which was a tight fit inside the threaded tube. A greased 'O' ring acted as a water seal. The sample could be withdrawn from the furnace by attaching an electric motor to the bottom of the threaded tube, via a flexible drive, to give a range of growth rates between 1.2×10^{-2} mm/s and 9.6 mm/s.

4) Temperature gradient determination

It is well known that the specimen temperature gradient may differ markedly from the furnace temperature gradient, depending on the magnitude of the applied gradient. Thus at low gradients the efficiency of heat input from the furnace and heat loss to the colder environment is lower, so that the position of the solid/

liquid interface in the sample is dictated partly by the relative lengths of material inside and outside the furnace, and by the cross-sectional area and conductivity of the specimen. At high gradients the efficiency of heat input and heat loss is much greater, and the sample temperature gradient is less dependent on the properties of the sample.

In order to measure the gradient, a 2 mm bore alumina tube was used, with the alloy replaced by a platinum/platinum-rhodium thermocouple made up from 0.3 mm diameter wire. The measuring junction was located about half way up the tube with wire continuing to the top, so that the thermal conductivity above and below the junction was the same. The tube was inserted in the furnace and withdrawn at 10 mm intervals, temperature being recorded at each interval. A temperature/distance plot was then made, and the gradient at the eutectic temperature taken as the specimen temperature [illegible] gradient for a given furnace temperature.

5) Apparatus for undercooling measurements.

Since, for this experiment it was necessary to record the output from a thermocouple located in a sample tube being withdrawn from a furnace, it was necessary to use an apparatus in which the tube was not rotated as it was withdrawn. Such an apparatus was constructed by Sharp and a detailed description is given in his D.Phil. thesis (56). The arrangement was similar to that illustrated in fig (11), differing in the way the sample was mounted inside the threaded tube - see fig (12)-. The sample tube was mounted on a hollow steel tube, so that the thermocouple wires could be taken out from the base of the sample to the end of the tube. This steel tube fitted inside an outer tube which was clamped to the threaded brass rod, while the inner tube was

clamped to a base plate. Thus the outer tube and threaded rod were free to rotate without the sample doing so, being driven via a worm reduction gear.

The thermocouple was made from platinum/platinum 13% rhodium wire of diameter 0.15 mm. Inside the sheath one wire was insulated by fine alumina tubing while outside both wires were insulated. In order to obtain as sharp an arrest as possible, a very fine thermocouple junction was needed, and in order to acheive this the wires were joined by a butt welding technique originally due to Jordan (6). In this method the wires are pressed together, end to end, inside a fine alumina insulator. The junction is then heated in an oxy-coal gas flame until a slight give indicates that the junction is molten. The weld is then allowed to cool and the alumina tube broken away from the thermocouple. Thus a weld about 0.5 mm long could be obtained. The thermocouple cold junctions were inserted into two test tubes filled with alcohol to improve thermal contact between the junctions and the ice/water mix in which the tubes were immersed. The junctions were a soldered join between the thermocouples and copper wire. Output from the thermocouple was fed into a Telsec chart recorder, some voltage being backed off using a Cambridge potentiometer so that a 0 to 0.5 mV scale could be used to record the arrests. The accuracy of the recorder was about 1/50 of the full scale deflection, corresponding to 0.1°C, and that of the backing off potentiometer was similarly about 0.01 mV or 0.1°C.

6) Microexamination techniques

After solidification, the alloy rods were broken out from their alumina tube containers and samples taken for microexamination. Longditudinal and transverse sections were cut from the middle of directionally frozen specimens, and for optical microscopy these

sections were mounted in transparent resin and ground on silicon carbide papers down to 600 grade. These specimens were polished with diamond paste on selvyt covered lapping wheels using successively 6-3 micron, 3-1μ and 1-$\frac{1}{4}\mu$ paste. It was found that 2-3 minutes polishing on each wheel, using moderate pressure, gave the best results. The specimens were washed in methanol and dried with compressed air to avoid drying marks.

Metal polish or alumina powder in distilled water were used to polish some specimens, but it was found that these methods did not generally produce a good finish on the aluminium phase.

Optical microscopy was carried out on specimens in the as-polished condition since, because of the difference in hardness between the two phases, the silicon particles stood proud of the aluminium matrix after polishing and showed up clearly under the optical microscope.

For scanning electron microscopy, specimens were prepared by a method due to Day (2). Samples were polished as for optical microscopy, removed from their plastic mounts and then deep etched in very dilute solutions (1-2%) of hydrochloric acid in water. This treatment etched away the aluminium matrix, leaving the silicon phase intact so that a three-dimensional view of the silicon morphology was obtained. Rapid etching resulted in the hydrogen produced by the chemical reaction forming bubbles, which tended to break up the very fine and brittle silicon particles, so very slow attack was needed, especially for specimens containing fibrous silicon. This was achieved by adding a little concentrated acid to the etching solution every few hours. Etching was continued until the surface of the specimen appeared dark, as this indicated that only the silicon phase could be seen.

Specimens were washed by immersing them very carefully in

distilled water followed by ethanol. They were dried by gentle warming to evaporate the ethanol and mounted on aluminium stubs using a conducting glue.

Transmission electron microscopy required that the silicon phase was extracted completely, and this was done by etching away all the aluminium matrix with dilute hydrochloric acid. A fine powder of silicon particles remained which was washed with distilled water followed by ethanol and dried by gentle warming. For examination under the electron microscope the powder was sprinkled onto a copper grid made sticky by a solution of sellotape glue in chloroform. The silicon stuck to individual strands of the grid, and particles projecting out from these strands could be examined.

7) Microscopy

The scale of dispersion of the fibrous silicon phase obtained in rapidly frozen or modified specimens lies near the limit of resolution of the optical microscope, and to obtain better resolution electron microscopy was employed.

The scanning electron microscope has the advantage of a much lower limit of resolution (about 200Å as compared with 2500Å for an optical instrument), although this was found to vary greatly, depending on the condition of the microscope. Its large depth of focus allowed the examination of silicon morphology in three dimensions using deep etched specimens. Contrast arises from variations in the number of secondary electrons produced at different points in the area scanned by the fine electron probe. The secondaries are attracted to a collector by a high positive voltage, and the resulting output is converted into a varying potential which is used to modulate the brightness of a cathode ray tube scanning synchronously with the electron probe.

Variations in brightness are thus produced by variations in surface topography or chemical composition. In these specimens only one phase was present and contrast arose from variations in topography.

Compared with the scanner, the transmission electron microscope has a limit of resolution an order of magnitude lower but because a transmitted image rather than a stereoscopic reflected image is obtained, it is less suited to the study of three-dimensional aggregates. The specimen preparation technique described above breaks up the silicon so that what could be seen under the microscope was small pieces of the original aggregate randomly heaped together. Thus the transmission electron microscope is suitable for the examination of the shape, and if transparent, the internal structure and orientation of small sections of the silicon aggregate. However these orientations cannot be clearly related to the macroscopic orientation of silicon with respect to the growth direction, since the silicon network has been broken up.

It was expected that in silicon particles sufficiently thin to be transparent to 100 KV electrons, twin boundaries parallel or nearly parallel to the electron beam would show up as dark lines or closely spaced sets of fringes. Selected area diffraction patterns taken from the particles would show their orientation and hence the direction of the traces. If the twin crystals were very narrow, streaking of the diffraction spots perpendicular to the direction of the twin traces would be expected since it is known (57) that when a single crystal is very narrow in one dimension, the corresponding reciprocal lattice points are elongated into spikes in a direction normal to the plane of the plate. Fig (13) shows the Ewald reflecting

sphere construction for a crystal narrow in a direction normal to the direction of the electron beam. The length of the spike is 1/W, where w is the width of the crystal, so that the angular spread of intensity is λ/w, where λ is the wavelength of the electrons. For a crystal 10Å wide this angle is about 10^{-3} radians, while the Bragg angle for a low order reflection is about 10^{-2} radians. Thus a rather narrow twin crystal is necessary for streaking of diffraction spots to be observed.

A similar construction can be used to show the range of orientations of the crystal for which measurable reflection occurs. In this case, it is spikes parallel to the electron beam, depending on the thickness t of the crystal perpendicular to the beam which must be considered - fig (14)-. Then the range of orientations ϕ over which significant reflection occurs is $\frac{1/t}{g}$, where g is the reciprocal lattice vector for the given point $\sim$ 1/d where d is the interplanar spacing. Thus $\phi \sim d/t$. The silicon crystals examined here are about 2000Å thick, so an orientation range of 2×10^{-3} radians is permissible, and patterns will be observed over a range of orientations.

If two twin crystals are present in an area from which an S.A.D. pattern is taken, two sets of spots would be expected to be present on the pattern. Similarly for more than two crystals, so that if a number of twin crystals are present in the same area, a rather complex pattern of spots would be expected to be observed.

Specimens were examined using a 100 K.V. E.M.6. electron microscope, and in order that given crystals could be observed over a range of orientations, a stage which allowed tilt in one direction was employed.

8) The flake-fibre transition results

In previous work (32) alloys of eutectic or near eutectic composition had been grown over a range of rates between 0.1 mm/s and 1.2 mm/s under a temperature gradient of about 10°C/mm. From optical and scanning electron microscopy on samples taken from these specimens it was concluded that a rather sharp transition in structure took place over a range of rates between 0.2 and 0.4 mm/s. This transition was reassessed and in order to discover whether the transition was temperature gradient dependent, another set of alloys were grown with a furnace temperature of 1300°C (compared to 1000°C for the lower gradient specimens) giving a temperature gradient of about 22°C/mm at the interface.

Plates 1 to 8 are optical micrographs of specimens grown at 0.12, 0.24, 0.48 and 0.96 mm/s under temperature gradients of 10°C/mm (plates 1 to 4) and 22°C/mm (plates 5 to 8). Plates 9 to 12 are scanning electron micrographs of specimens grown at the above rates under a gradient of 22°C/mm and plates 13 to 16 are transmission electron micrographs of specimens grown at 0.24, 0.48, 0.96 and 1.2 mm/s under a gradient of 10°C/mm.

From the optical micrographs it can be seen that at G~22°C/mm the transition from the coarse flake morphology starts between V = 0.12 and V = 0.24 mm/s, while at G ~10°C/mm the transition starts between V = 0.24 and V = 0.48 mm/s. With increasing velocity the dispersion becomes finer and less easily resolved.

The progress of the transition at G ~22°C/mm is illustrated in plates 9-12 scanning electron micrographs. These micrographs confirm that there is a transition from a coarse flake morphology between V = 0.12 and V = 0.24 mm/s. It can be seen that at

V = 0.24 mm/s the silicon morphology is by no means exclusively fibrous but rather consists of a mixture of flakes and fibres. At higher growth rates the proportion of fibrous silicon appears to increase, while the scale of dispersion becomes finer. A corresponding progression was observed at higher growth rates in specimens grown at $G \sim 10^{\circ}C/mm$.

Plates 13-16 are transmission electron micrographs illustrating the transition at $G \sim 10^{\circ}C/mm$, and once again a transition from flake to mixed flake and fibre to finer fibres can be observed.

From these results it can be seen that there is a temperature gradient dependence in the breakdown of the coarse flake morphology, so an additional line can be drawn on fig (8) to represent the growth velocity and temperature gradient dependence of this transition giving fig (15). Thus increasing temperature gradient appears to favour the fibrous relative to the flake morphology.

9) Observations on twins by transmission electron microscopy

Using the tilting stage a search was made for twin traces in a number of specimens covering both the flake-like and fibrous morphologies. Generally the silicon flakes were too thick to be transparent to electrons, but in those that were transparent, traces were quite often observed. When a single crystal could be picked out for selected area diffraction, the resulting pattern usually showed that the traces lay along a $\langle 110 \rangle$ direction. When the S.A.D. aperture covered more than one twin, very complicated diffraction patterns were obtained, - plates 17, 18 - showing a number of crystals sharing a common $\langle 110 \rangle$ direction. On one crystal the twin axis was $\langle \bar{2}11 \rangle$ - plates 19, 20 - and this diffraction pattern shows some streaking perpendicular to the

direction of the traces. The trace spacing is about 200Å or larger, so it seems that since streaking occurs, the traces must represent bands of very fine (~30Å) twins. Morphologically this crystal appears primarily plate-like, and the presence of traces along the axes of the fine 'fingers' growing out from the plate cannot be taken as evidence that fibrous silicon particles are generally twinned. Indeed examination of a substantial number of unambiguously fibrous silicon particles failed to reveal any definite twin traces. The fibre axis usually lay along ⟨110⟩ as in the fibre with its corresponding diffraction pattern shown in plates 21, 22. It is possible that the fibres are twinned on the two {111} planes which contain the common ⟨110⟩ axis, in which case traces would not be expected to be visible, but in view of the simplicity of the diffraction patterns obtained from the fibres, it is also possible that the fibrous form of silicon is not heavily twinned and that individual fibres are monocrystalline.

10) Undercooling measurements

The freezing temperature of pure aluminium, since it is a non-faceting material, does not vary much with growth velocity, so the thermocouple and general experimental set-up were tested using a specimen of pure aluminium and measuring the freezing temperatures at various growth velocities. A table of growth rate against freezing temperature is given below:

Pure Aluminium:	Growth rate mm/s	Arrest temperature
	0.1	659.5°C
	0.2	661.0°C
	0.3	660.2°C

Thus the measured freezing temperatures were within about 1°C of the melting point of pure aluminium, so it was concluded that the apparatus was sufficiently satisfactory to measure the

relatively large undercoolings expected for the aluminium-silicon eutectic at these growth rates, and that the measured arrest temperatures were accurate to about 1°C.

A typical eutectic arrest of the type from which freezing temperature measurements were taken is shown in fig 16. The freezing temperature was taken to be the point at which straight lines drawn along the traces in the liquid and solid regions met. The temperature gradient as measured from the chart recordings was about 8°C/mm using a furnace temperature of 1100°C. The gradient is lower for a given furnace temperature than that observed previously for directionally frozen specimens, because here the sample is being pulled into a water cooled copper toroid rather than into water. Continual difficulty was experienced due to the tendency of the eutectic to expand and crack the thermocouple sheath, often shorting the thermocouple and thus restricting the number of satisfactory undercooling measurements obtained. At high pulling rates, arrests became rather indistinct, the slope of the mV/time trace changing over an increasingly wide range about the arrest temperature. This was probably due to build up of latent heat at the interface at high pulling rates.

A table of growth rate V against undercooling ΔT is given below:

V mm/s	ΔT°C
0.01	4.6, 3
0.03	9.0, 5.5
0.07	11.6
0.1	12.5, 11.0
0.15	14.4
0.2	18.0, 15.5
0.3	16.0
0.4	16.8
0.6	21.0

ΔT is plotted against log V in fig 17 and against $\sqrt{V}$ in fig 18.

The $\log_e V$ vs ΔT plot yields a relationship $\Delta T = 4 \log_e V - 6$ (V in μm/s) while the ΔT vs $\sqrt{V}$ plot gives $\Delta T = 1.2\sqrt{V}$. The large scatter in the results makes a choice between the two relationships difficult. It can be seen that the parabolic relationship does not fit the high velocity results very satisfactorily, and extrapolation of the relationship to a growth rate of 10 mm/s would give an improbably high undercooling of over 100°C. However it is possible that the undercooling of the fibrous silicon is less sensitive to growth rate, so that another relationship may take over at higher rates. In this connection it was unfortunate that limitations of the experimental technique precluded undercooling measurements at growth rates where the silicon morphology was fibrous.

The exponential relationship fits the high velocity results more satisfactorily and extrapolation to a rate of 10 mm/s gives an undercooling of 30°C, which is quite plausible. However extrapolation to lower growth rates gives zero undercooling at a rate of 5 μm/s, so another relationship must take over at these rates, corresponding to the transition to $\langle 100 \rangle$ eutectic silicon - see fig (15) -. Thus from the experimental results it is not clear which of the above relationships is correct.

Fig 10

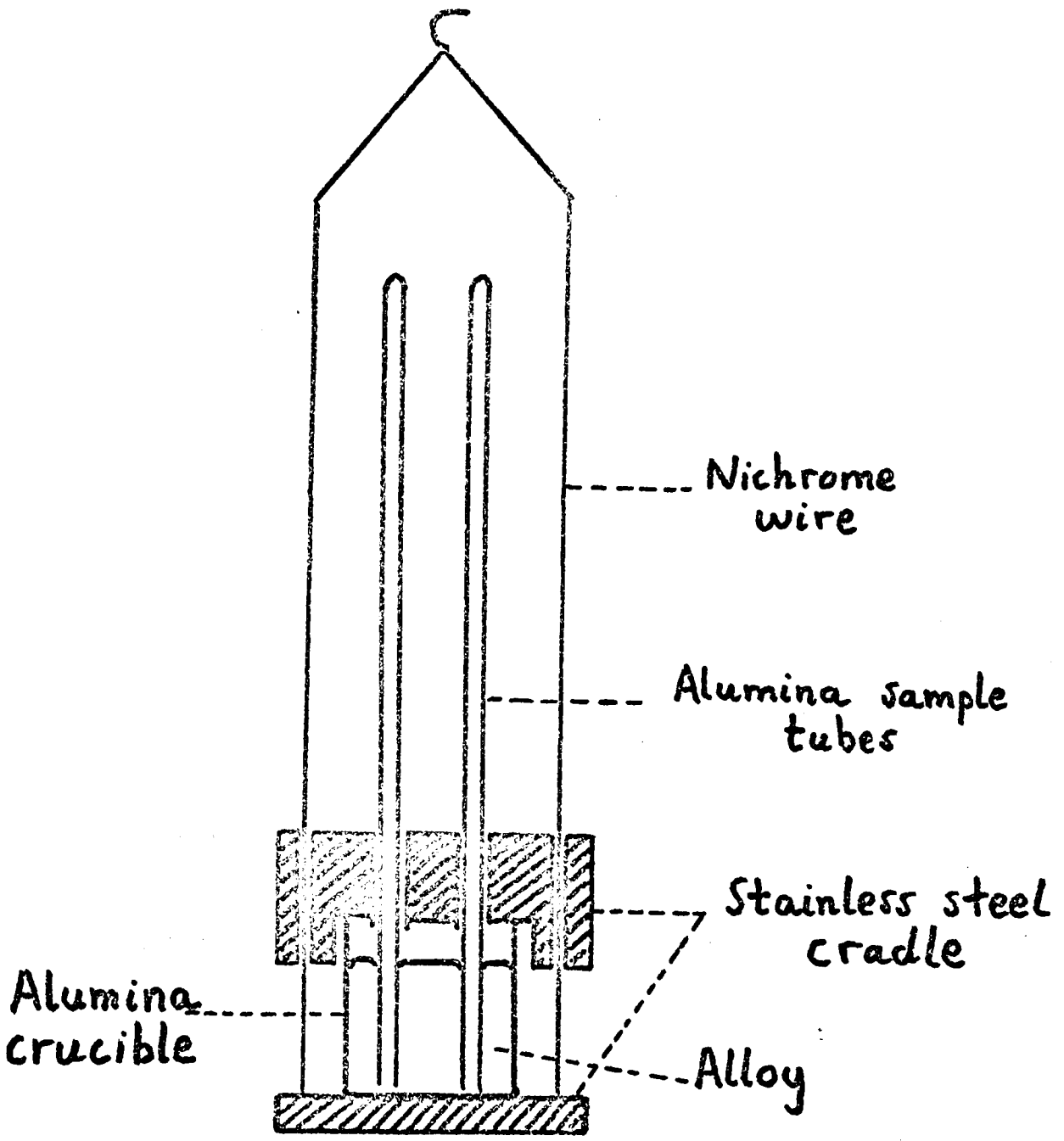

Rig for loading sample tubes

Fig 11

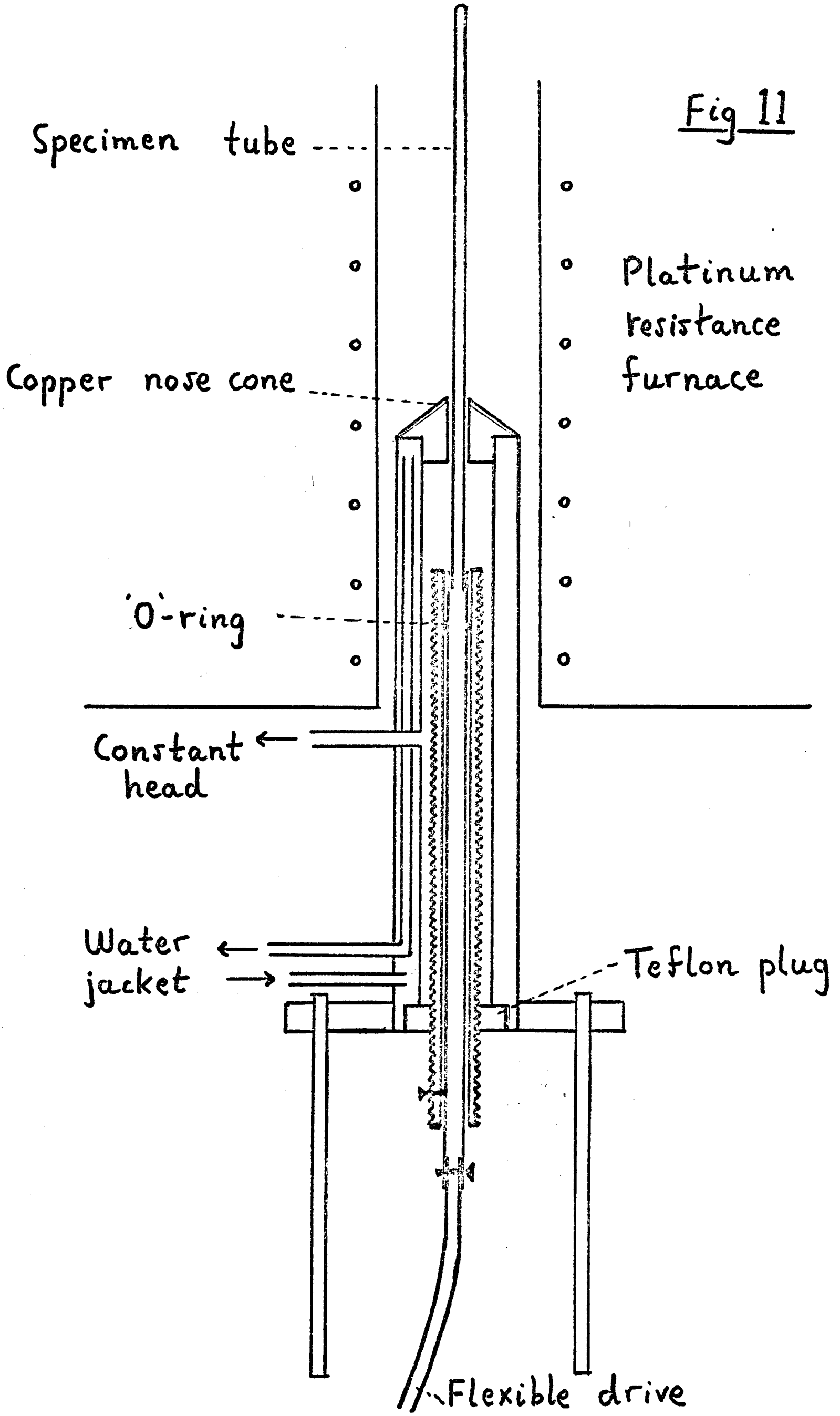
Specimen tube
Copper nose cone
'O'-ring
Constant head
Water jacket
Platinum resistance furnace
Teflon plug
Flexible drive

Fig 12

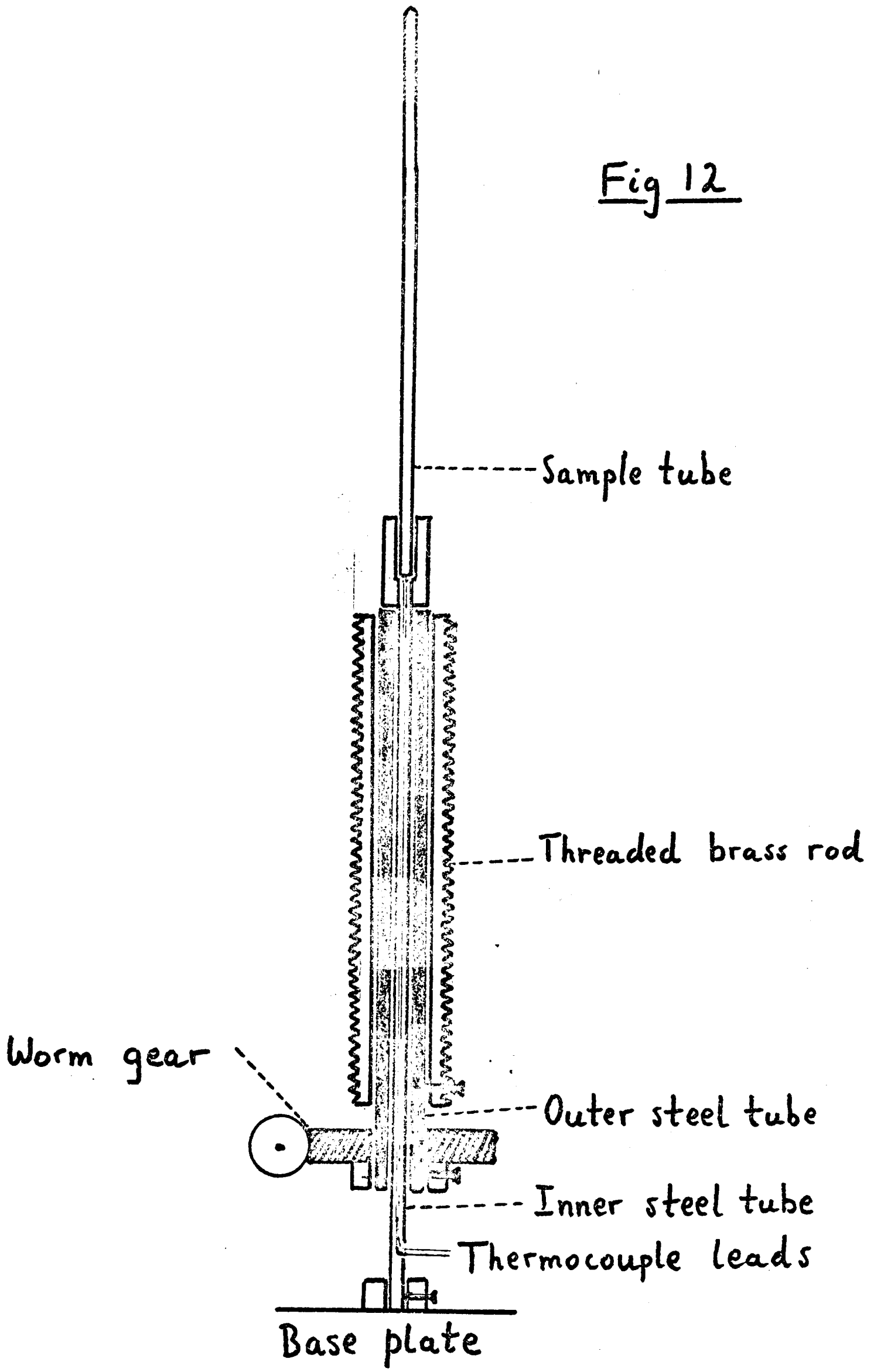
Sample tube
Threaded brass rod
Worm gear
Outer steel tube
Inner steel tube
Thermocouple leads
Base plate

Fig 13

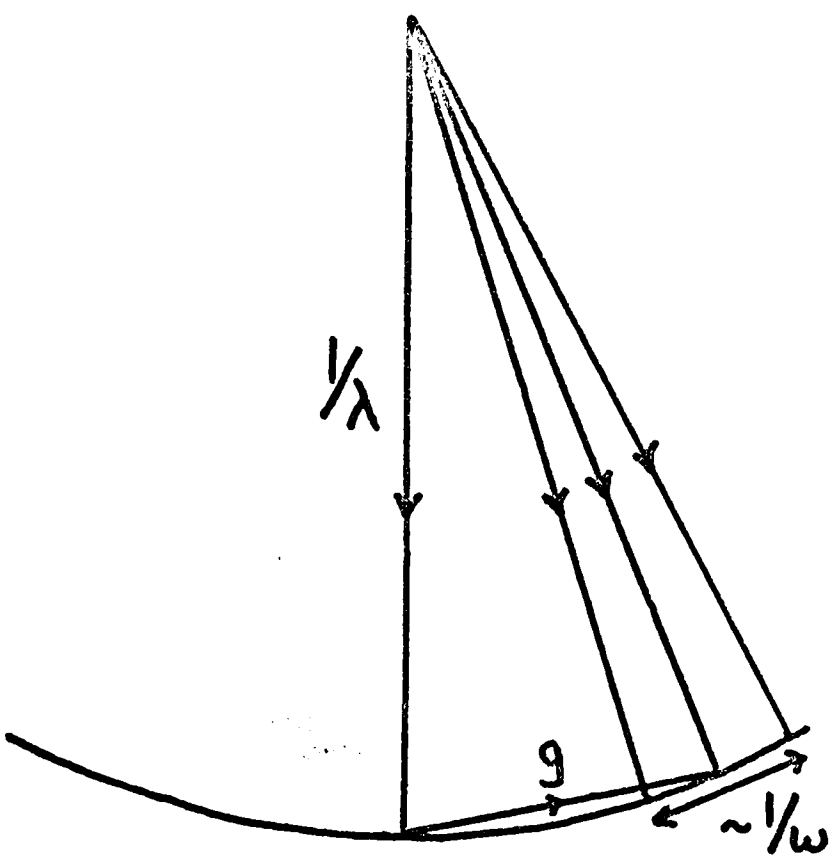

Fig 14

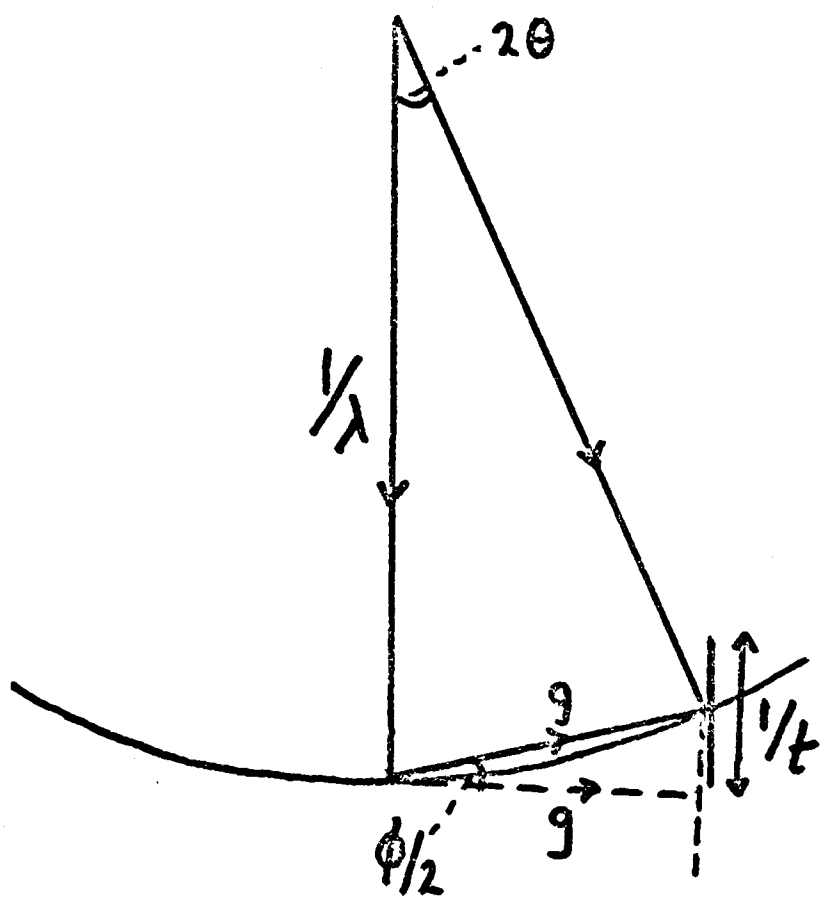

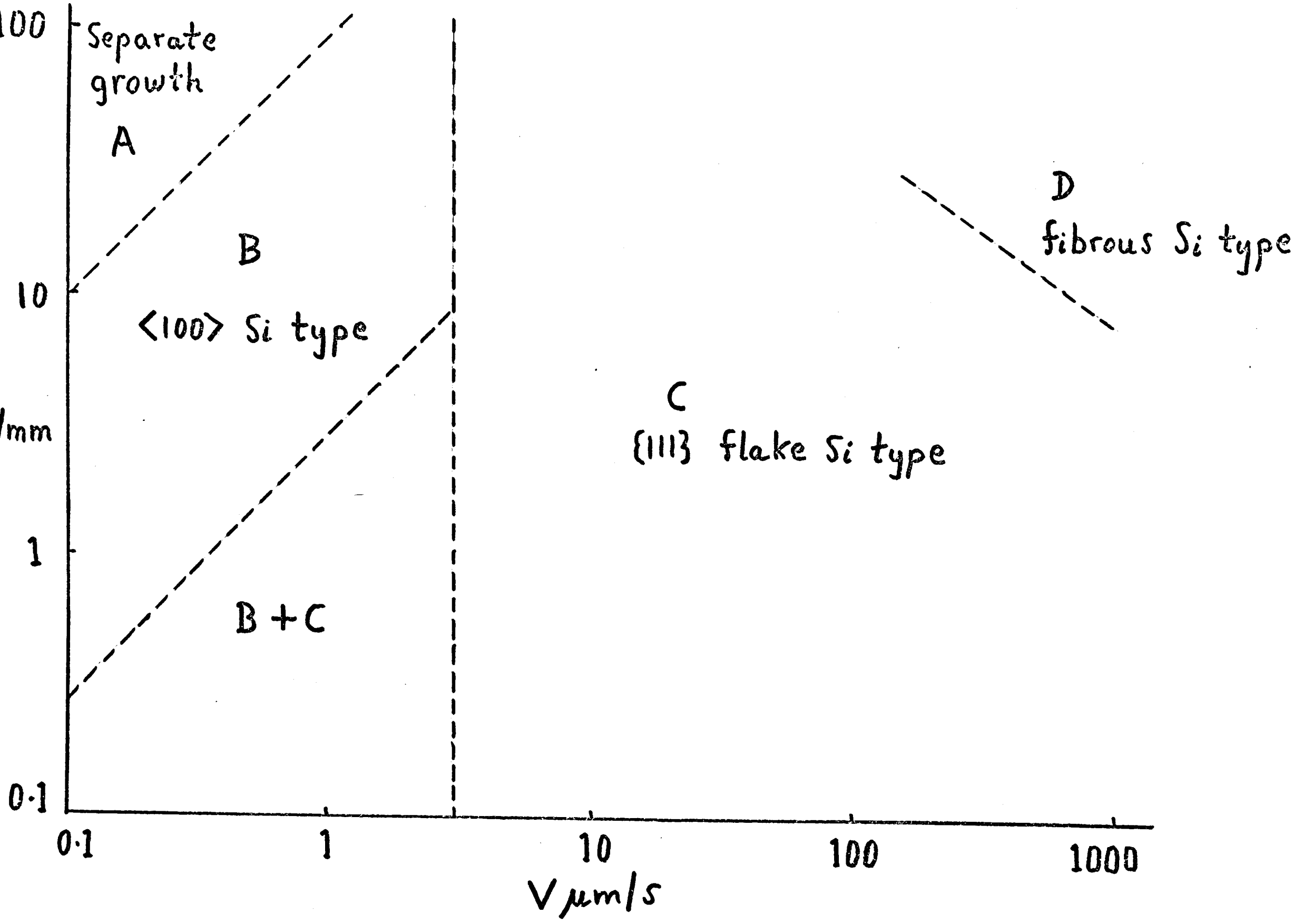
100
Separate growth
A
B
10
<100> Si type
G °C/mm
1
B + C
0·1
0·1
1
10
100
1000
V μm/s
D
fibrous Si type
C
{111} flake Si type

Fig 15

Fig 16.

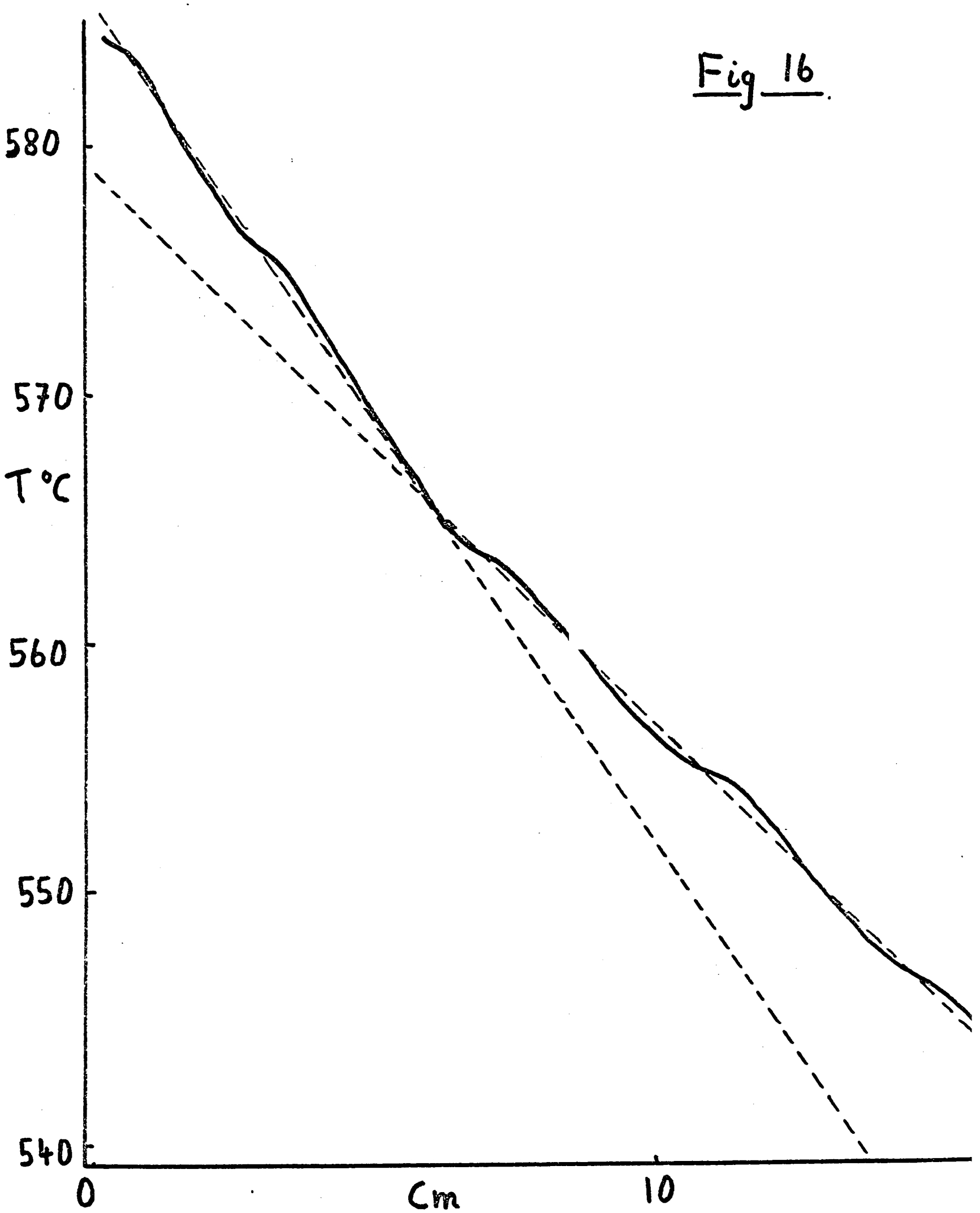

Fig 17

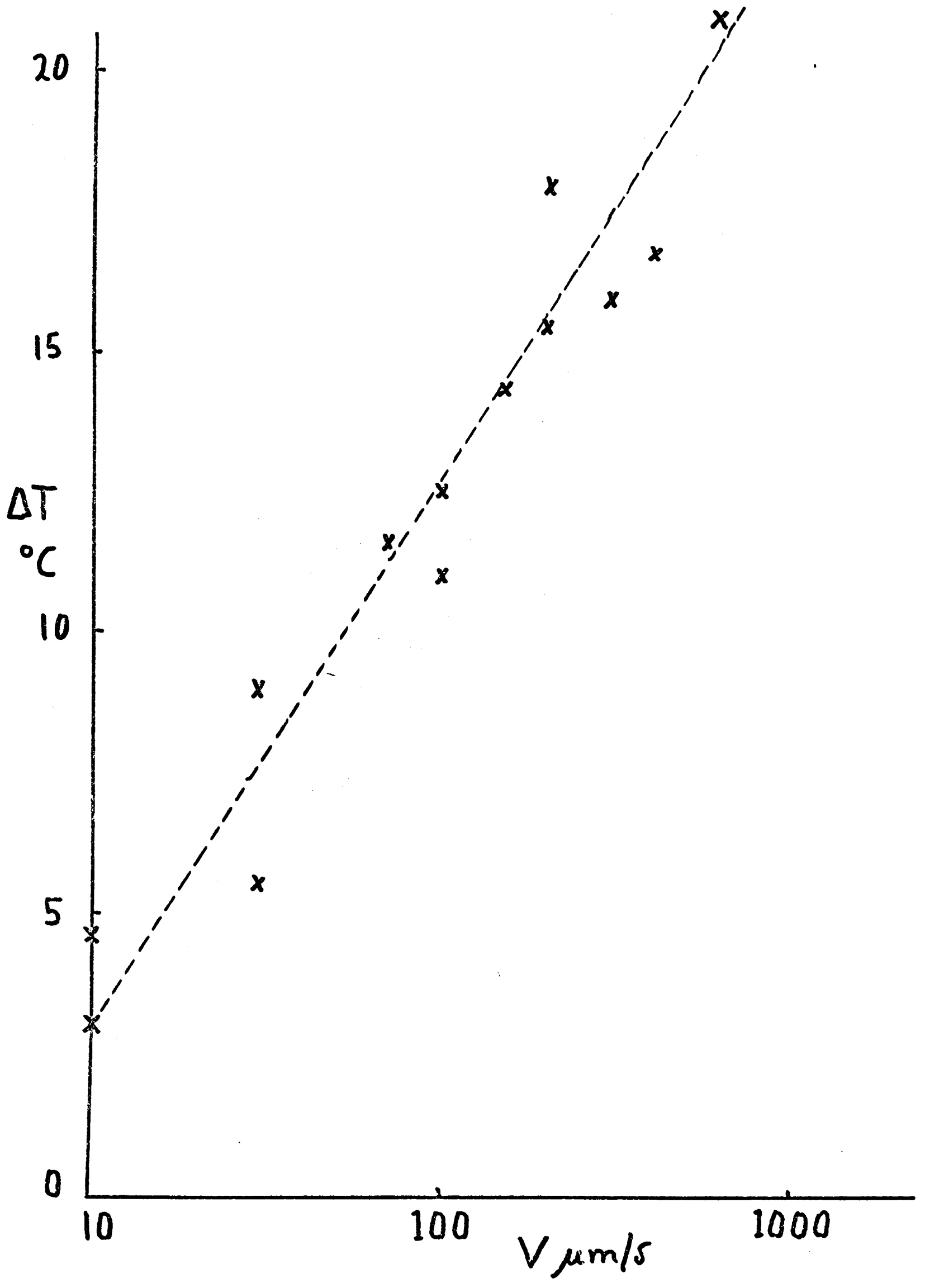

Fig 18

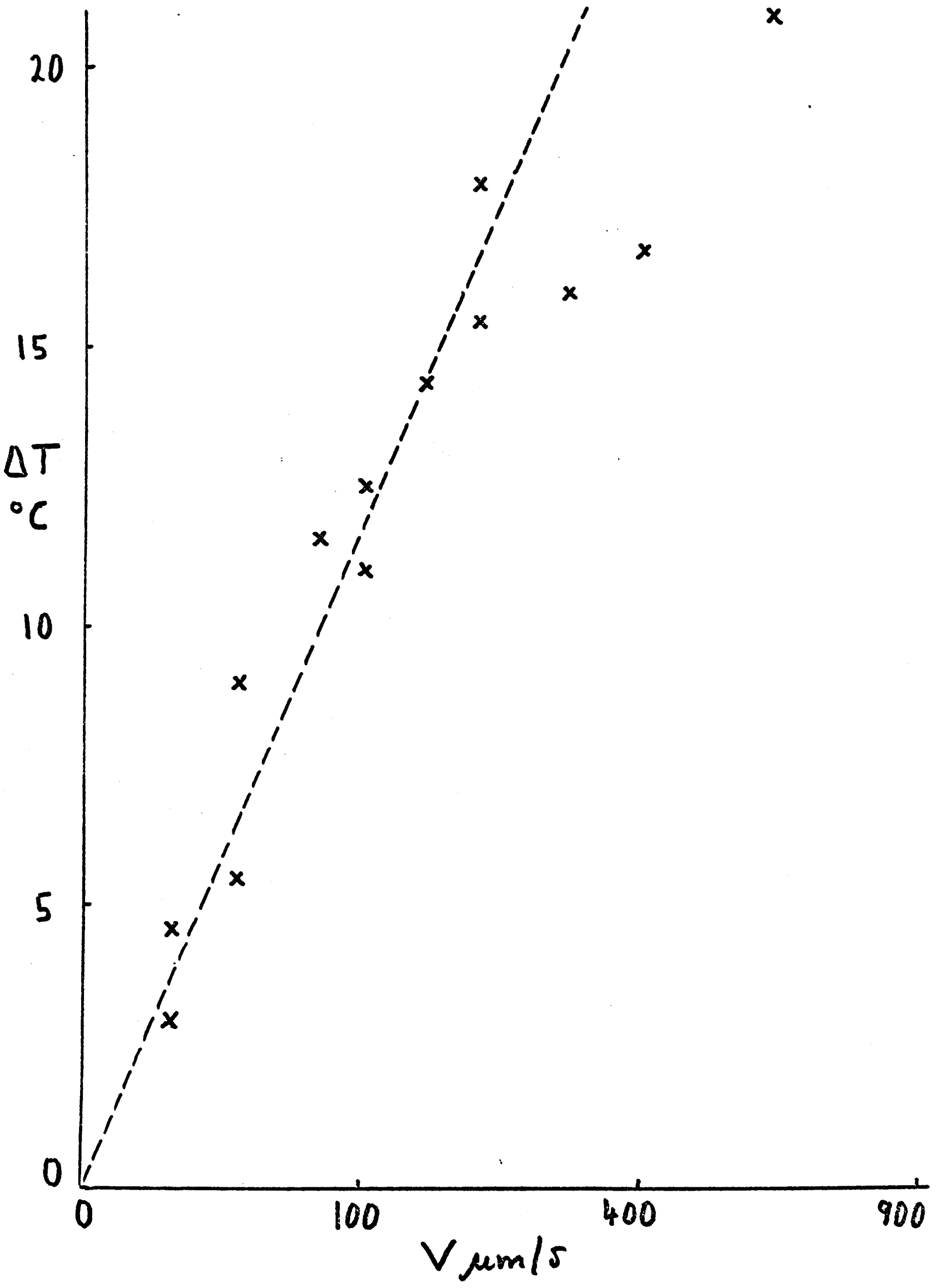

Plate 1 V = 0.12 mm/s, G = 10°C/mm X 1000

Plate 2 V = 0.24 mm/s, G = 10°C/mm X 1000

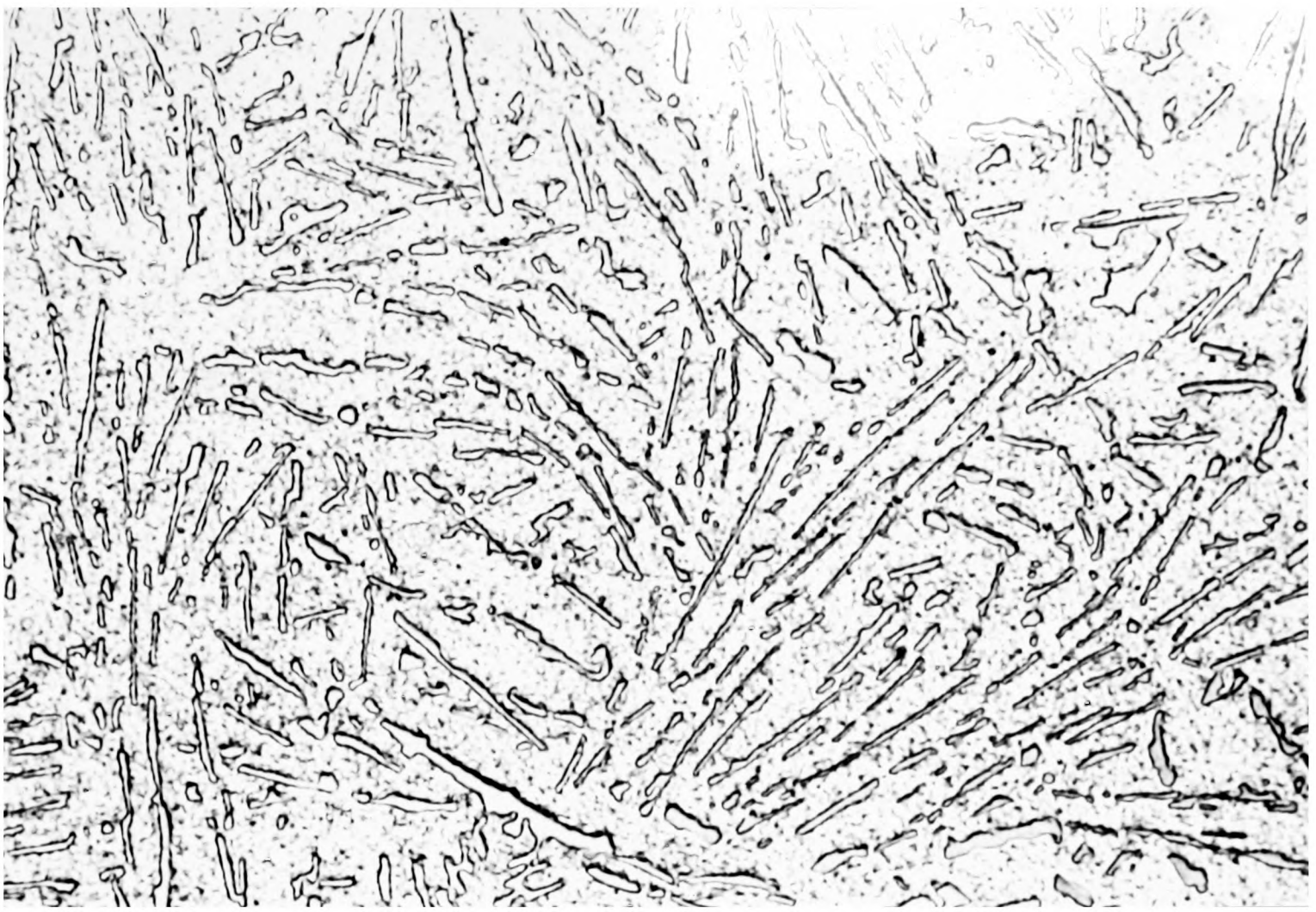

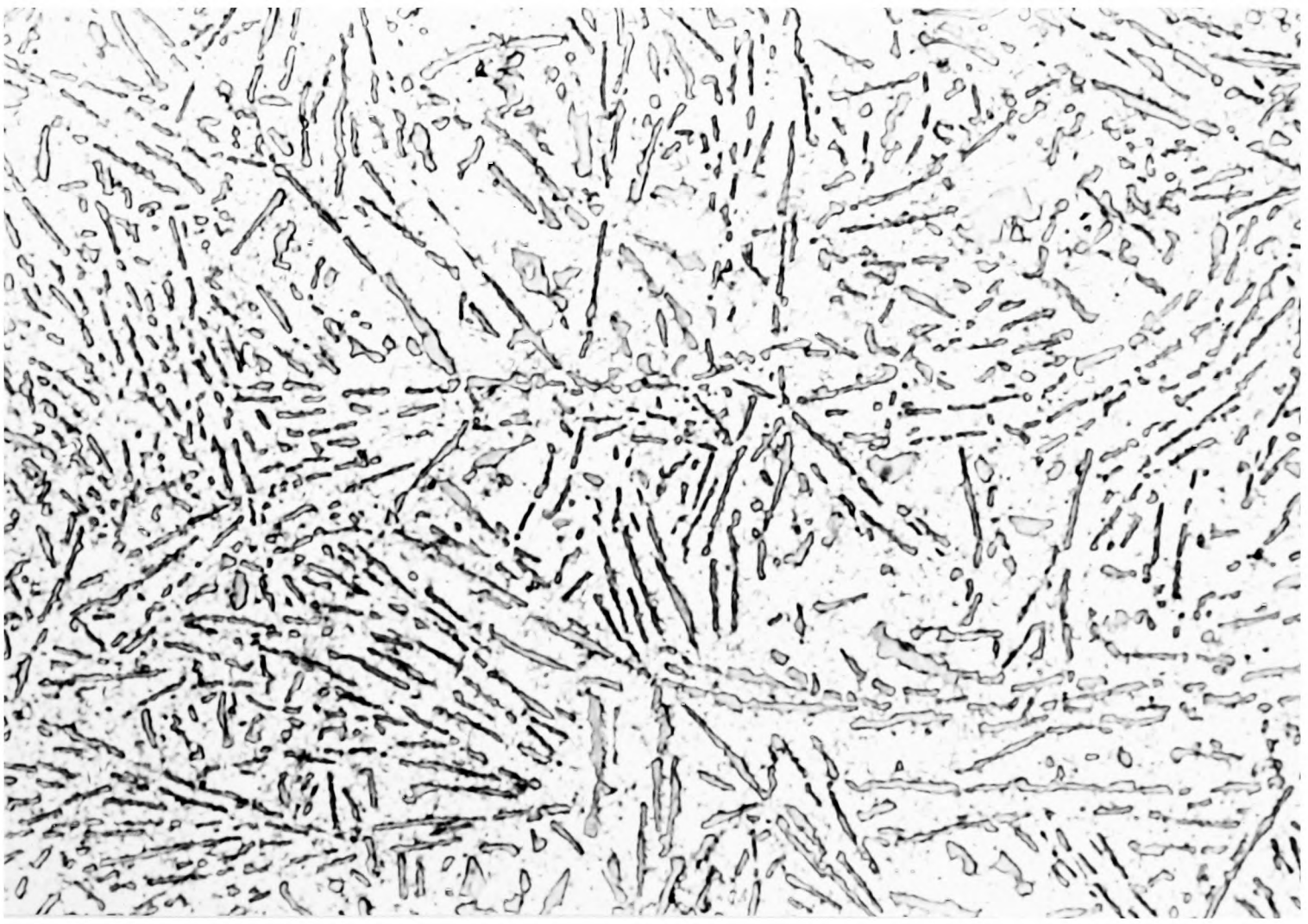

Plate 3 V = 0.48 mm/s, G = 10°C/mm X 1000

Plate 4 V = 0.96 mm/s, G = 10°C/mm X 1000

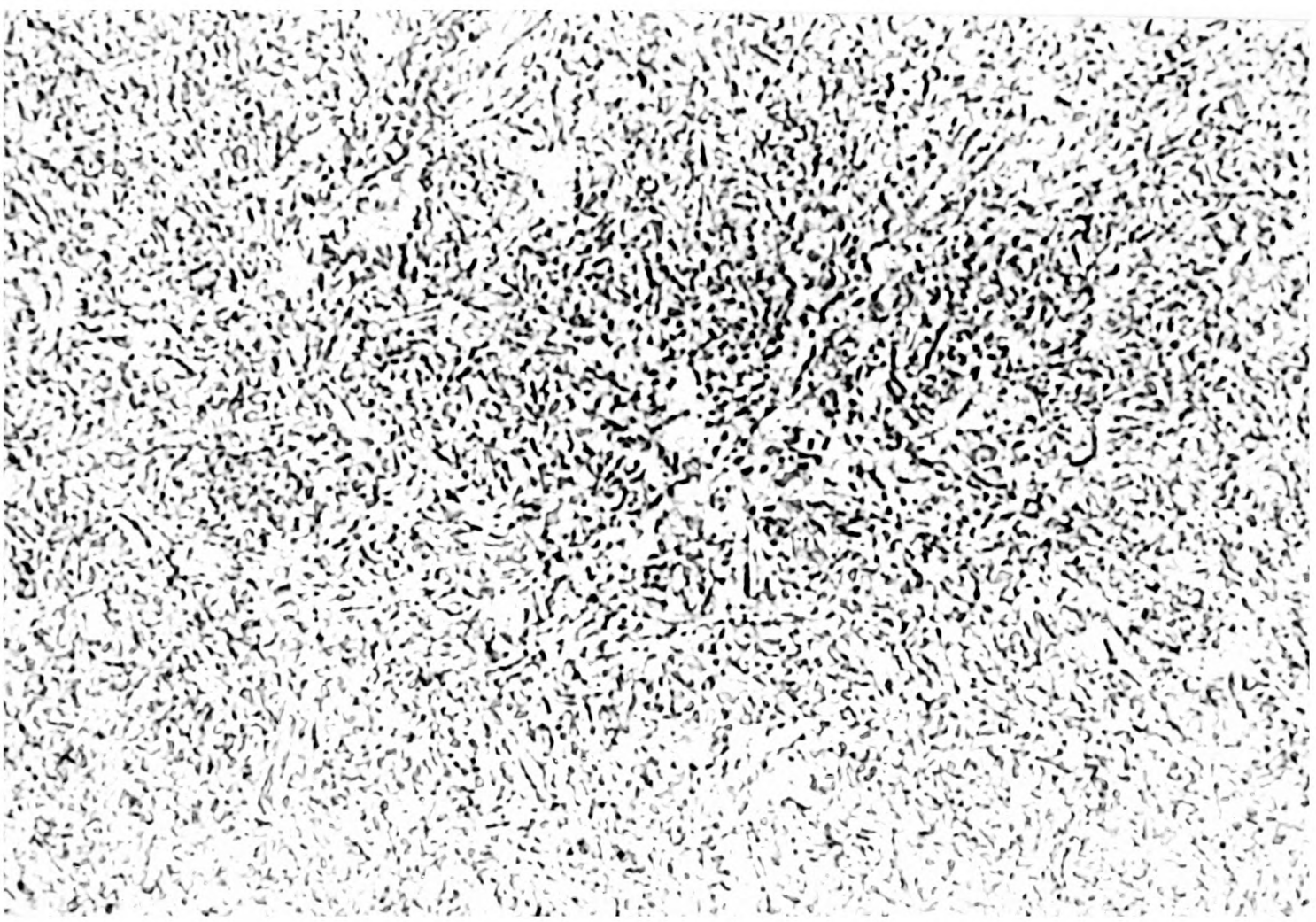

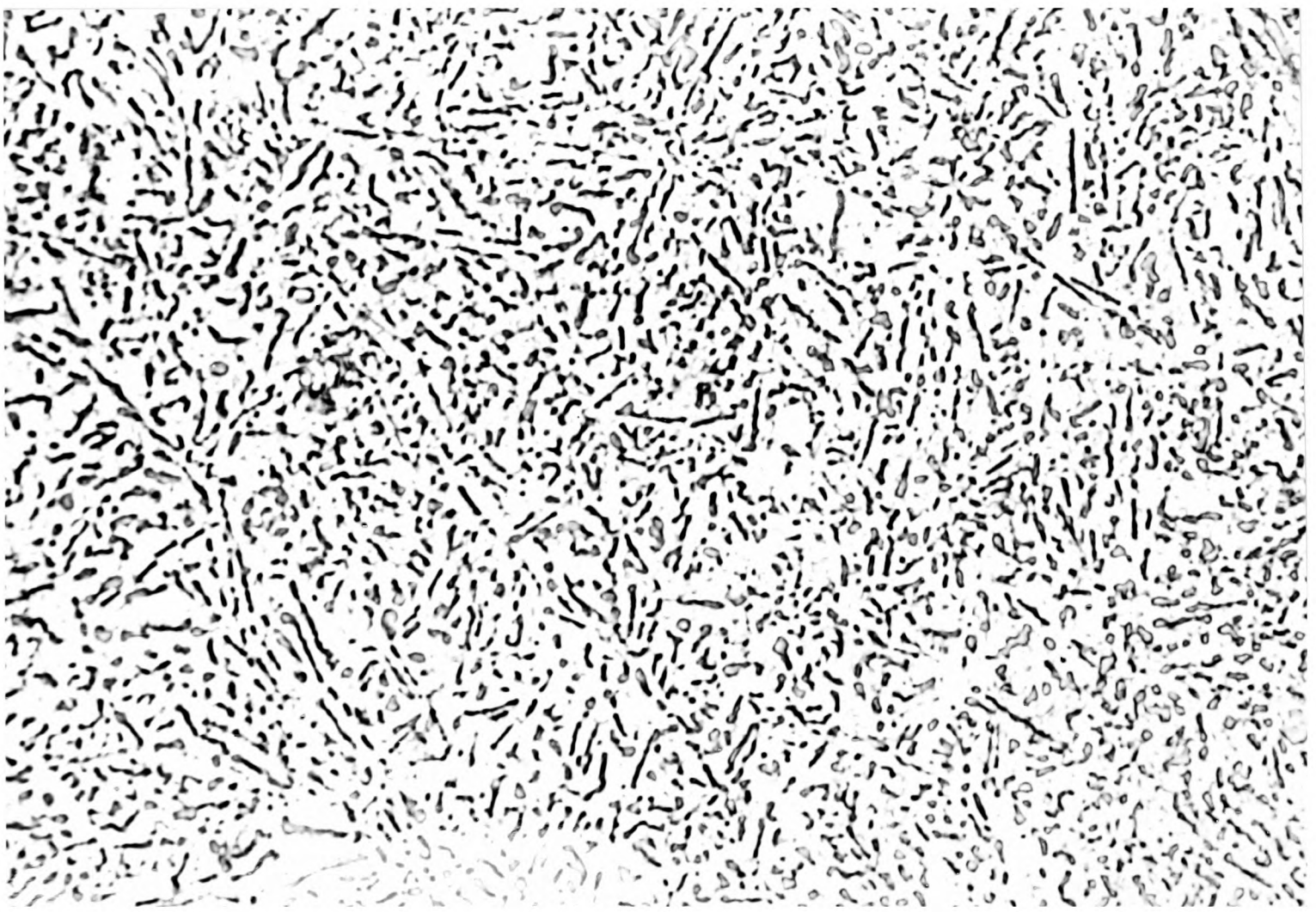

Plate 5 V = 0.12 mm/s, G = 22°C/mm, X 1000

Plate 6 V = 0.24 mm/s, G = 22°C/mm X 1000

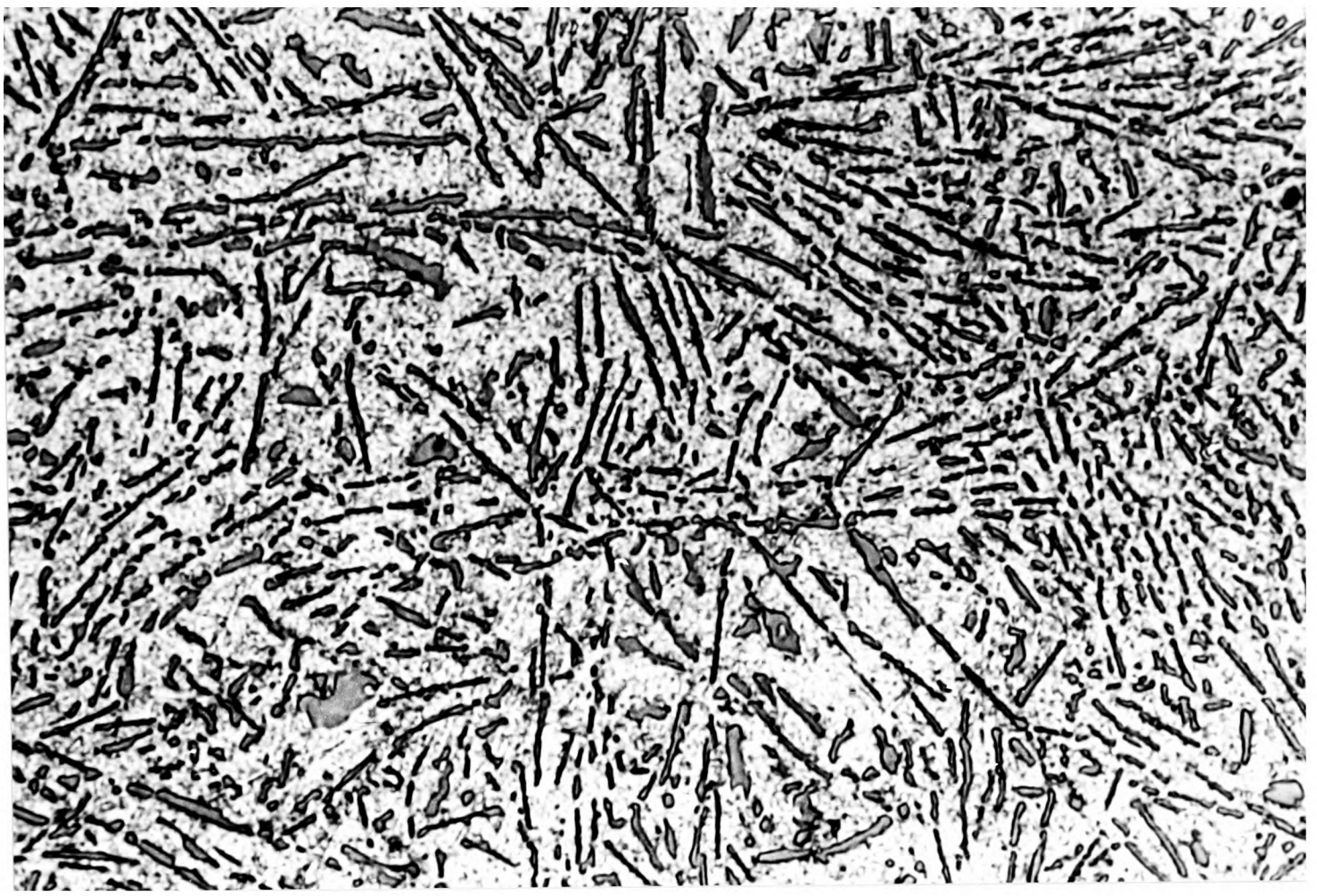

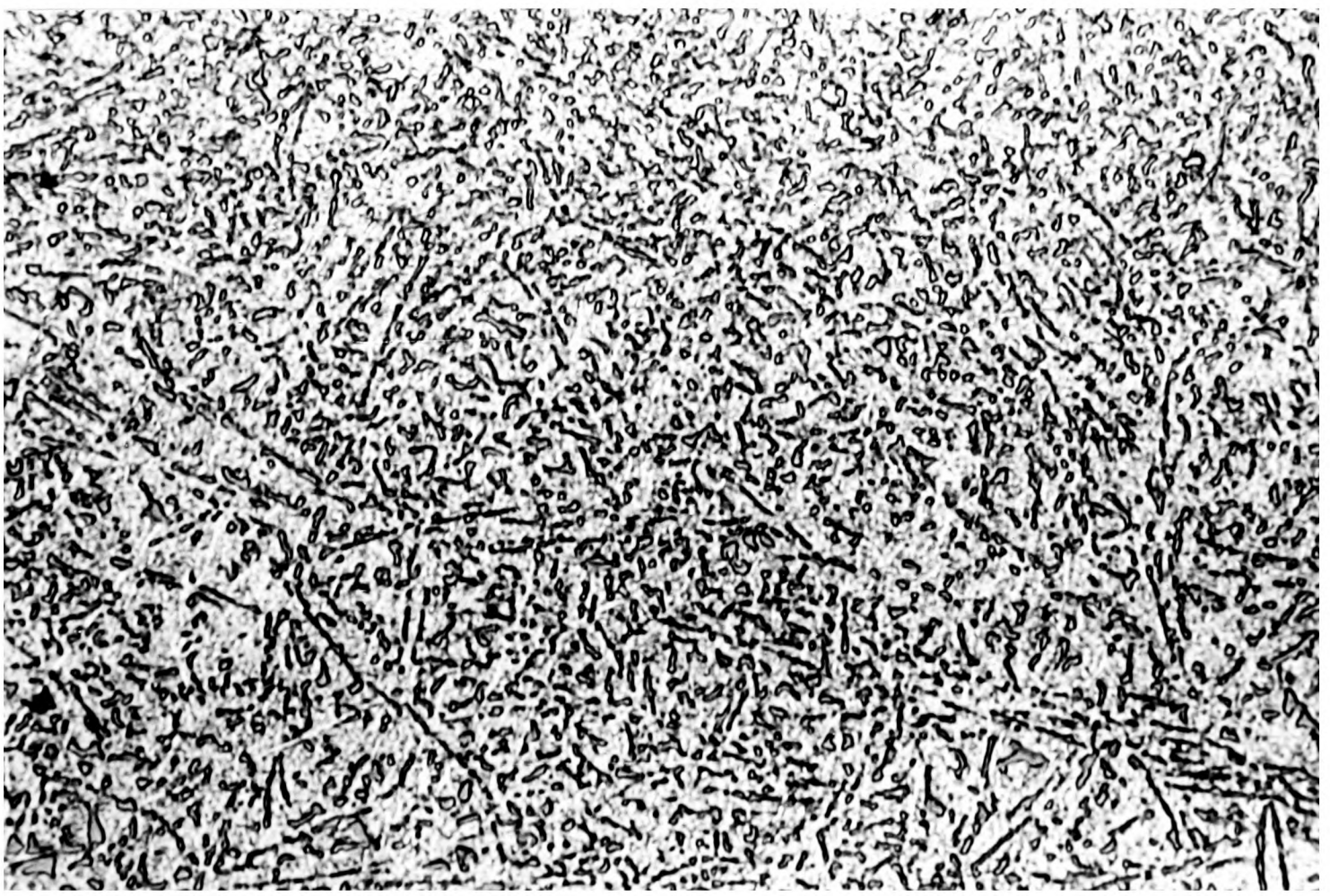

Plate 7 V = 0.48 mm/s, G = 22°C/mm X 1000

Plate 8 V = 0.96 mm/s, G = 22°C/mm X 1000

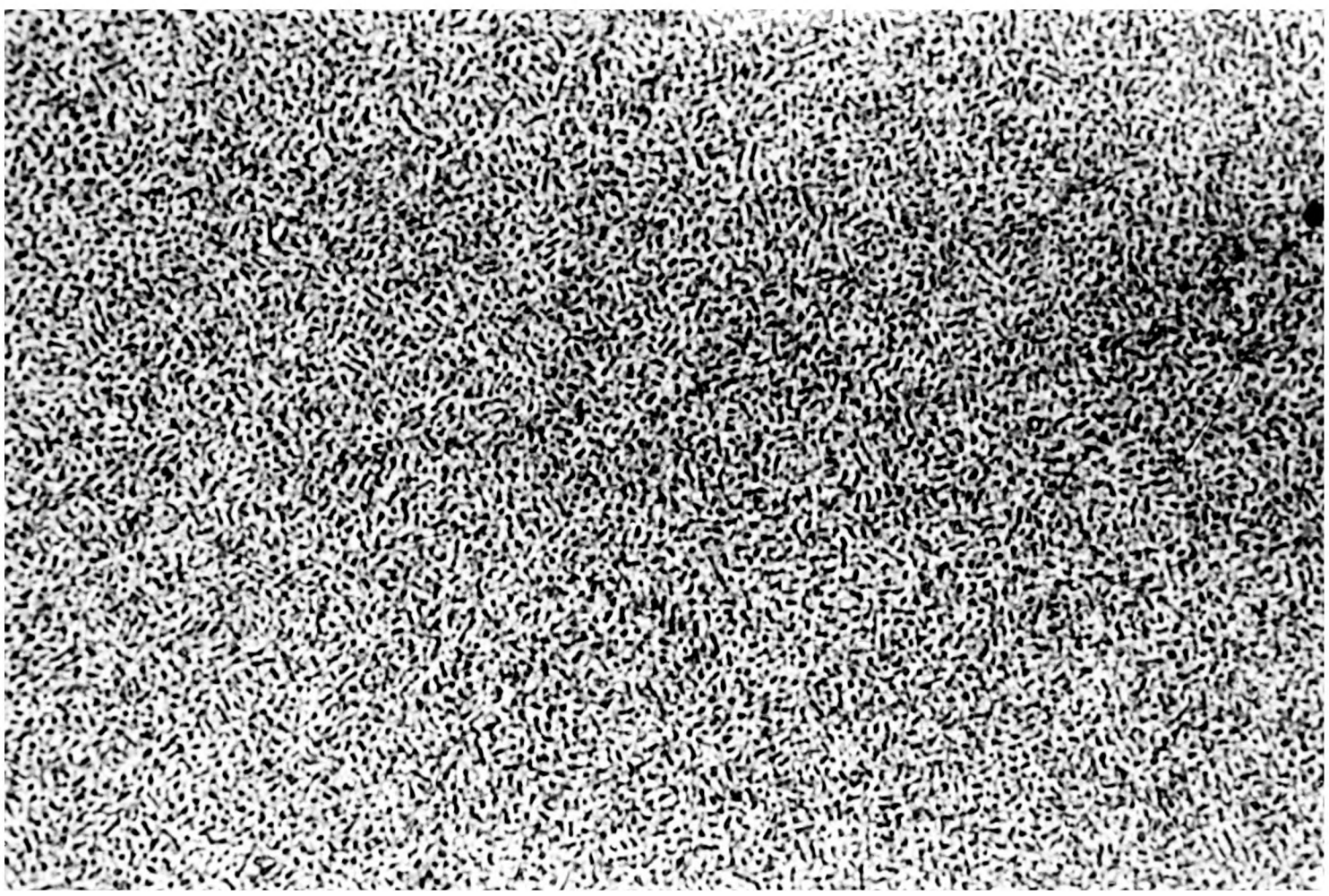

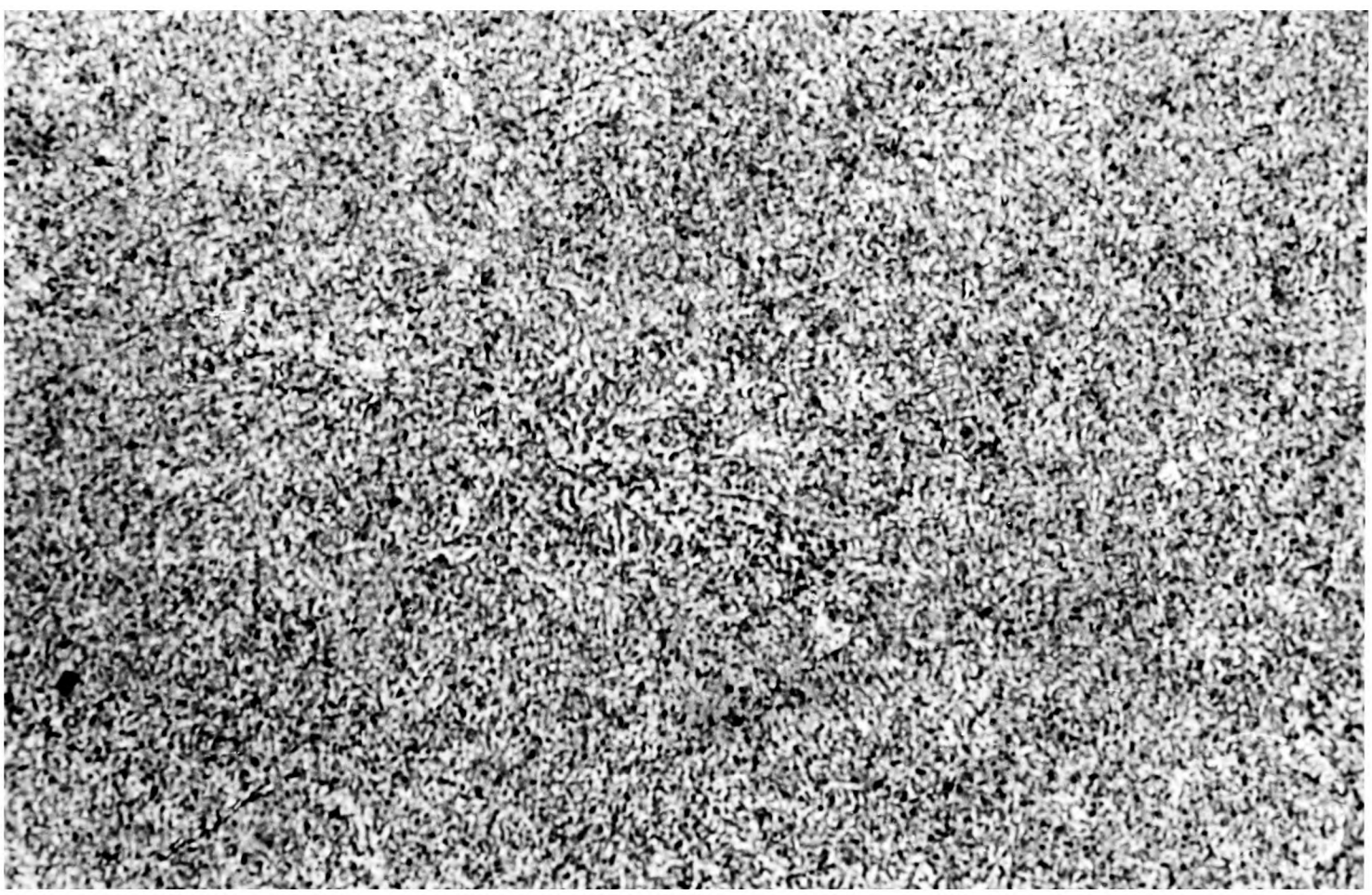

Plate 9

V = 0.12 mm/s, G = 22°C/Mm,

X 10,000, Scanning electron micrograph

Plate 10

V = 0.24 mm/s, G = 22°C/mm

X 10,000, Scanning electron micrograph

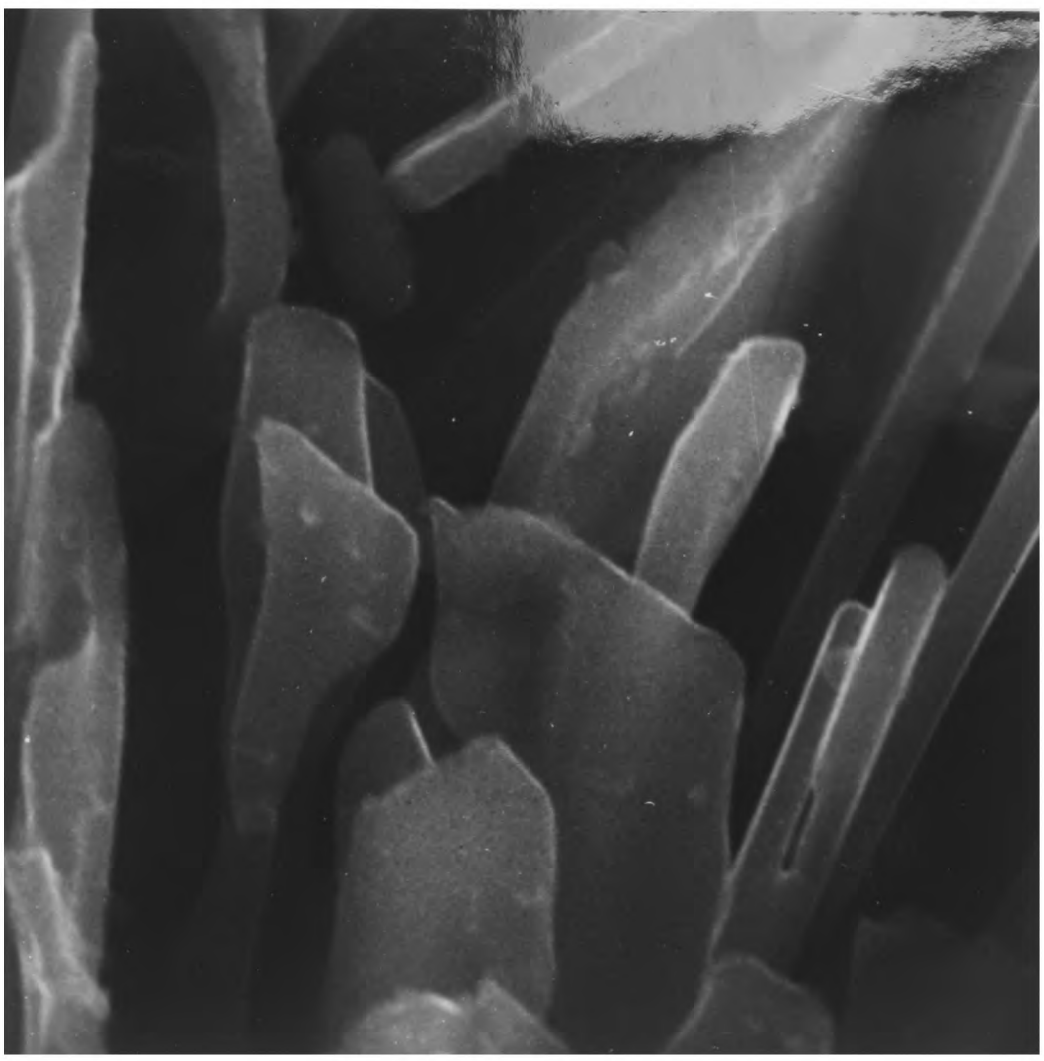

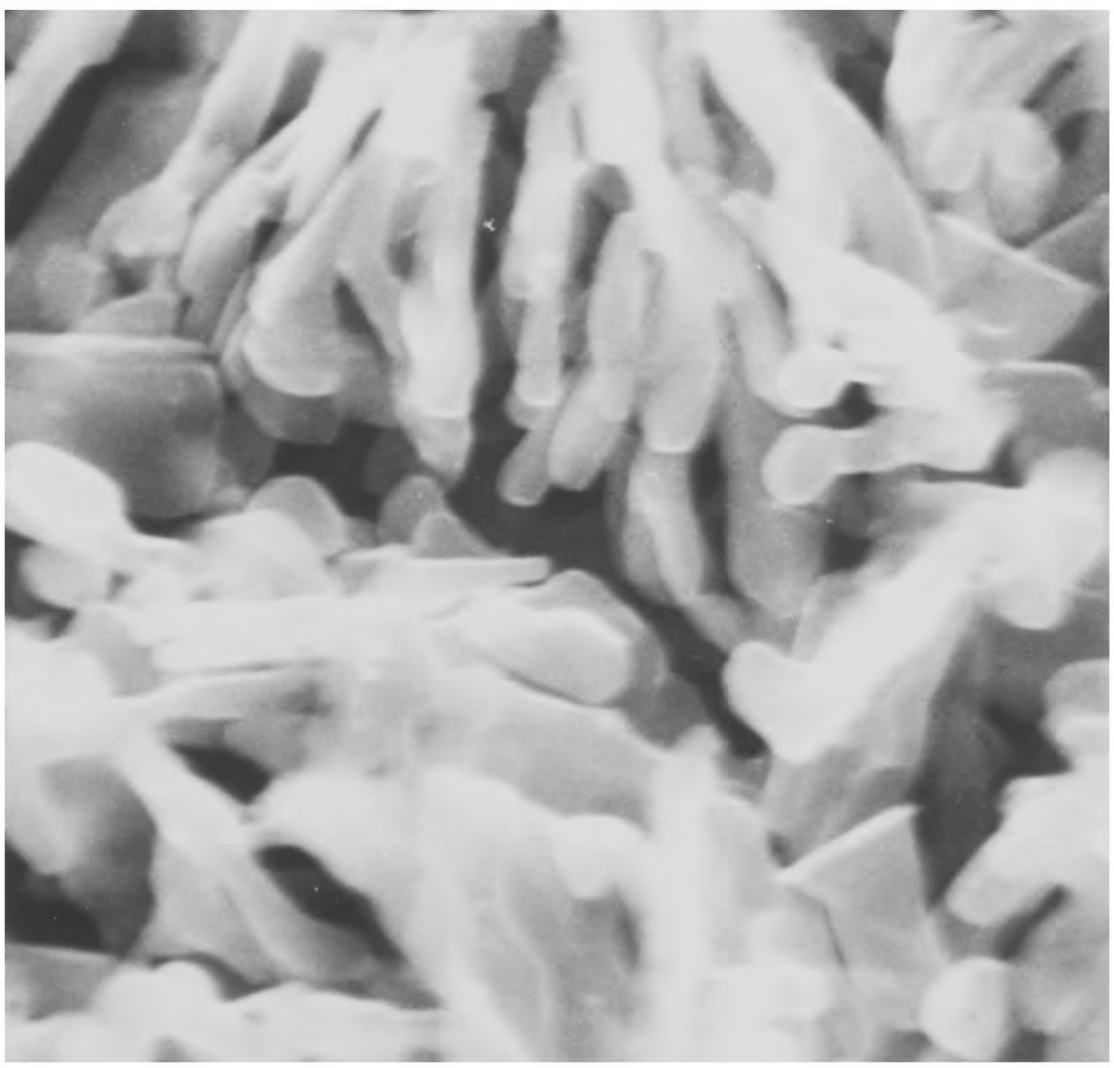

Plate 11

V = 0.48 mm/s, G = 22°C/mm

X 10,000, Scanning electron micrograph

Plate 12

V = 0.96 mm/s, G = 22°C/mm

X 10,000. Scanning electron micrograph

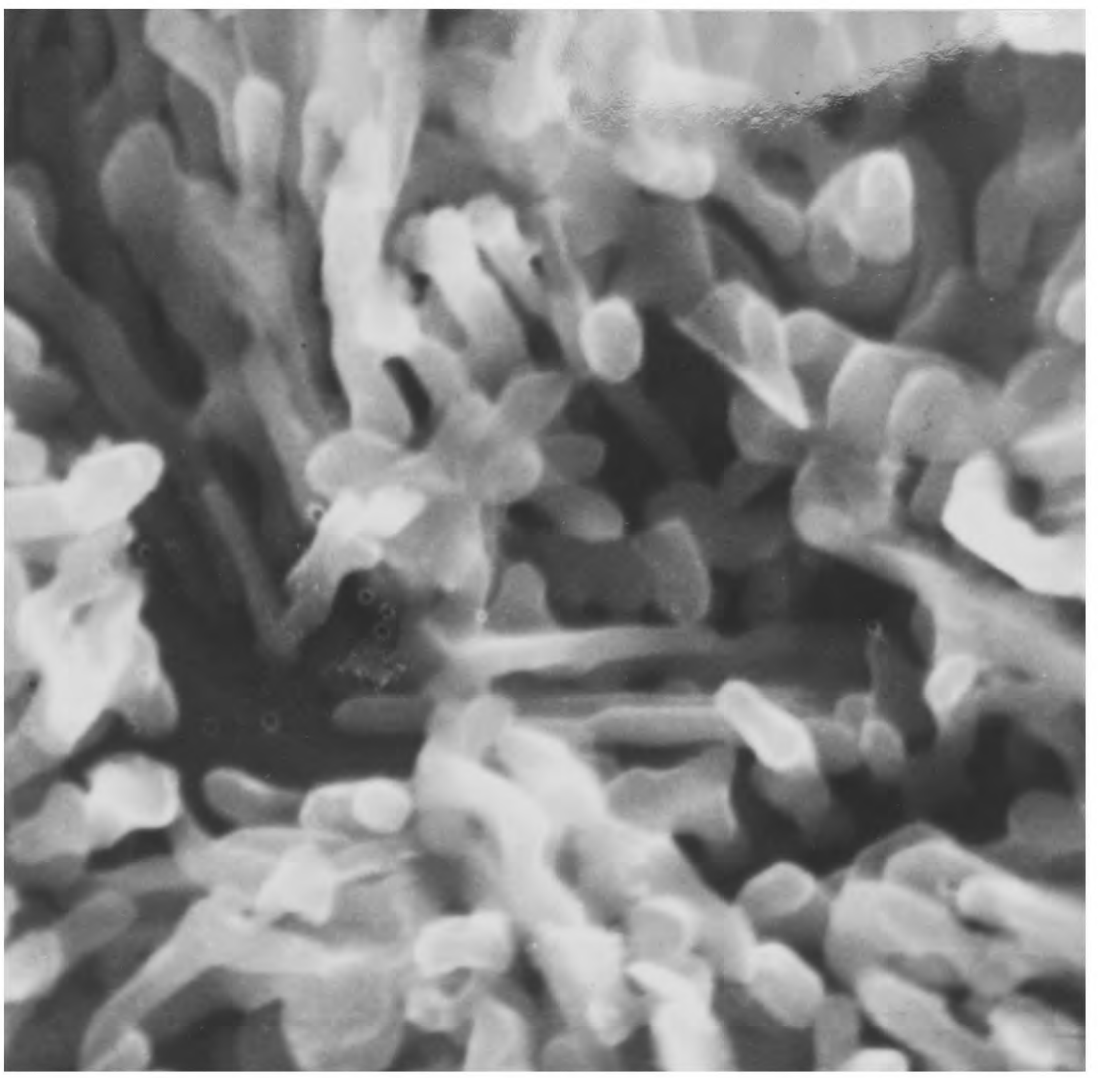

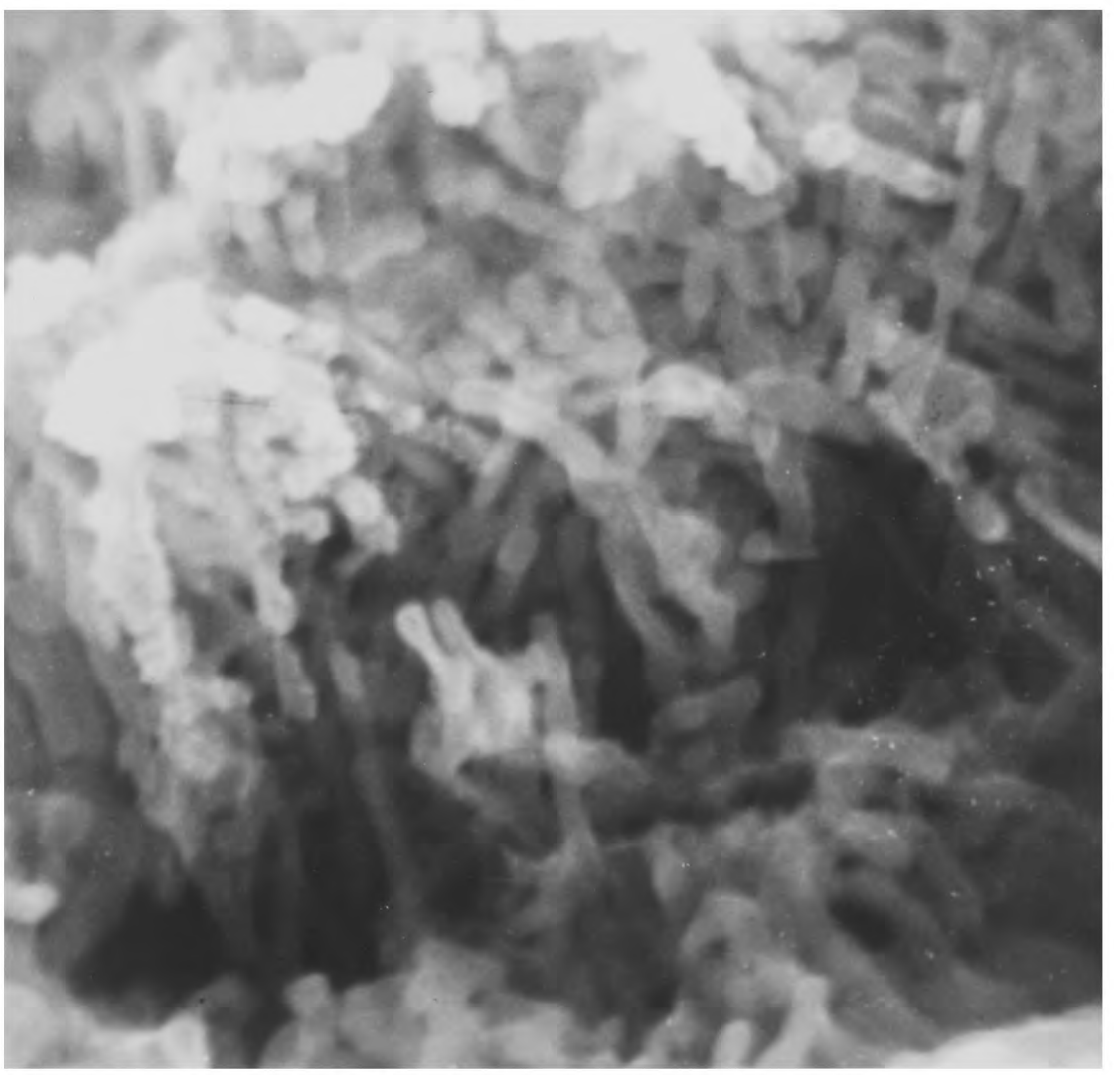

Plate 13

$V = 0.24$ mm/s, $G = 10^{\circ}C/mm$

X 9000. Transmission electron micrograph

Plate 14

$V = 0.48$ mm/s, $G = 10^{\circ}C/mm$

X 9000. Transmission electron micrograph

Plate 15

$V = 0.96$ mm/s, $G = 10^{\circ}C/mm$

X 21,000. Transmission electron micrograph

Plate 16

$V = 1.2$ mm/s, $G = 10^{\circ}C/mm$

X 9000. Transmission electron micrograph

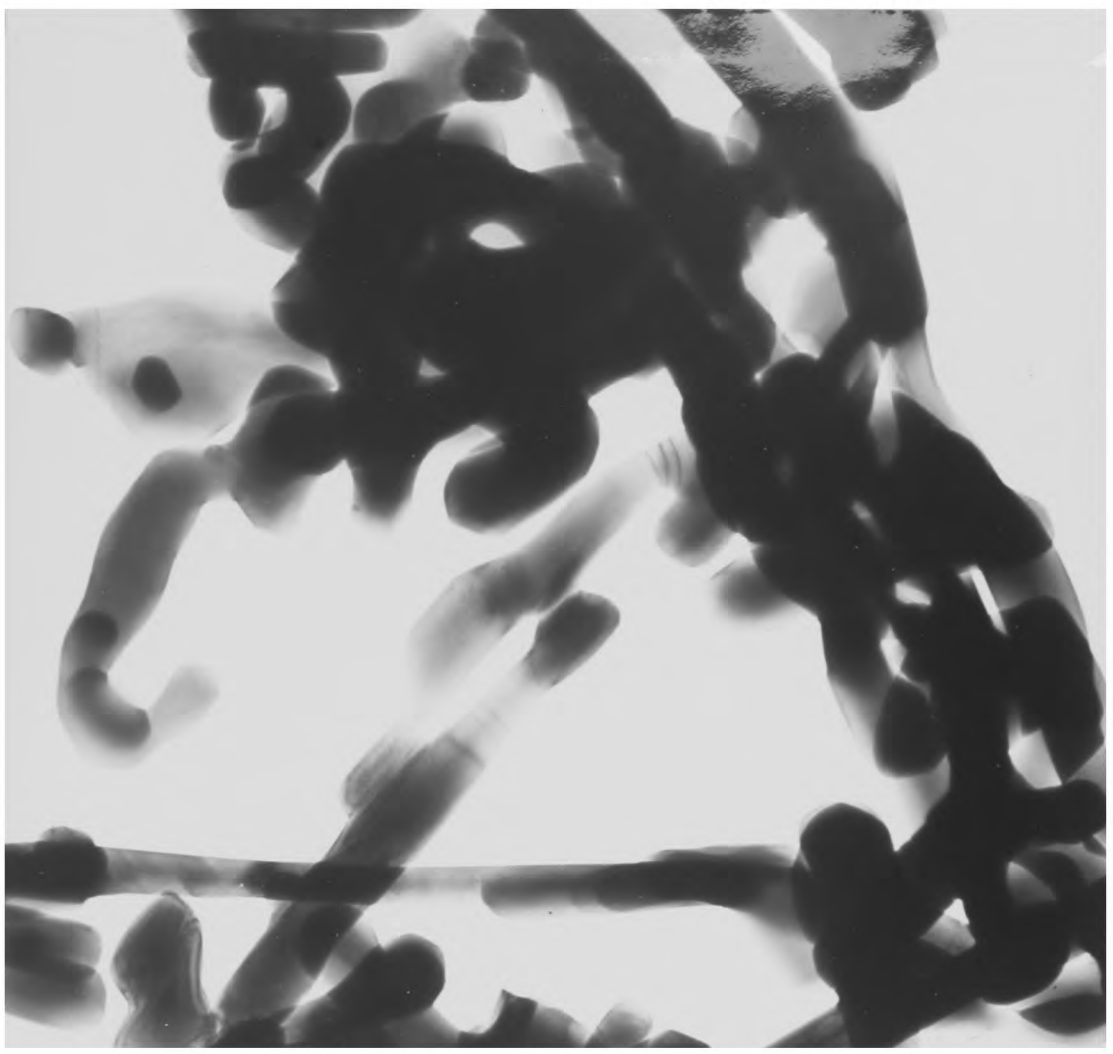

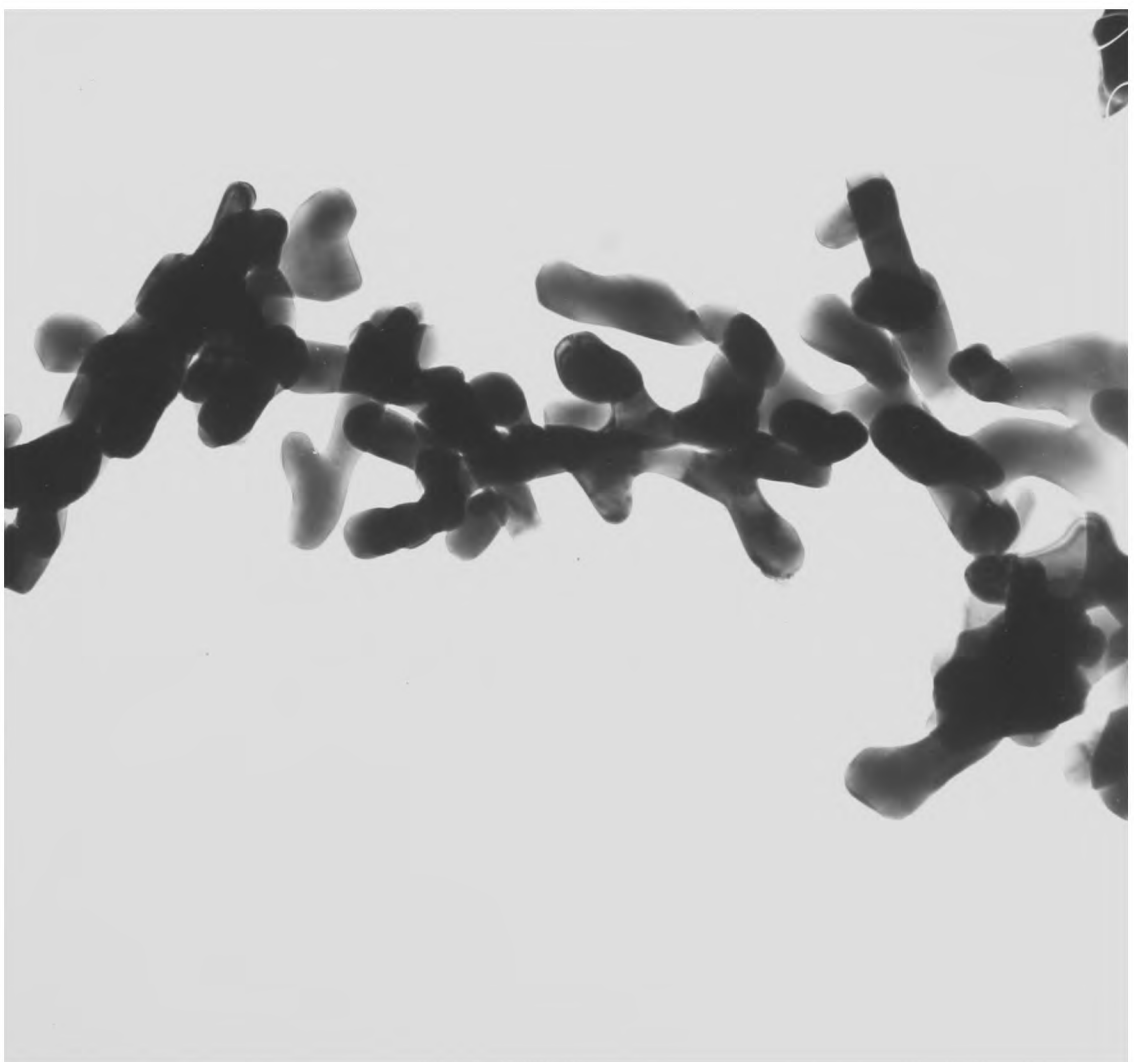

Plate 17

V = 0.24 mm/s, G = 20°C/mm

X 65,000. Transmission electron micrograph

Plate 18

Selected area diffraction pattern from crystal illustrated in plate 17.

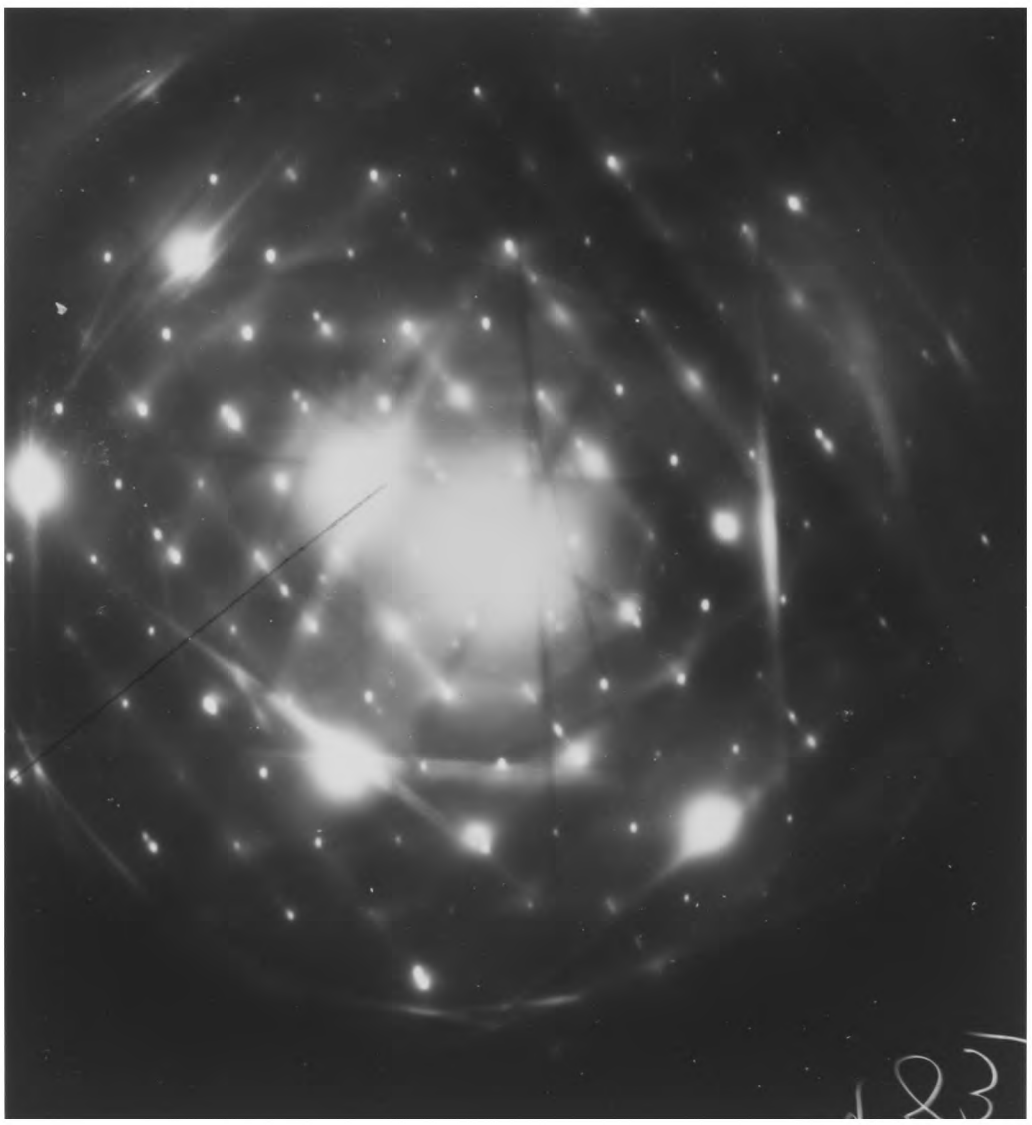

⟨011⟩⊥

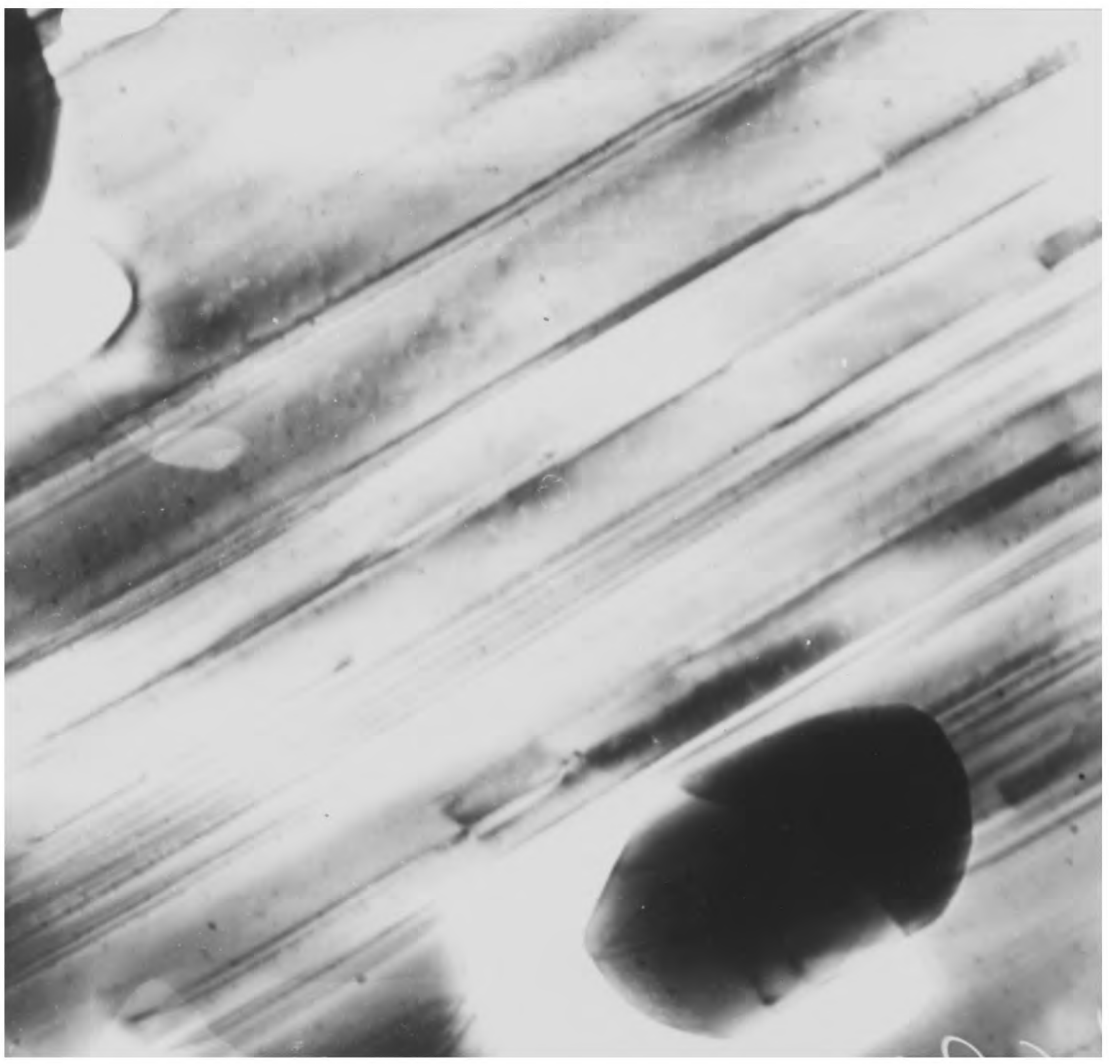

⟨011⟩

Plate 19

V = 1.9 mm/s, G = 20°C/mm

X 65,000. Transmission electron micrograph

Plate 20

Selected area diffraction pattern from crystal illustrated in plate 19.

<2117>

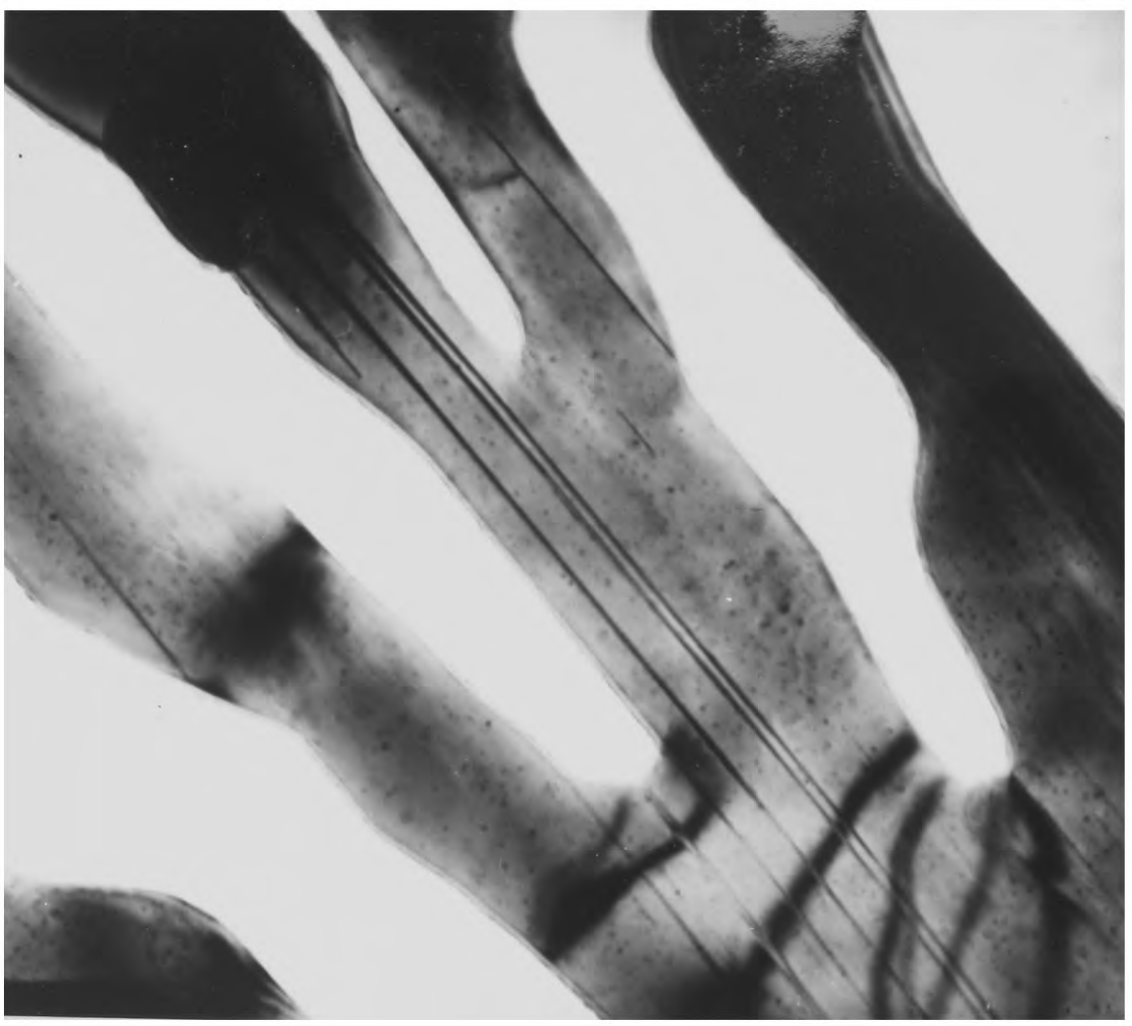

<2117>

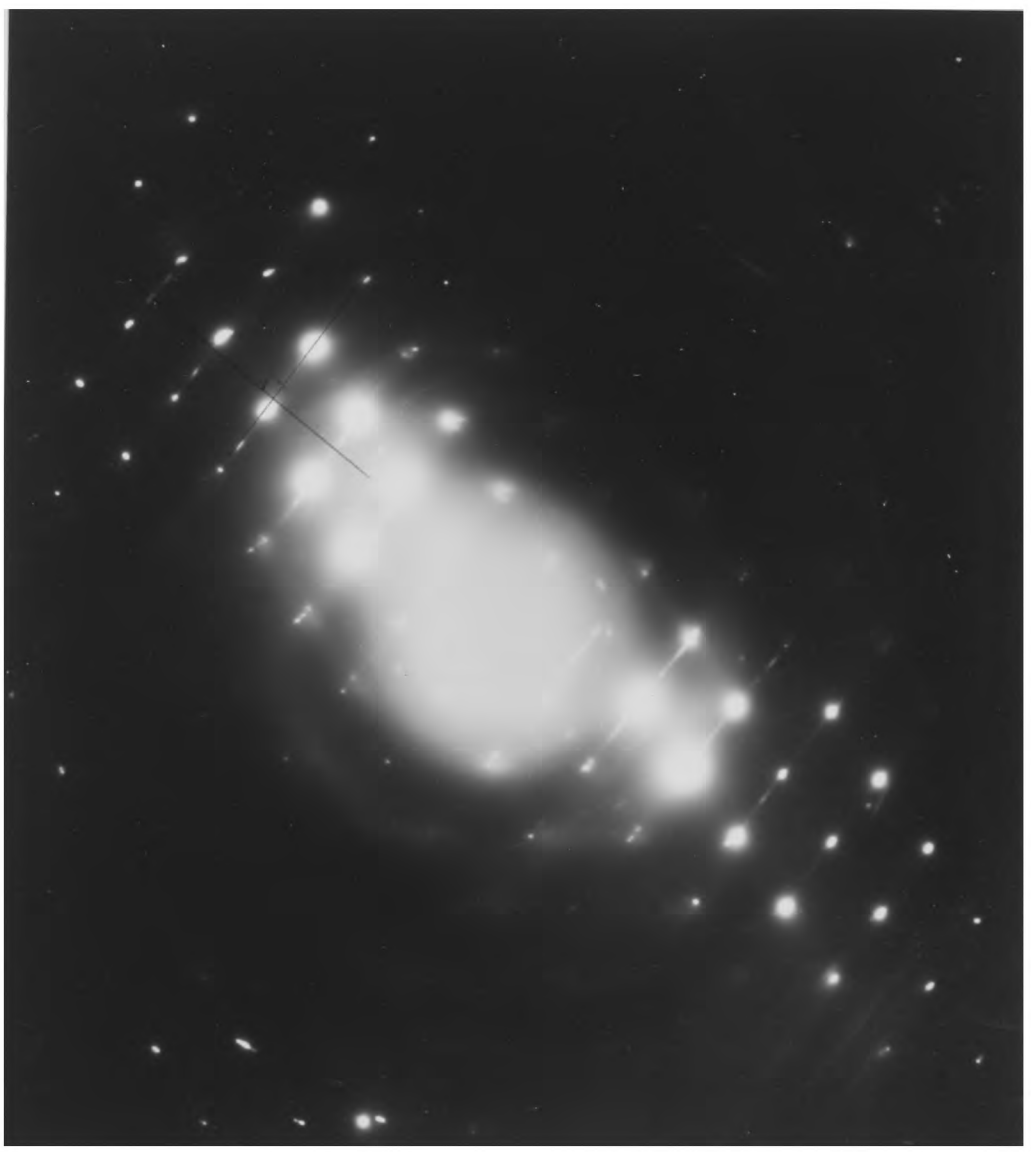

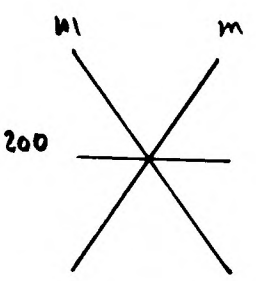

{1103}

Plate 21

V = 1.9 mm/s, G = 20°C/mm

X 65,000. Transmission electron micrograph.

Plate 22

Selected area diffraction pattern from crystal illustrated in plate 21.

{111}

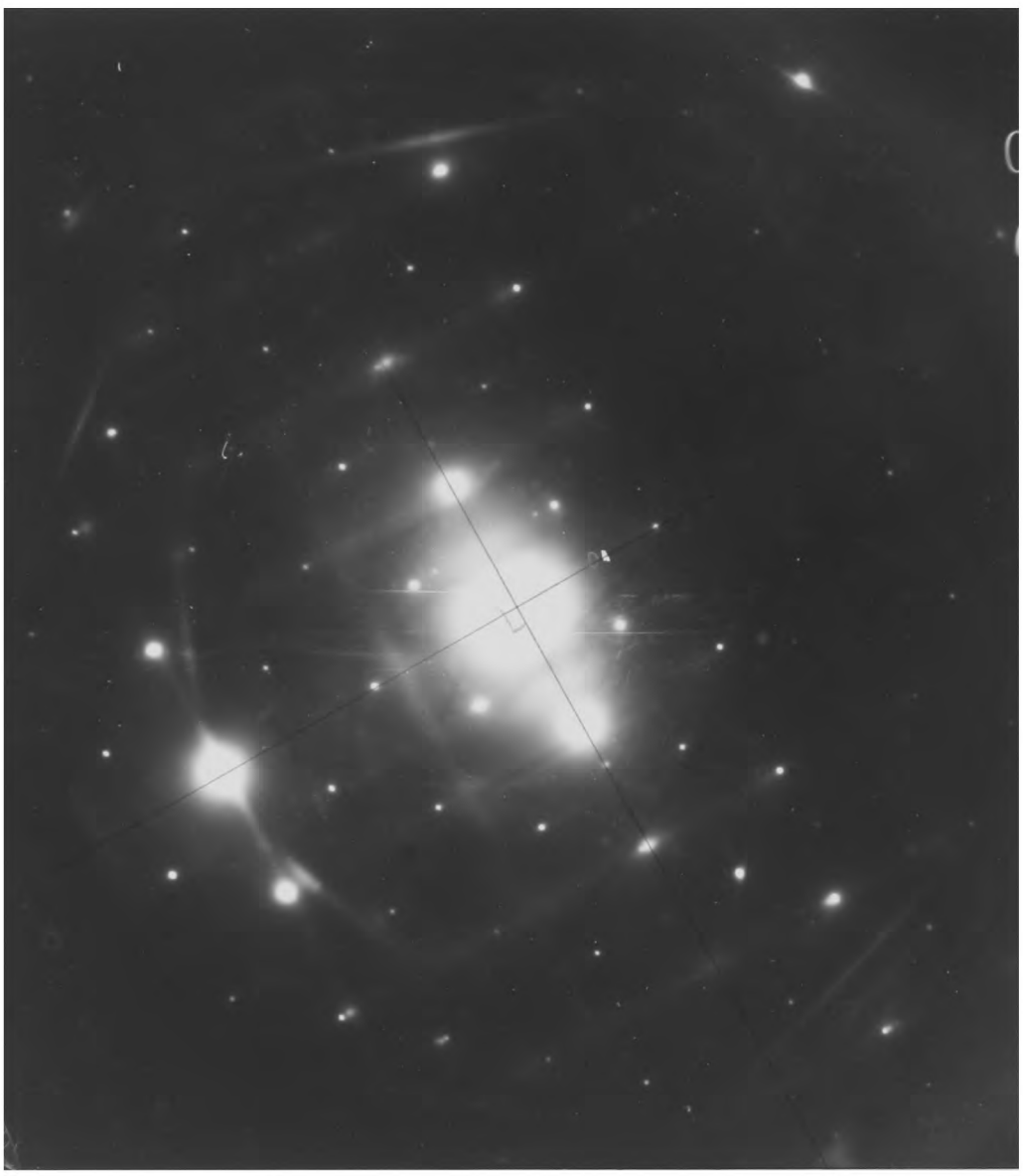

<111>

VI Droplet experiments

1) Introduction

It has been concluded that the eutectic microstructure in the aluminium-silicon system depends primarily on the growth kinetics of the silicon phase. Thus the basic problem concerns the growth of silicon into aluminium solutions, and it was decided to attempt to study this by melting droplets of aluminium or eutectic on variously oriented faces of monocrystalline silicon. The silicon substrate is then dissolved back until the composition of the droplet reaches the silicon liquidus composition at some temperature. When the droplet is cooled, the composition moves down the silicon liquidus, and silicon is deposited on the substrate, forming a growth layer which thickens until the eutectic nucleates and the remainder of the droplet solidifies. Examination of the growth layer after the manner of Davies and West (41), should then reveal whether growth took place with a rough or a smooth interface and whether or not twins were present in the growth layer.

Provided that it is possible to bring a thermocouple into good thermal contact with the substrate, it should also be possible with a large number of small droplets to determine undercoolings for nucleation of eutectic on silicon substrates. This experiment requires in-situ observation of the droplets as they melt and freeze and a sufficiently high vacuum (found to be $< 10^{-5}$ T) so that oxide layer formation on the droplets does not obscure the change of surface appearance accompanying melting and freezing.

It is known that under the influence of a temperature gradient a droplet containing a (saturated) solution of one phase in another will migrate through solid of the matrix phase up the temperature gradient, since solute is preferentially dissolved at the hotter

and deposited at the cooler end of the droplet. As will be discussed later, the rate of movement of a droplet in a given temperature gradient is expected to depend on the kinetics of dissolution or deposition of the solute, in this case the silicon phase, amongst other factors. Thus by comparing the migration rates of droplets with and without small concentrations of modifying elements, some conclusions may be drawn about how the impurity element affects the growth of silicon. Since this experiment was to be carried out under vacuum, it was found most convenient to use a non-volatile modifying element, and of the group I and II elements reported to produce modification, strontium seemed the most suitable.

Strontium was also used to see whether growth layers were affected by the presence of a modifying agent, although droplets were also melted under alkali halide fluxes in an argon atmosphere.

2) The hot stage apparatus

The stage: This is illustrated in fig 19. The main body was machined out of copper and wound with copper tubing for water cooling. The wall of the main body contained three entry ports, two to accommodate thermocouple leads, the other the current supply for the heating element. Inside the chamber the thermocouple leads were soldered to the pins of two insulated lead-throughs which were themselves soldered into recesses in the wall. Thermocouple wires matching those inside the chamber were soldered to the outside ends of the pins and taken to a cold junction where they were soldered to copper wire. The heating current was taken in via a water cooled copper 'finger' insulated from the chamber with a P.T.F.E. bush. 'O' ring seals between the 'finger' and the bush and between the bush and the main body ensured that the entry

was vacuum tight. The heating element used was a tantalum strip, one end of which was screwed onto the end of the cold finger, and the other onto a part of the chamber. The tantalum strip was bent into a flattened U shape in order to make it resistant to distortion on heating. The cold finger, friction allowing, was free to slide in and out on its 'O' ring seal, so longditudinal expansion of the heater strip was possible. The chamber was sealed via an 'O' ring to a water cooled copper lid in which a small hole, covered by a quartz disc on an 'O' ring seal, made possible observation of the specimens.

A pair of 40 mm diameter brass bellows connected the chamber to a vacuum system, allowing the chamber to be moved up and down on the stage of a Beck microscope so that the X4, long focus objective could be focussed on the specimen. The ends of the bellows were soldered onto brass discs containing 'O' ring seals. One disc fitted into a hole in the base of the chamber and the other onto the top plate of a baffle valve which also contained an inlet for argon. The valve fitted onto a liquid nitrogen trap above a 40 mm oil diffusion pump backed by a rotary pump. According to the manufacturer's specifications this system should have been capable of pumping down to $10^{-7}\gamma$. Vacuum measurement was by an Edwards ionisation gauge able to measure vacua down to $10^{-9}\gamma$. The gauge head was attached to the top plate of the baffle valve. It was found that given sufficient time (a few days) the experimental system would pump down to about $5 \times 10^{-7}\gamma$, but a vacuum of $5 \times 10^{-6}\gamma$ was sufficient to keep the surfaces of droplets clean enough for melting and freezing to be observed.

<u>The heater circuit</u>: The heater circuit is shown in fig 20. Power from the mains was fed via a variac transformer into a D.C. transformer which gave a high direct current output at a potential

of 2V. Current was carried to the hot stage by thick copper braid, the earth lead being screwed onto a tab on the outside of the chamber, and the other lead screwed to the end of the water cooled finger. Current on the input side of the D.C. transformer was measured with an ammeter, and from this and the variac setting, knowing that the D.C. output was at 2V, the current passing through the heater was calculated. It was found that a current of 150A heated the strip to as high a temperature as was needed. Because of the low voltage, particular care had to be taken to ensure good electrical contact in the circuit. The heater temperature depended on the variac setting, so in order to obtain slow cooling rates it was necessary to turn the variac down slowly and evenly. An aluminium disc with a groove in the circumference was fitted to the spindle of the variac. One end of a piece of fine wire was pinned to a point on the circumference, and the wire taken round the groove to a variable speed motor. Thus the variac could be wound down at a constant rate. It was found that at the high variac outputs concerned, turning down at a constant speed gave a closely linear cooling rate, although Jordan (6) has shown that to give a linear drop in power output from a variac, a cam should be employed, the radius of which at a given point is proportional to the voltage at that point, rather than a disc.

By varying the rate at which the variac was turned down it was possible to obtain cooling rates between 0.6°C/s and 15°C/s. In order to produce faster cooling rates a gas quench was necessary, so a fine tube which could be attached to an argon cylinder was led through the lid of the hot stage, the end of the tube being positioned so as to direct a jet of argon onto the silicon substrate. Thus a fast cool was obtained by closing the baffle, switching off the power to the heater and opening a valve which

allowed a stream of argon to flow through the tube and quench the substrate. This way cooling rates of the order of 120°C/s were obtained. Cooling curves were obtained but since the argon stream quenched the thermocouple as well as the substrate, it was not clear how closely the measured cooling rate approximated to the actual cooling rate of the substrate.

The heating strip: As mentioned above, the tantalum heating strip was bent into a flattened U shape for general purposes. In order to obtain a temperature gradient, a heater of cross-section ⌐ was used. It was found that such a heater produced a much larger temperature gradient across the slice than could be obtained by longditudinal variations in the heater cross-section. The gradient could be estimated by comparing the outputs of thermocouples on either side of the silicon slice. It was found initially that the thermocouples picked up some current from the heater via the silicon, and in order to obviate this it was necessary to insulate the heater electrically while maintaining good thermal conductivity. To this end the heater was coated with a film of boron nitride, using an aerosol spray. The film was dried and baked out under vacuum before use, after which treatment it maintained its insulating properties for about ten runs.

Temperature measurements: In the hot stage it was found to be difficult to maintain thermocouples in close thermal contact with the silicon slices. Most intimate contact could be obtained by melting the thermocouple bead, using an oxy-coal gas flame, onto the silicon. This technique however, resulted in the formation of an exceedingly brittle platinum-silicon compound in the bead which rendered the specimens too fragile to be of much practical use. Moreover the thermocouple output was found to be

affected by the compound. In practice the thermocouple bead was pressed into a shallow groove cut in the surface of the silicon slice with a fine carbide wheel. The thermocouple was calibrated by observing the melting of a droplet under the microscope. Generally melting occurred when the thermocouple recorded a temperature about 50°C lower than the eutectic temperature. Undercoolings for nucleation of individual droplets were taken as the difference between the apparent melting and freezing temperatures for that droplet. Temperatures above the eutectic to which droplets were heated were taken as the difference between the apparent melting temperature and the maximum temperature recorded. Thus the temperature measurements were sensitive to changes in thermal contact between thermocouple bead and substrate which could be caused by thermal contraction or expansion of the platinum wire and of the tantalum heating element.

Sodium modification: The hot stage apparatus was not suitable for the melting of droplets under alkali halide fluxes, and for this purpose the radio frequency induction furnace described in the section on alloy preparation was used. In order to ensure a clean surface the droplet was initially melted onto the substrate in the hot stage under high vacuum. The specimen was transferred to an alumina crucible and covered with the appropriate flux. The crucible fitted into a graphite susceptor which was heated under an argon atmosphere. Cooling rates were estimated from a thermocouple in contact via an alumina sheath with a graphite lid which fitted over the susceptor.

3) Sample preparation

In order to produce a large droplet, a small piece of eutectic, previously cleaned in dilute H.F., was placed in the hot stage on

the polished surface of a silicon slice of the desired orientation. Enough alloy was used to give a droplet between 1 and 2 mm diameter on melting.

Small droplets were obtained by melting very fine particles of eutectic on the silicon substrate. These particles were produced by filing a cleaned eutectic ingot with a fine, clean file. Iron particles were removed with a magnet and oversize particles by sieving the powder through a fine copper grid. The resulting powder was sprinkled carefully on the appropriate silicon substrate in the hot stage. For the purpose of comparing the migration rates of modified and unmodified droplets, modified particles were sprinkled on one side and unmodified ones on the other side of a line through the middle of the substrate axial with the temperature gradient.

4) Specimen preparation for metallography

For microscopical examination the silicon slice supported by a wire former was mounted in transparent plastic, and a flat was ground perpendicular to the plane of the slice so that a section through both droplet and slice was revealed. This section was ground on silicon carbide papers down to 600 grade and then polished on a selvyt covered lapping wheel using fast cutting alumina. It was found that alumina powder gave a less pronounced relief effect between the hard silicon substrate and the softer eutectic droplet than that obtained using diamond pastes or metal polish. For examination of substrates with small droplets, the relief effect was further minimised by the use of taper sections. The wire former was bent so that the ground surface made an angle of about 45° with the surface of the silicon, so that a larger area of droplet (and substrate) was available for examination.

Sections were examined both unetched and etched, under the

optical microscope. Unetched sections showed the microstructure of the droplet and the silicon-eutectic interface up most clearly, while etched sections revealed the growth layer in the substrate, and the internal structure of this layer and any primary silicon particles present in the droplet. A modified C.P.4 etch given by Day (2) was used, the composition of which was one part HF, two parts concentrated HNO_3 and fifteen parts glacial acetic acid. This etch produced little attack on eutectic aluminium while delineating any internal structure in silicon. Etching times of 15 to 120 seconds were employed.

Fig 21(a) illustrates a transverse section through droplet and substrate. In order to allow examination of the surface of the growth layer, the aluminium phase of some droplets was etched away, using a dilute solution of hydrochloric acid in water. This produced a 'pit' in the substrate formerly occupied by the droplet, and the sides and base of the pit were the surface of the growth layer. This arrangement is illustrated in fig 21(b).

5) Previous work on droplet migration

No previous work appears to have been done on the thermomigration of droplets using the aluminium-silicon system, but Wernick (50) has examined the migration of wires of aluminium laid perpendicular to the temperature gradient across and through variously oriented germanium single crystals. He noted an orientation dependence in the behaviour of molten zones migrating across a surface of the germanium substrate in that the zone would not cross an oblique $\langle 110 \rangle$ direction, but tended to lie along this direction. When the temperature gradient was perpendicular to a $\langle 110 \rangle$ direction, the zone lay along this direction and migrated slowly parallel to the temperature gradient. His experiments were carried out using $\{100\}$, $\{110\}$ and $\{111\}$ substrates so that the $\langle 110 \rangle$ directions corresponded to intersections of $\{111\}$ planes with the plane of the substrate, and it was concluded that $\{111\}$ planes impede zone movement normal to them.

The migration rate of molten zones across the surface was found to increase rapidly for small increases in temperature, so that, as a zone moved about 20°C up a temperature gradient, its migration rate increased by a factor of about 2. Some experiments were also carried out involving the thermomigration of wire zones of different diameters through the germanium substrate. Here it was found that the migration rate was zone size dependent, larger diameter zones migrating faster.

Thermomigration of liquid zones through solids can be considered as three processes which are: dissolution at the hotter interface, diffusion, and deposition at the cooler interface. Migration takes place because the equilibrium concentration of solute increases with temperature, and diffusion

tends to reduce the resulting composition gradient between the hot and cool ends of the zone, while dissolution and deposition act so as to maintain the gradient. From the observation that {111} planes impeded zone movement, Wernick concluded that dissolution was the rate determining step in this process, and that the solution rate was lowest for {111} planes.

From the rapid change in migration rate with temperature he inferred that the rate determining step was one with a large activation energy. This condition is satisfied if the controlling process is dissolution or freezing, the activation energy being required for a two-dimensional nucleation event or to form defects to provide favourable sites for growth or dissolution. It has been shown by Cline (52) that the kinetics of dissolution rather than freezing is the rate determining process here, since the freezing interface is concave in migrating droplets and favourable sites for the nucleation of new layers are always available. The dissolving face on the other hand is convex (towards the solid), and when the interface is faceted, favourable sites for dissolution depend on the presence of defects in the facets.

Expressions for the migration velocity of droplets in accelerational fields (52), and in temperature gradients (53, 54), have been derived. The driving force for migration is the chemical potential difference ΔG_S between solute atoms in the solid at the melting and freezing interfaces. Considering fig (22) K_S and K_D are the kinetic free energy barriers for solidification and dissolution and ΔG_l is the chemical potential difference between solute atoms in the liquid at the melting and freezing interfaces. If V is the migration velocity, C_S the solute concentration in the solid, C_l that in the liquid, l the length

of the droplet and B the mobility of the solute, then by mass balance considerations:

$$VC_S = BC_L \frac{\Delta G_L}{l}$$

$$\therefore V = \frac{C_L}{C_S} \frac{D}{RT} \frac{\Delta G_L}{l}$$

$$\text{Now } \Delta G_L = \Delta G_S - (K_D + K_S)$$

$$\therefore V = \frac{C_L}{C_S} \frac{D}{RT} \left[\frac{\Delta G_S}{l} - \frac{(K_D + K_S)}{l} \right]$$

If we consider migration due to the presence of a temperature gradient G, ΔG_S is $\Delta T f(c)$ where f(c) is some function of the particular system and absolute temperature.

$$\therefore V = \frac{C_L}{C_S} \frac{D}{RT} \left[Gf(c) - \frac{(K_D + K_S)}{l} \right]$$

Physically the first term represents the driving force for migration and the second term the driving force necessary to overcome the kinetic barriers at the melting and freezing interfaces. The equation predicts that below a certain droplet size, V will be zero since the combined kinetic barriers will be greater than the overall drop in chemical potential across the droplet in the solid. Such a minimum droplet size for migration was observed by Antony and Cline (54). As the droplet size increases above this minimum, V is initially strongly dependent on l, and as l becomes large, approaches a constant value given by the first term in the expression. Tiller (51) has shown that if the variation of V with l is known for a given system, $(K_D + K_S)$ can be calculated. From $(K_D + K_S)$ he is able to discuss whether interface motion is layer motion dependent or layer source dependent either on screw dislocations or on two-dimensional nucleation events. Analysing Wernick's results he suggests that in that case the migration of liquid zones through germanium was screw dislocation layer source limited.

If kinetics are neglected, an approximate expression for

the migration velocity may be derived as follows. Considering fig (23), we assume that the liquid compositions at both melting and freezing interfaces are the same as the mean liquid composition, in other words that the liquid is fully mixed. Then by mass balance:

$$V(C_L - C_S) = D\frac{dc}{dx}$$

$$\text{Now } \frac{dc}{dx} \sim \frac{\Delta C}{L} \text{ and } \quad C = \frac{\Delta T}{m}$$

$$\therefore VC_L(1-k) = \frac{D\Delta T}{lm}$$

$$\therefore V = \frac{DG}{mC_L(1-k)}$$

6) Droplet migration results

Preliminary experiments were carried out with $\{111\}$ and $\{110\}$ substrates to find out how the relative orientations of substrate crystals to the applied temperature gradient influenced the shape and migration behaviour of small eutectic droplets.

On a $\{111\}$ substrate, the molten droplets assumed a roughly equilateral triangular shape, rounded at the corners, the edges lying along $\langle 110 \rangle$ directions. Considering fig 24(a), it was found that when the temperature gradient was positive along $[121]$, the droplet did not migrate as a compact unit, but tended to spread out, the edge normal to the temperature gradient moving up the gradient while the other edges remained stationary.- fig 24(b) -. When the temperature gradient was positive along $[\bar{1}\,\bar{2}\,\bar{1}]$ on the other hand, the droplet migrated as a compact mass, its size not changing with time. Thus migration always took place along the direction of the imposed temperature gradient.

On a $\{110\}$ substrate it was found that whatever the direction of the imposed temperature gradient, perceptible migration only took place along the $\langle 110 \rangle$ direction, and if

these directions were normal to one another, no migration was observed. This can be explained if we consider the intersections of {111} planes with a {110} plane - fig 25 -. In the {110} plane, here the plane of the substrate, two intersecting sets of {111} planes lie along the <110> direction, making angles of 35^{o} with the {110} plane, and two sets each normal to the {110} plane lie along <211> directions making angles of 54^{o} with the <110> direction. If, as predicted {111} planes are the most immobile, a molten droplet should lie is a V shaped groove bounded by intersecting {111} planes, with the front and back of the groove formed from the sets of {111} planes normal to the plane of the substrate. Migration is then difficult normal to the <110> direction, as was observed by Wernick (50). After migration across a {110} oriented substrate, the droplets were etched away using dilute HCl, and examination under the microscope revealed that the droplets had lain in shallow grooves - plate (23)-. Droplets were also examined unetched after migration, and it was observed that they were rounded at the freezing interface and most were faceted at the dissolving interface - plate (24) -, the angle between the facets being about 108^{o}, corresponding to the angle between the two {111} planes normal to the {110} surface. This indicated that there was a significant kinetic barrier to dissolution but not to growth.

Migration rate measurements were made with unmodified and strontium modified eutectic droplets on a {110} slice of silicon, with a temperature gradient applied parallel to the <110> direction. Plate (25) shows a specimen after migration. The <110> direction and temperature gradient are vertical, the unmodified droplets are on the left and the modified ones on the right. Measurements were made under the microscope of the

migration distance of each droplet. This distance was taken as the distance travelled by the dissolving interface of the droplet, as dissolution was expected to be the rate determining process. As can be seen from plate (25), the migration distance and hence the temperature gradient decreased near the ends of the slice, so measurements were taken near the centre of the specimen.

On some specimens droplet width was also measured but no correlation was found between width (and hence length since most droplets were approximately equiaxed) and migration distance. The shape of droplets was not observed to change during migration.

Migration velocity was altered by varying the temperature gradient (by propping up the cooler end of the substrate on a sliver of alumina) and the ambient temperature.

The migration velocity was calculated for the modified (V_m) and unmodified (V_u) droplets on each specimen by measuring the migration distances of a number ($\sim$20) of droplets of each type, taking the mean for each type and dividing by the time over which migration had taken place. The scatter in migration distances for each species of droplet can be attributed to two factors:

1) Local variations in temperature gradient on the substrate
2) The change in absolute temperature across the droplet due to the temperature gradient, as it was observed that migration distances were longer near the hotter end of the substrate.

From these measurements a plot was made of ΔV against V_u - fig (26) - where $\Delta V = V_u - V_m$.

From the results it can be seen that the presence of a modifying agent does slow down the migration of droplets, and

if the modifier inhibits dissolution by adsorbtion on the dissolving interface, this indicates that the kinetic term in the expression for migration velocity is significant. However if this is so, a dependence of migration velocity on droplet size would be expected, and no such dependence was found. It is possible that in this experiment variations in velocity due to local temperature gradient differences and changes in ambient temperature masked any variation due to differences in droplet size. In order to make satisfactory measurements of droplet size against velocity it would be necessary to maintain a constant and uniform temperature gradient across the substrate. The present experiment was designed to give the ratio of unmodified to modified droplet velocities under unspecified conditions of temperature gradient and ambient temperature.

7) Undercoolings for nucleation

Undercoolings for nucleation for a number of droplets were measured as described in section 2) of this chapter, using a cooling and heating rate of 0.6°C/S. Droplets were cooled through their freezing points and then heated to their melting points, the difference between these temperatures being taken as the undercoolings for nucleations. Melting and freezing caused a change in the surface appearance of droplets and could readily be detected. A {111} silicon substrate was used for this experiment.

Undercoolings were measured for 15 droplets, and in 14 of these lay between 15°C and 30°C. The other droplet was only partially melted and solidified at a 3°C undercooling.

Since thermal analyses have shown that the eutectic generally nucleates at an undercooling of less than 10°C, it is concluded that the {111} face of silicon is not an active nucleating agent for the eutectic.

8) Aluminium-silicon orientation relationship

In order to determine whether or not any epitaxial relationship existed between the aluminium phase in the eutectic droplets and the silicon substrate, back reflection Laue X-ray photographs were taken of a number of droplets. The camera had a specimen to film distance of 30 mm, and the exposure time was about three hours.

Each photograph showed reflections from the silicon substrate as well as the eutectic aluminium - plate (26) -, but the aluminium reflections formed Debye rings, indicating that the aluminium phase was polycrystalline.

This does not however rule out the possibility of an epitaxial relationship being present at nucleation since as

Hogan et al (55) have shown, the orientation of the aluminium phase of the eutectic changes during growth due either to the nucleation of new grains of the development of subgrams.

9) Growth layers - results

Growth layers were formed using eutectic droplets of about 0.2 mm and 2 mm diameter melted onto {111} oriented silicon substrates, heated about 200°C above the eutectic temperature and cooled at rates of 0.6°C/S and 150°C/S. Both undoped and strontium doped droplets were examined, and one 2 mm droplet was melted under a sodium flux and slow cooled. Sections through large and small droplets are shown in plates (27 to 30).

The experimental observations are summarised below.

1) Both modified and unmodified droplets formed a growth layer on cooling. This layer was of approximately constant thickness, extending up the sides as well as across the base of the droplet. Often sections showed that the growth layer was thickest in the centre of the droplet. Etching revealed no systematic differences between the growth layers of modified and unmodified droplets.

2) The 2 mm diameter droplets, both slow and fast cooled and both modified and unmodified contained large crystals of primary silicon in the body of the droplet. Etching showed these crystals to be twinned - plate (31) -, while the growth layer did not show any twin traces - plate (32) -. These twinned crystals were observed both growing up from the base and down from the top of the droplets. It was shown that some of the twinned crystals were continuous with the growth layer by etching away the aluminium phase and looking

vertically downwards into the pit dissolved out in the substrate. By this technique twinned silicon crystals could be seen projecting out of the growth layer - plates (33 to 36) -. All these crystals that were examined contained two or more twin planes, each face thus containing at least one ridge and groove - fig (27) - Sections through the 0.2 mm diameter droplets did not always reveal any twinned crystals.

3) Growth layer thicknesses were about 10^{-2} mm for the small 0.2 mm diameter droplets and about 5×10^{-2} mm for the large 2 mm diameter ones. Growth rates were calculated by dividing the thickness of the growth layer by the time taken to cool from the maximum temperature to the eutectic temperature. A cooling rate of $0.6^{\circ}C/S$ gave a growth rate of about 10^{-4} mm/s while a rate of $150^{\circ}C/S$ gave a rate of the order of 10^{-2} mm/s.

4) The surface of the growth layer - plate (37) - showed some curious "rivulet' markings, apparently due to irregularities in the surface.

10) Growth layers - discussion

The results indicate that layer growth perpendicular to the $\{111\}$ plane in silicon can proceed at rates up to at least 10^{-2} mm/s. When twins were present, probably formed by growth accidents in the growth layer, they enabled much more rapid growth of silicon to occur, the twin plane reentrant grooves providing favourable sites for the nucleation of new layers. Since the layers appeared to be thicker in the middle of the droplets than at the edges it would seem that new atomic layers nucleate and grow at sites on the layer, rather than propagating

across the layer from favourable sites for deposition where the layer meets the concave droplet sides. Thus there would appear to be no great difficulty in nucleating new atomic planes on a {111} facet in silicon growing from an aluminium solution.

According to the Jackson model of a solid-liquid interface, the change in free energy ΔF of a plane when a proportion x of surface sites are occupied or vacant is given by, (4),

$$\Delta F = \frac{NkL\xi\, x(1-x)}{R} + NkT_E\left[x\log_e x + (1-x)\log_e(1-x)\right]$$

Where L is the latent heat of fusion.

N, k, are constants.

R is the gas constant.

T_E is the temperature.

ξ is the proportion of nearest neighbour atoms lying in a given plane.

The equilibrium concentrations of additional atoms or vacancies are obtained by differentiating this expression and putting the result equal to zero. Thus we obtain:

$$\alpha(2x - 1) = \log_e\left[x/(1-x)\right]$$

Considering only terms to the first order in x, which is justified for faceted crystals where x is small, the solution is

$$x = \frac{1}{e^{\alpha} - 2\alpha + 1}$$

Where $\alpha = \frac{L\xi}{RT_E}$

Thus x varies with α which depends on the latent heat of fusion of the crystal, the temperature at which it grows and the orientation of the growing face. For a {111} face on silicon ($\xi \sim 1/2$) at the eutectic temperature (750°K), α is calculated to be 4. Inserting this value in the expression for x gives the equilibrium proportion of additional atoms to be 2×10^{-2}. If these were arranged in steps, their spacing would

then be about 50 atomic spacings, so the velocity of lateral propagation of steps needs to be about 50 times faster than the rate of addition of new layers normal to the close packed plane. A growth rate of 10^{-2} mm/s thus requires a lateral propagation velocity of 0.5 mm/s.

Knowing the equilibrium concentration of additional atoms, the Kinetic undercooling during growth of a plane at a given velocity can be calculated as follows. See fig (28).

V is the growth rate.

R_F is the freezing rate.

R_M is the melting rate.

ν is the molecular vibration frequency.

d is the molecular diameter.

Δg is the activation energy for diffusion in the liquid.

ΔG is the difference in bulk free energy between liquid and solid.

$$V = R_F - R_M$$

$$\therefore V = \frac{\nu d}{p}\left[\exp\left(\frac{-\Delta g}{RT}\right) - \exp\left(\frac{-\Delta g - \Delta G}{RT}\right)\right]$$

Where p is the probability of a molecule in the liquid jumping to a favourable site on the surface. The probability of a jump in a given direction is 1/6, and if the step spacing is 50 atoms, the probability of a jump towards the surface reaching a favourable site is 1/50. Thus here p = 1/300.

As $x \longrightarrow o$, $\exp(-x) \longrightarrow 1$, and since ΔG is much greater than Δg we can approximate

$$V = \frac{\nu d}{300}\left[1 - \exp\left(-\frac{\Delta G}{RT}\right)\right]$$

When x is small, $1 - \exp(-x) \simeq x$

so $$V \simeq \frac{\nu d}{300}\ \frac{\Delta G}{RT}$$

or since $\Delta G = \Delta S\, \Delta T$

$$V \simeq \frac{\nu d \Delta S \Delta T}{300\ RT}$$

$$\text{i.e. } \Delta T \simeq \frac{300\ RTV}{\nu d \Delta S}$$

Inserting numerical values, for the {111} facet of silicon at the aluminium-silicon eutectic temperature

$$\Delta T \simeq 0.1V, \text{ V being in mm/s}$$

Thus at $V = 10^{-2}$ mm/s, $T = 10^{-3}$°C, so under these conditions, layer growth of silicon normal to {111} does not require a large kinetic undercooling.

It has been pointed out that there was no apparent qualitative difference between modified and unmodified growth layers. If, as has been suggested, the function of the modifying impurity is to impede growth by adsorbtion on the most favourable sites, the effect will be to reduce the probability of a jump to a favourable site by a further factor, so increasing ΔT. Thus layer growth will still take place, but at a higher kinetic undercooling, depending on the proportion of sites poisoned.

The observation that the growth layers are thicker in the middle than at the edges is thought to be due to the rejection of solute at the edges from both the base and sides of the droplet slowing growth there. Assuming mixing by diffusion only, Tiller (58), derives an expression for the concentration of solute in the liquid ahead of a growing interface. He obtains an expression for a characteristic distance in which the solute concentration reaches an equilibrium value. This distance is given by D/kR where D is the diffusion coefficient, k the solute partition coefficient and R the growth rate. Because k for aluminium in silicon is very small ($\sim 10^{-4}$), this distance is large, of the order of centimetres, so in these droplets an equilibrium concentration of solute at the interface is never reached.

Hot Stage

Fig 19

Section

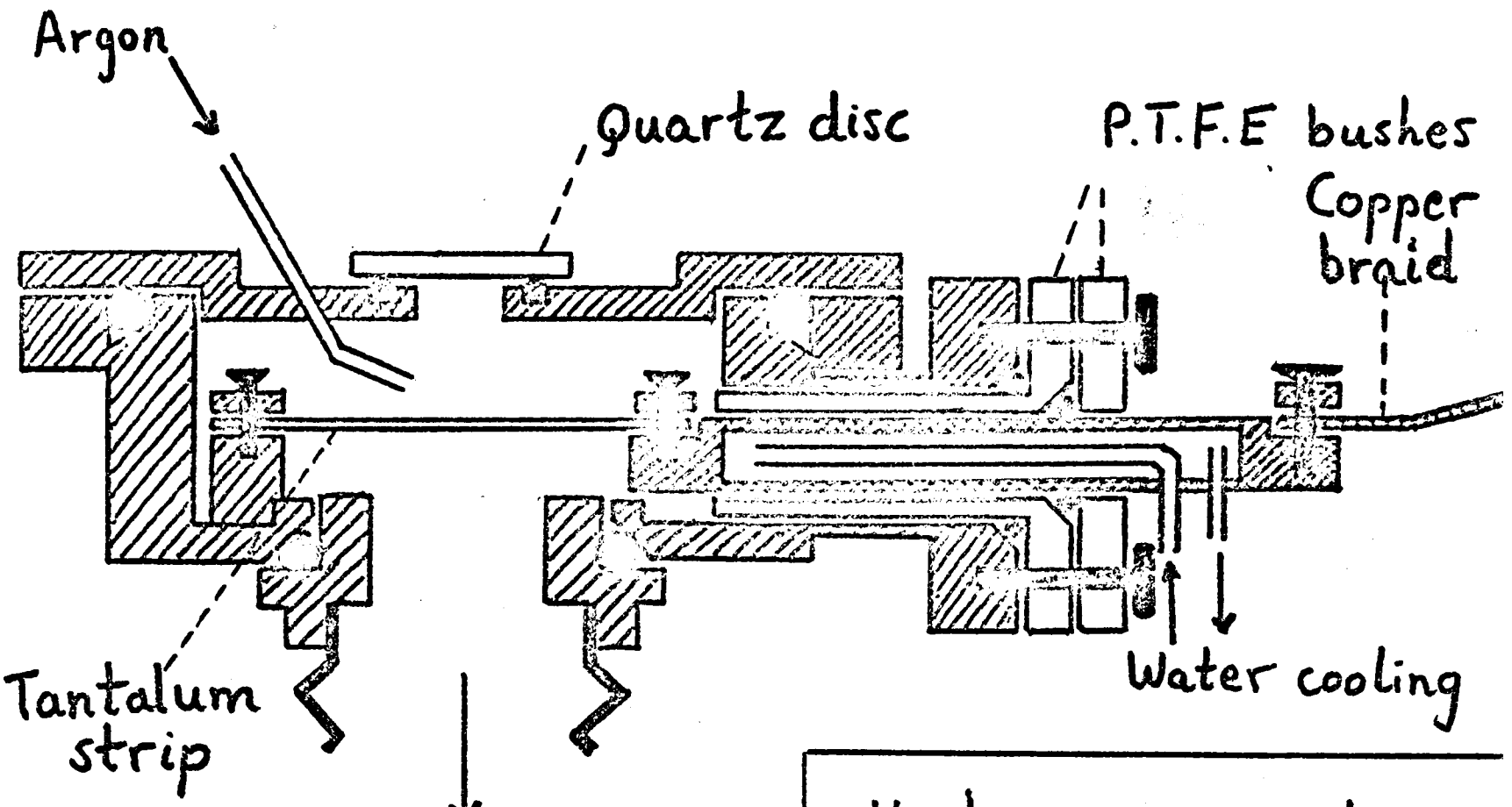

Heater cross-sections

Normal

G

Temperature gradient.

Top view.

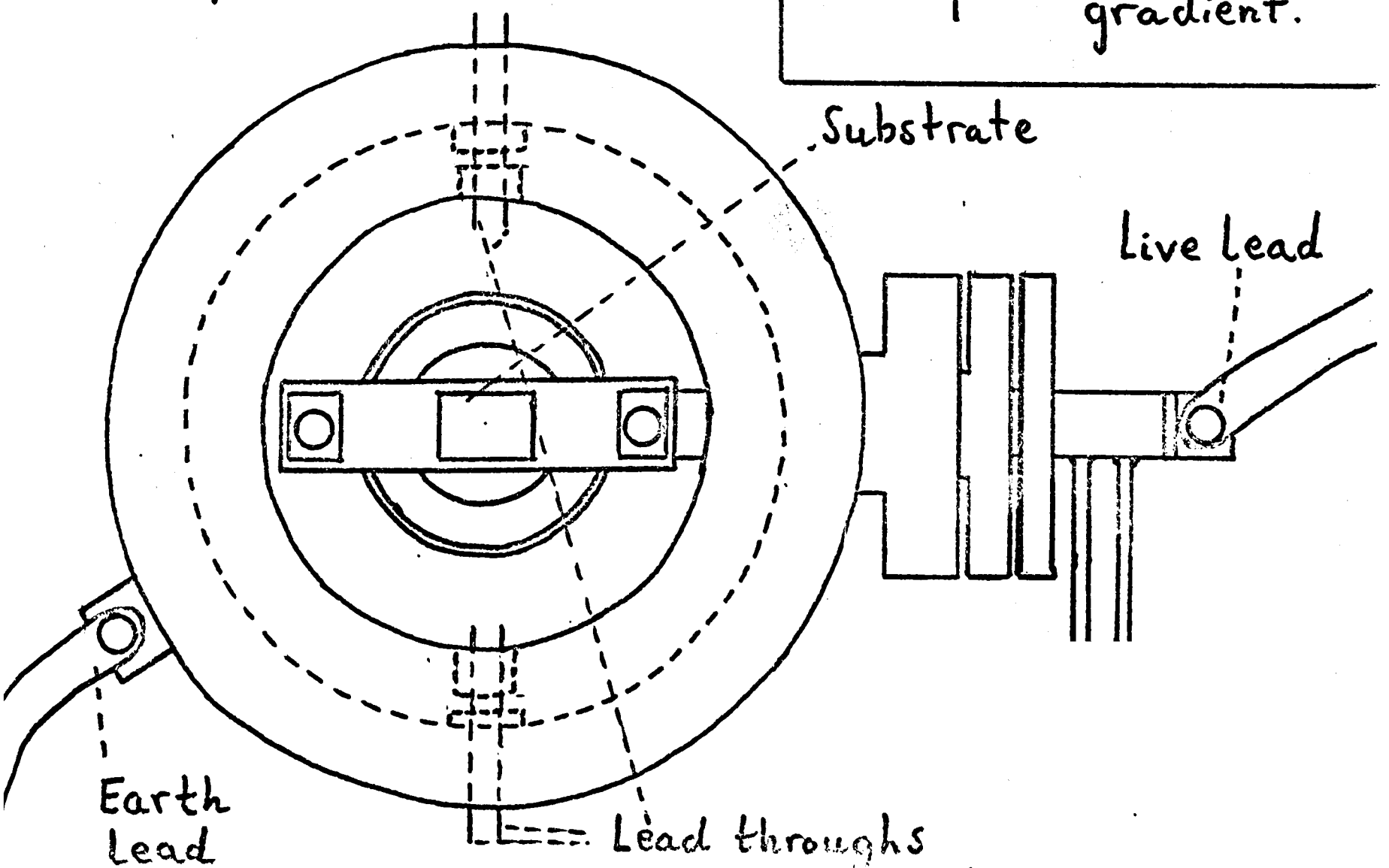

Fig 20

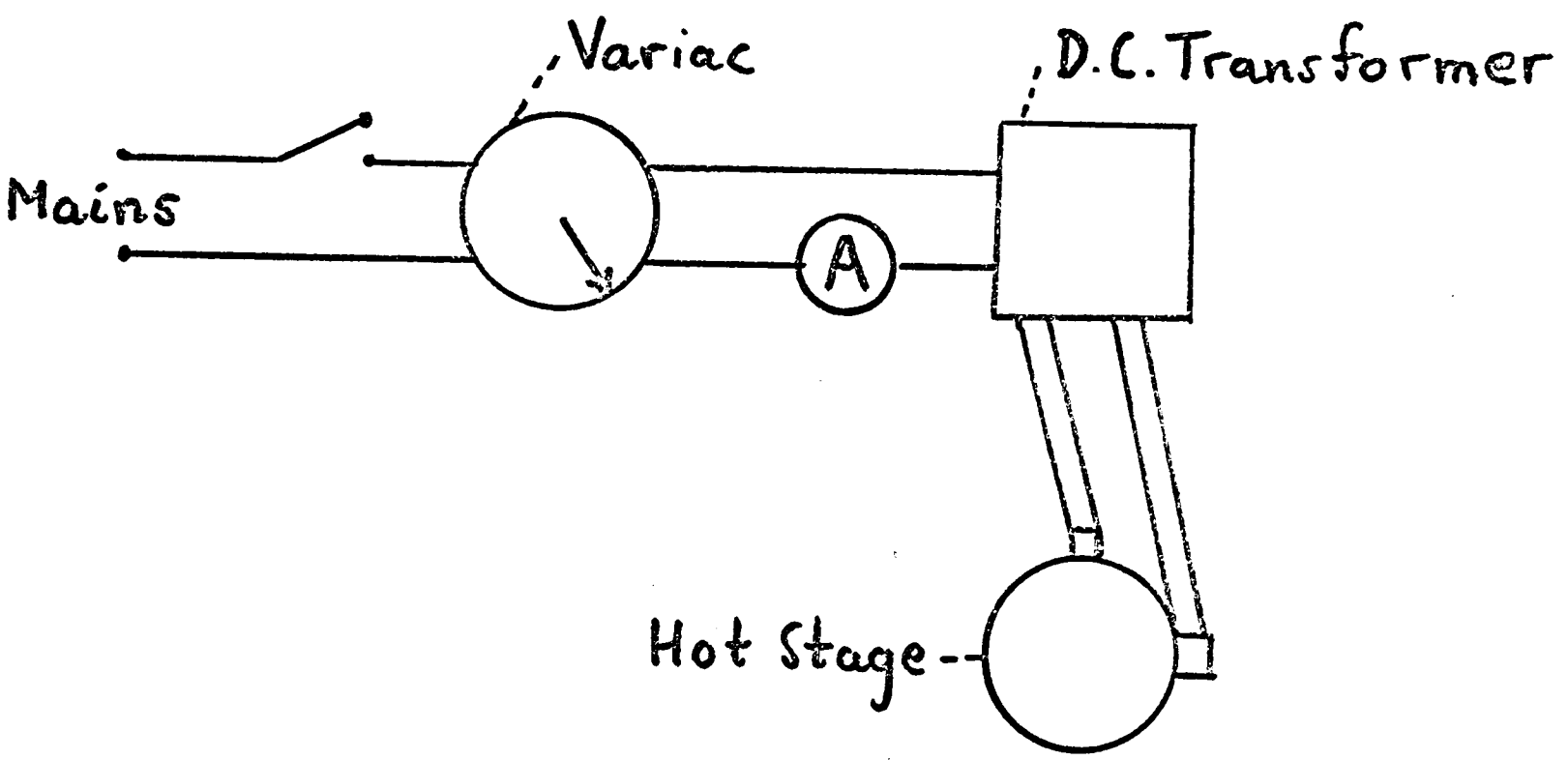
Variac
D.C. Transformer
Mains
A
Hot Stage

Fig 21

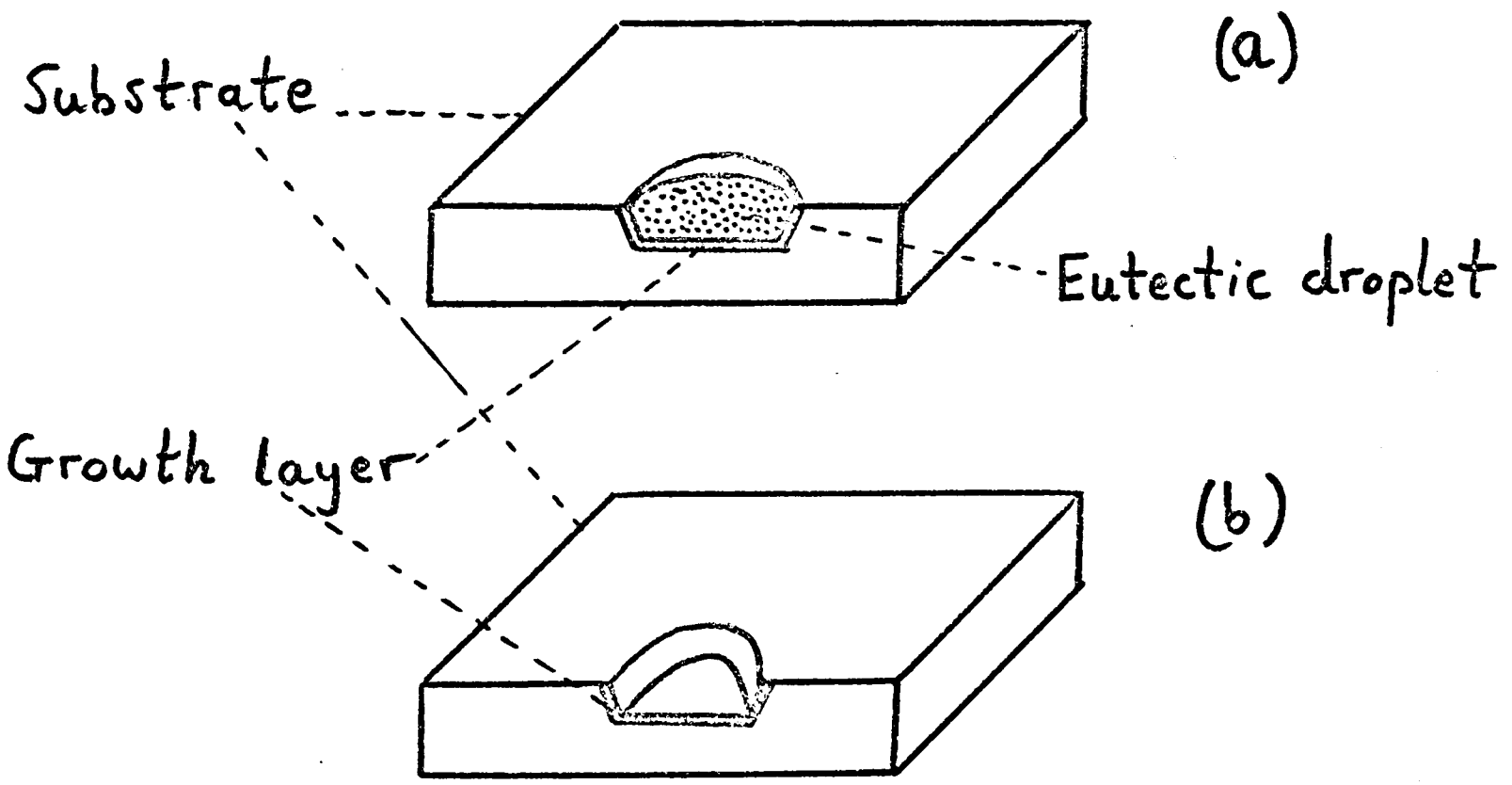
Substrate
(a)
Eutectic droplet
Growth layer
(b)

Fig 22

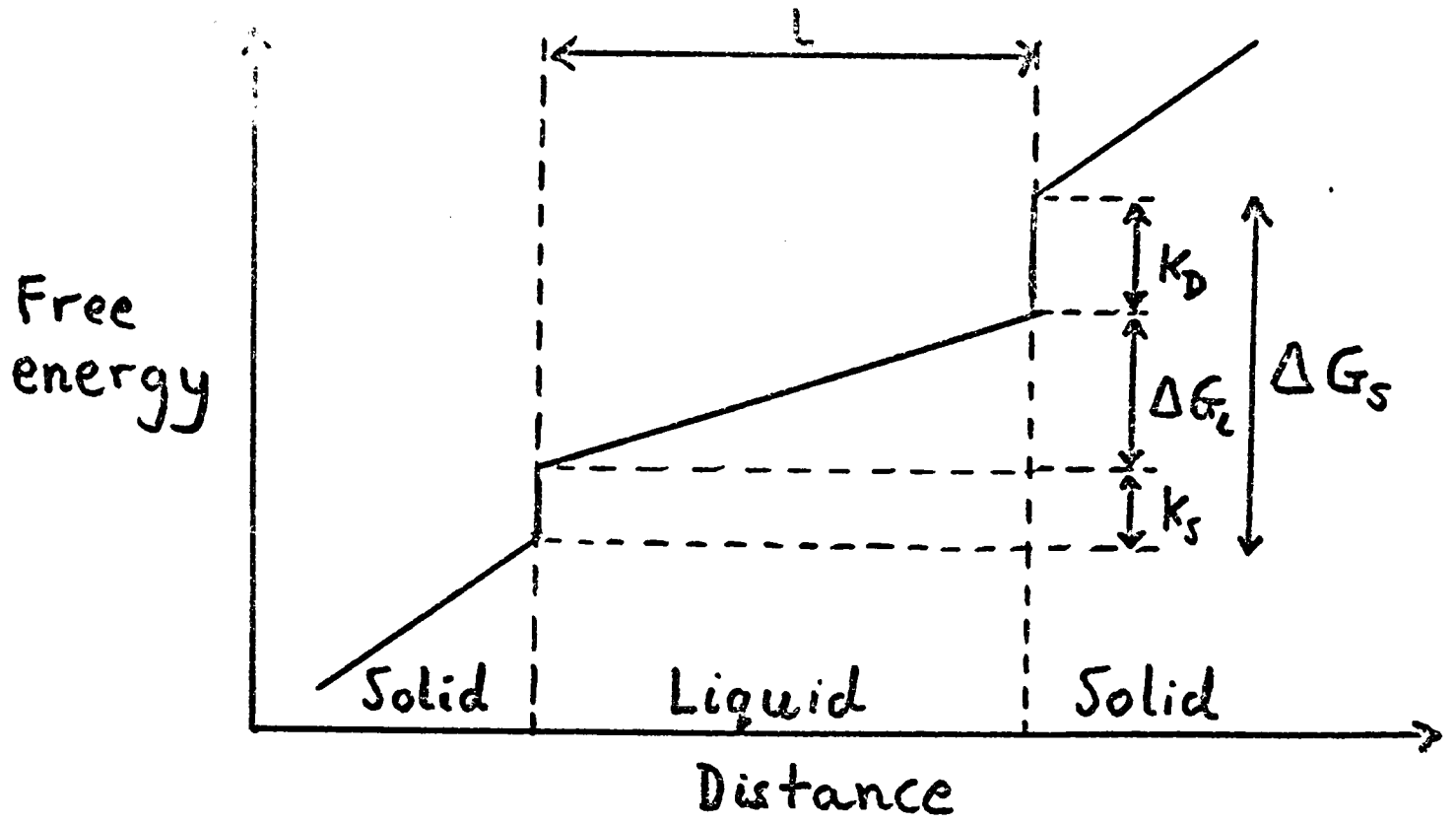

Fig 23

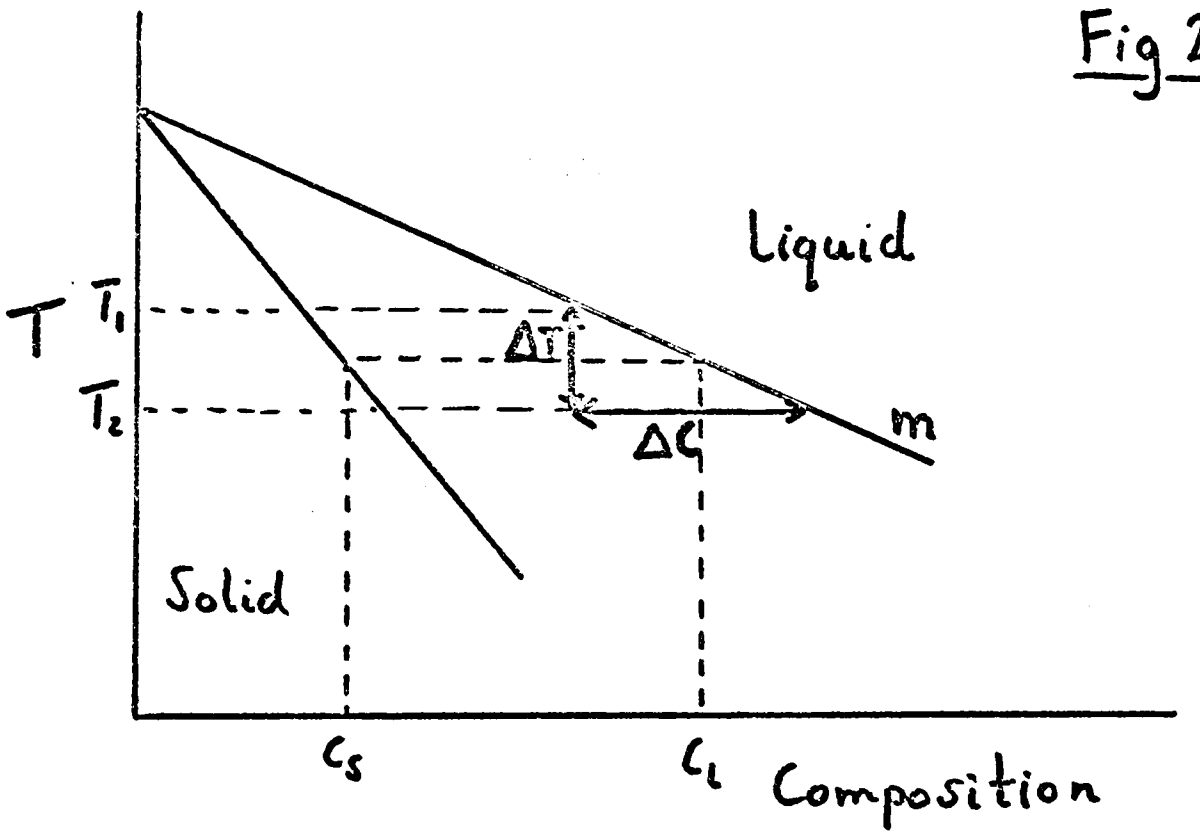

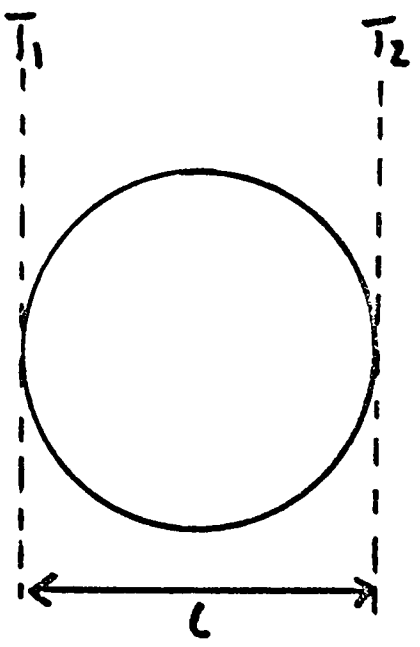

$$G = \frac{T_1 - T_2}{l}$$

Fig 24(a)

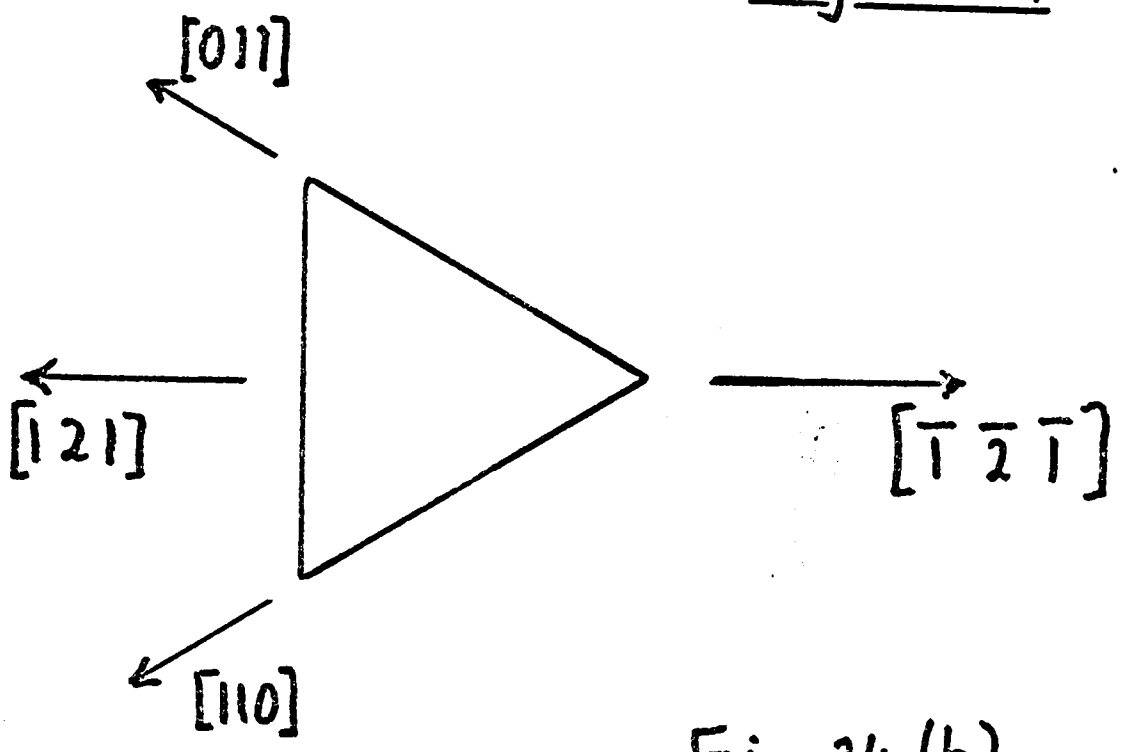

Fig 24(b)

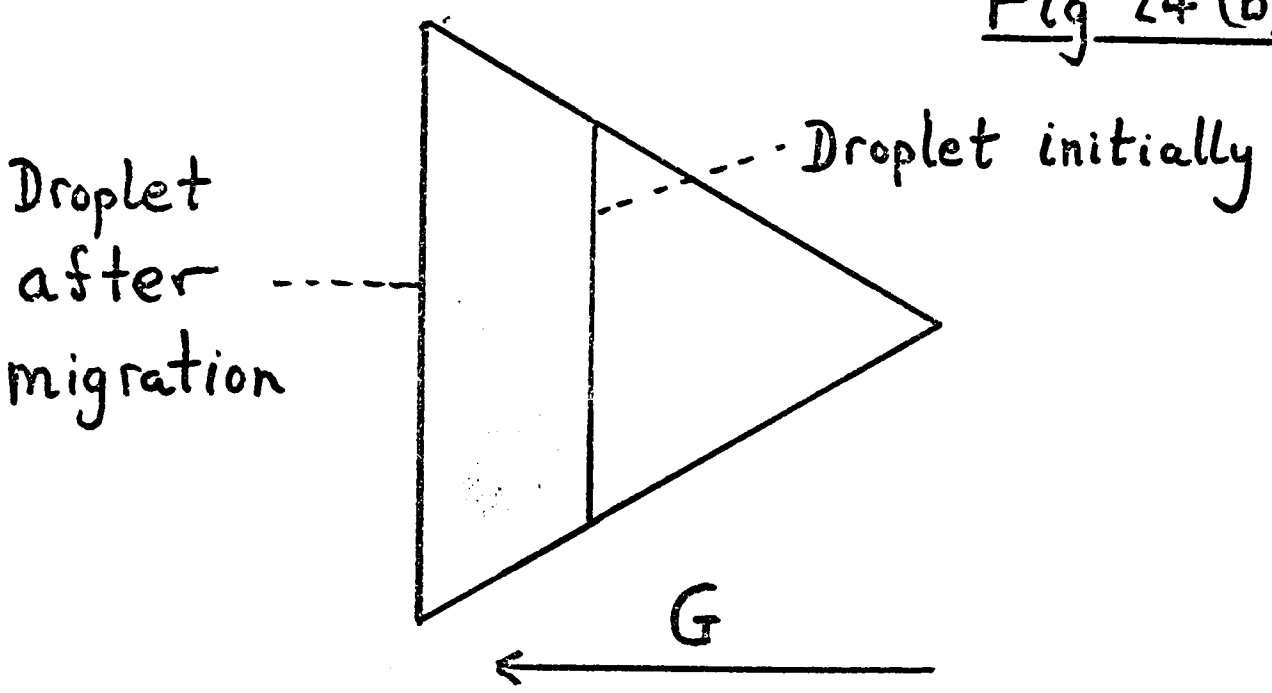

Fig 25

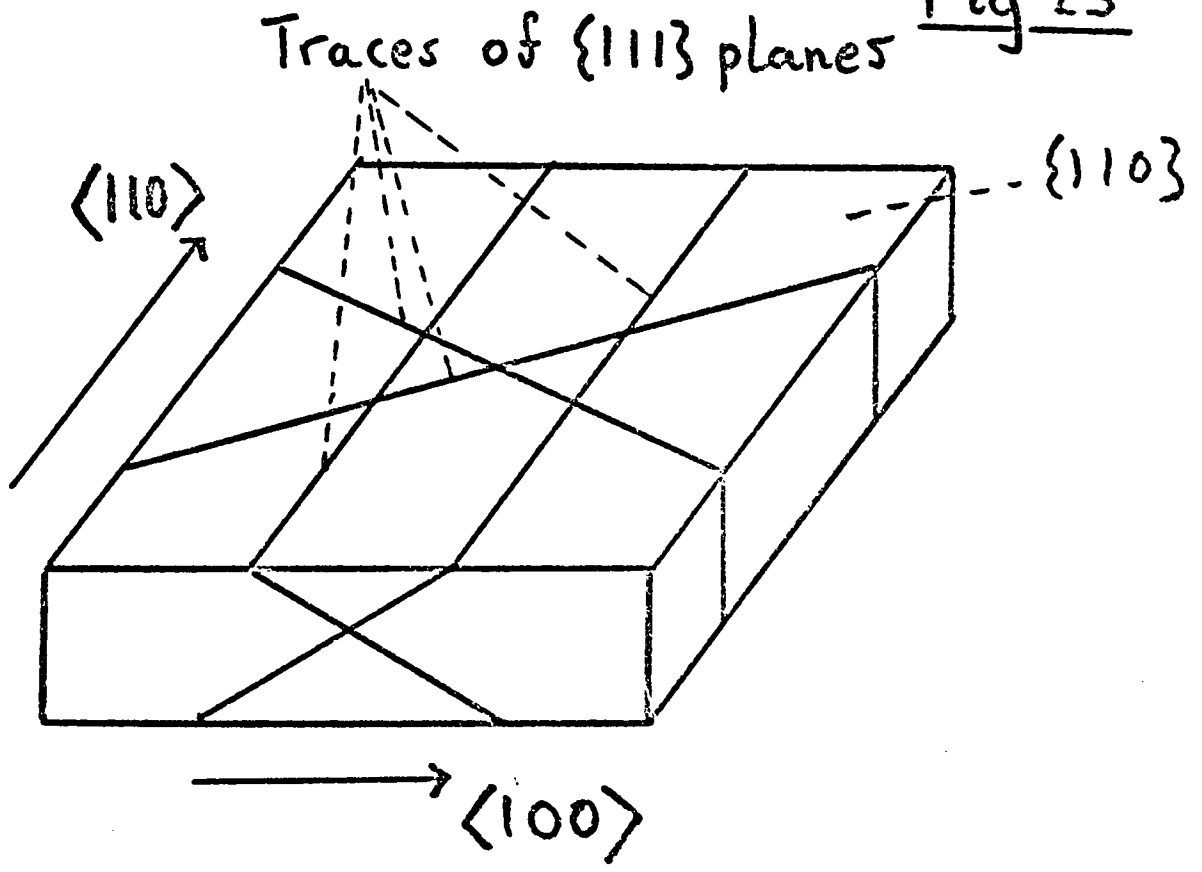

Fig 26

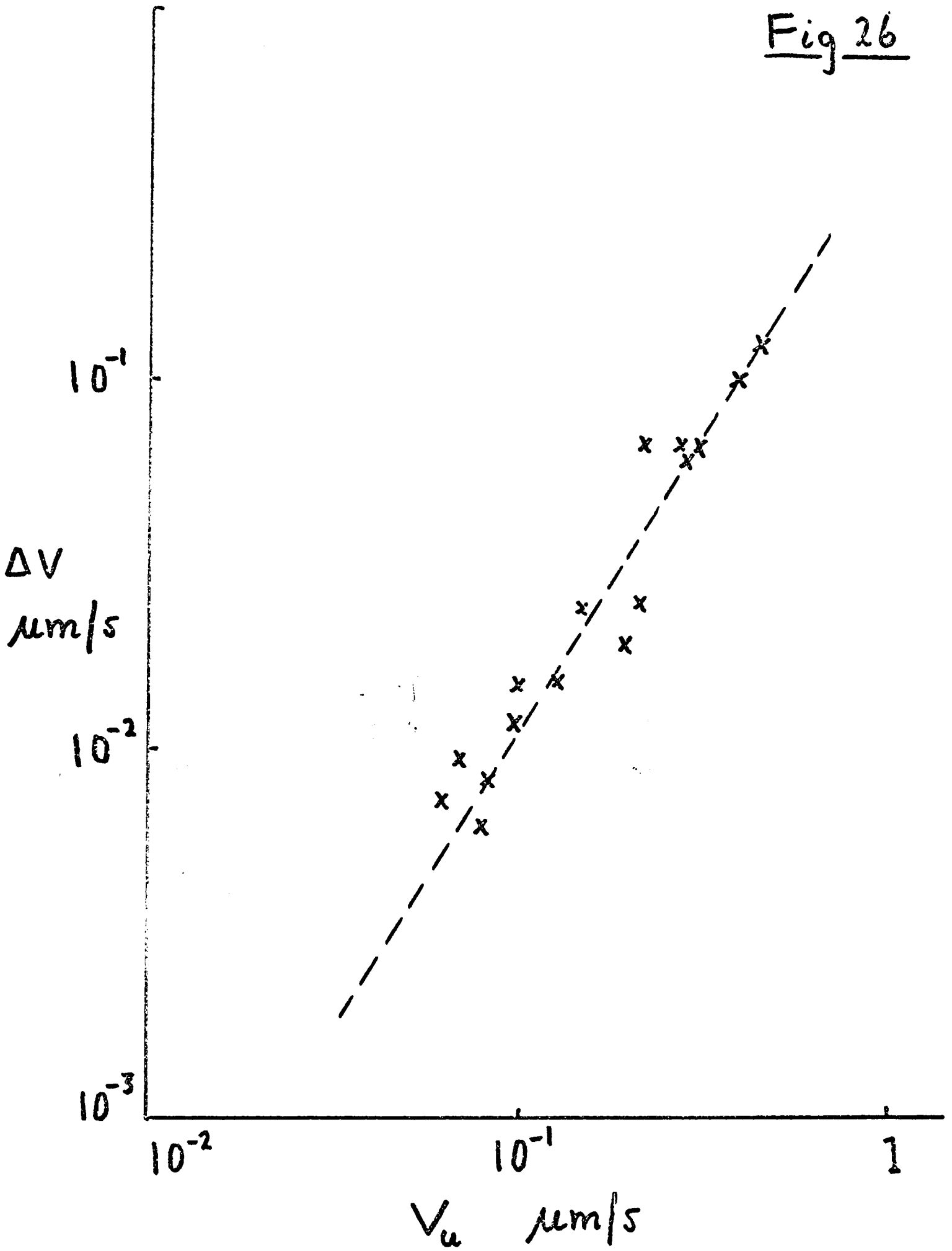

Fig 27

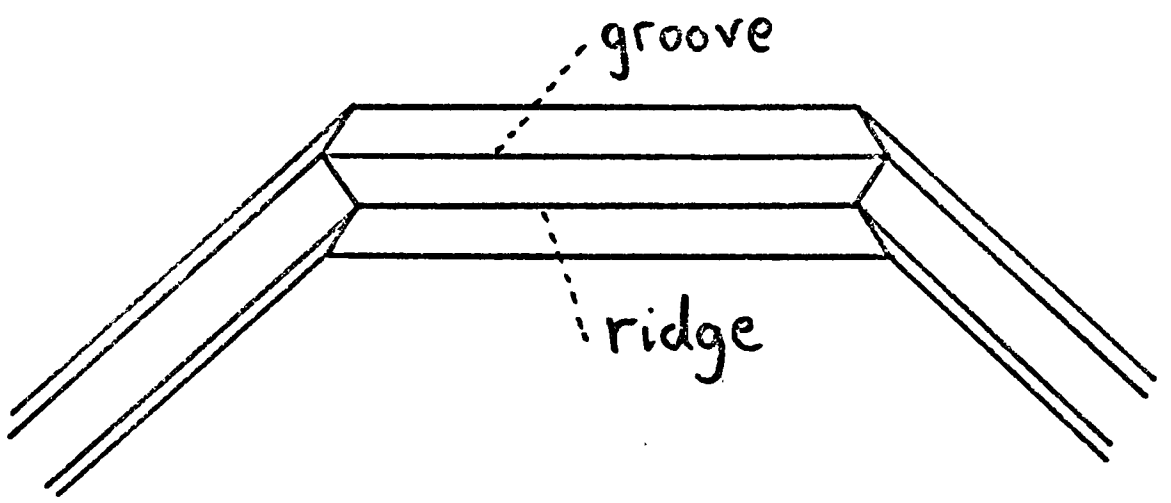

Fig 28

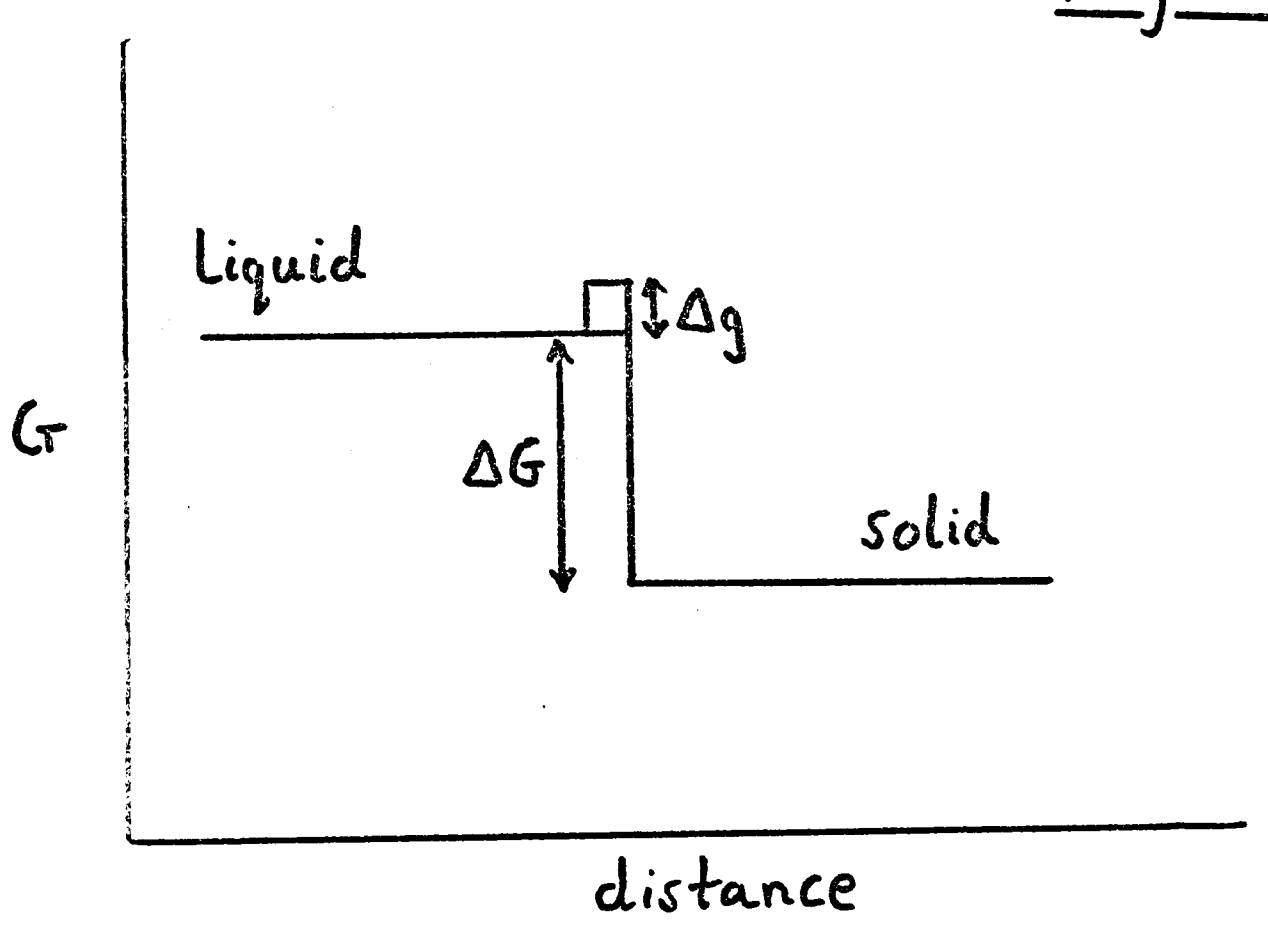

Plate 23 Droplet etched away after migration on {110} substrate

X 700

Plate 24 Droplet after migration on {110} substrate

X 140

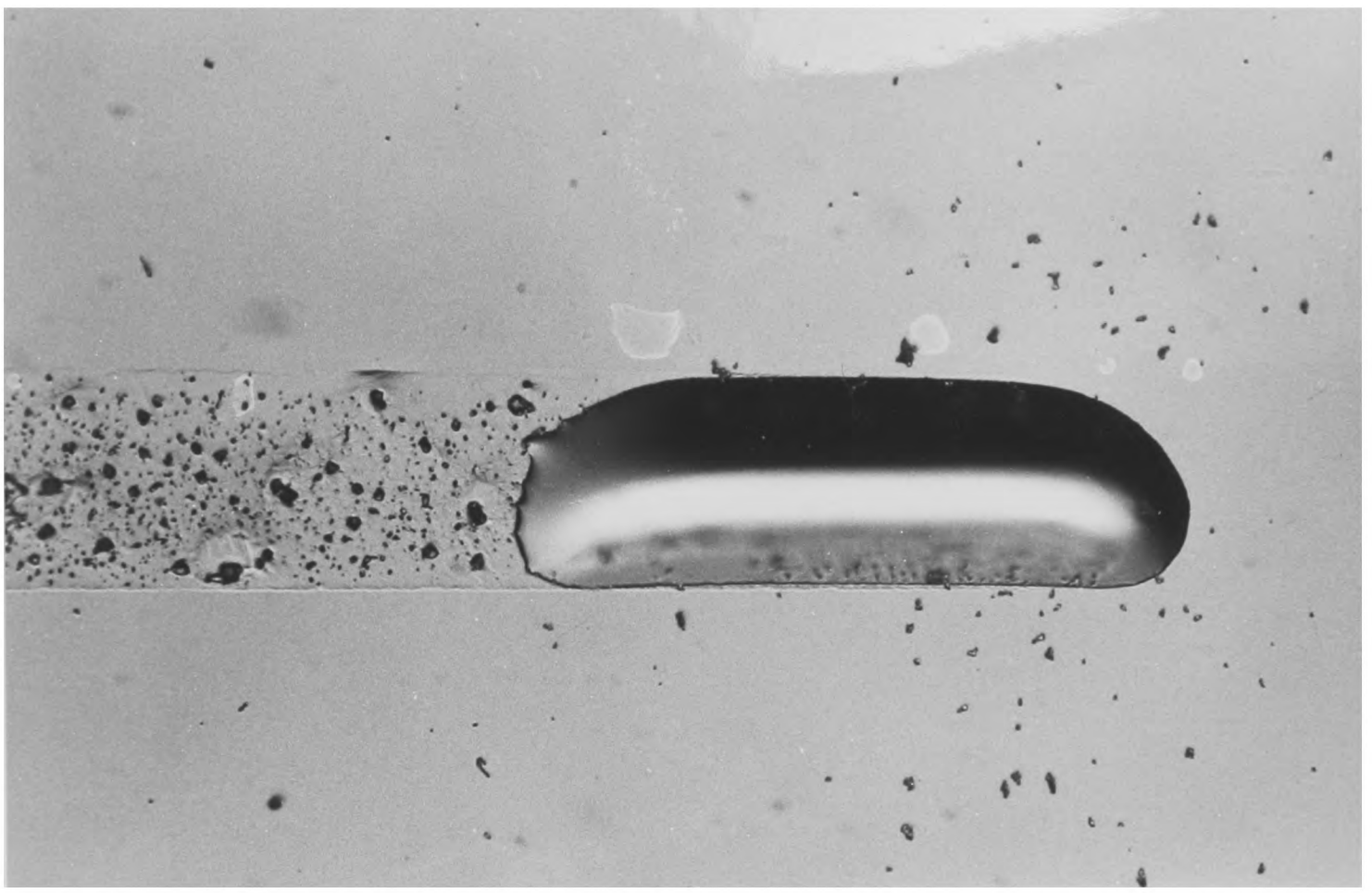

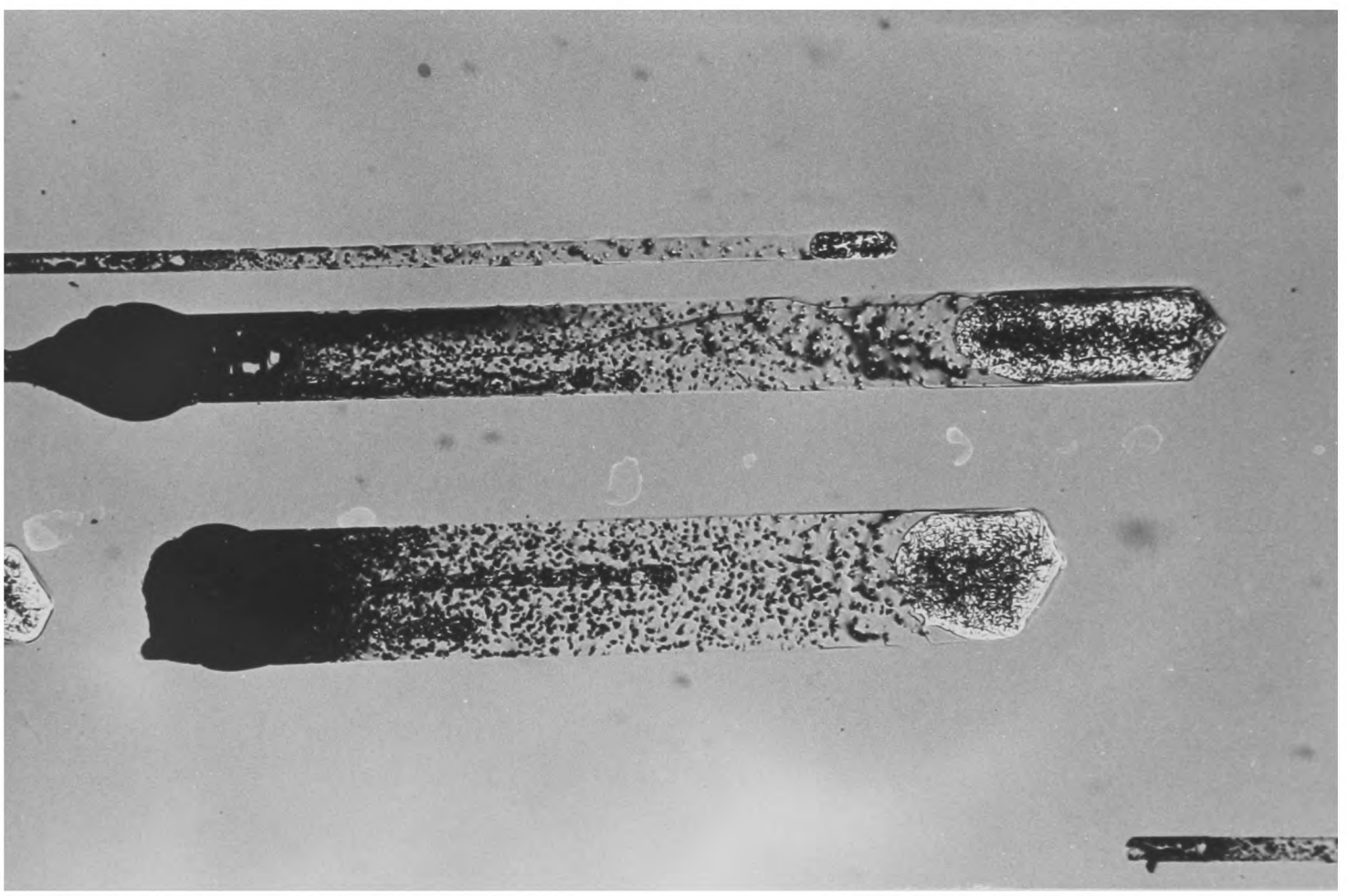

Plate 25 Macrograph of a {110} substrate from which droplet migration measurements were taken.

Plate 26 Back-reflection lane X-ray photograph of eutectic droplet on {111} silicon substrate.

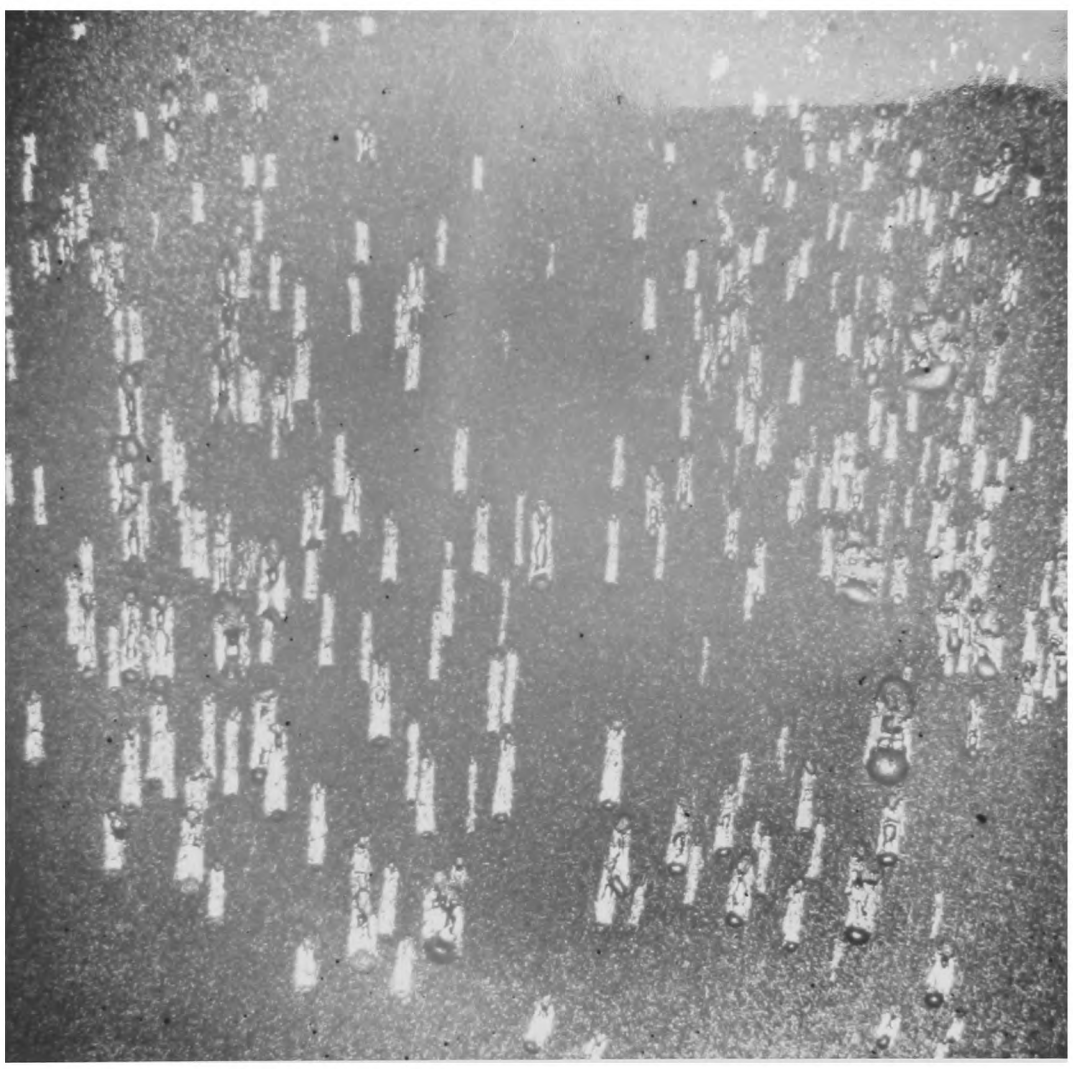

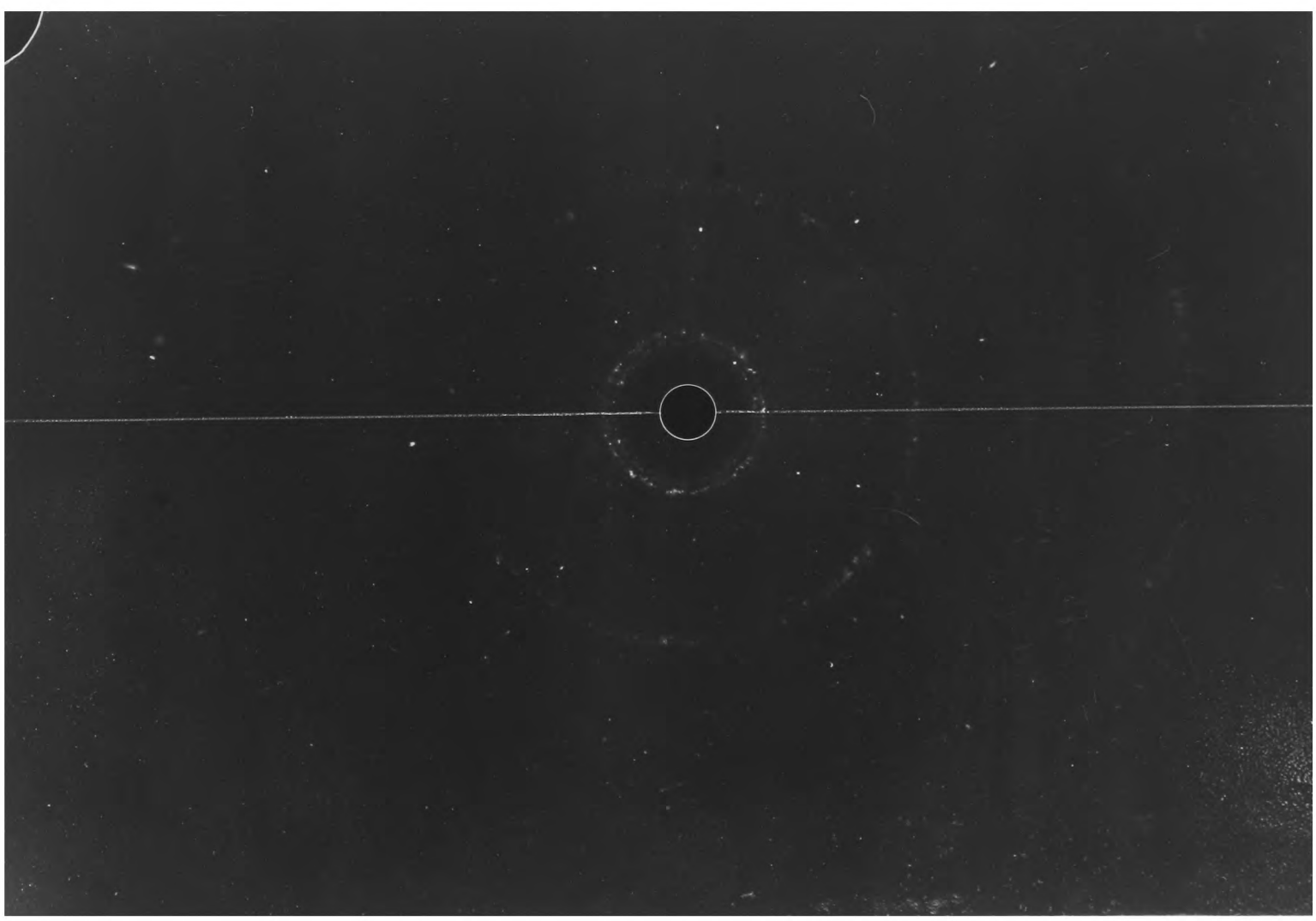

Plate 27 Macrograph of etched section through large droplet. Cooled at 18°C/S. Unmodified. X 40

Plate 28 Macrograph of etched section through large droplet. Cooled at 27°C/S. Strontium modified. X 40.

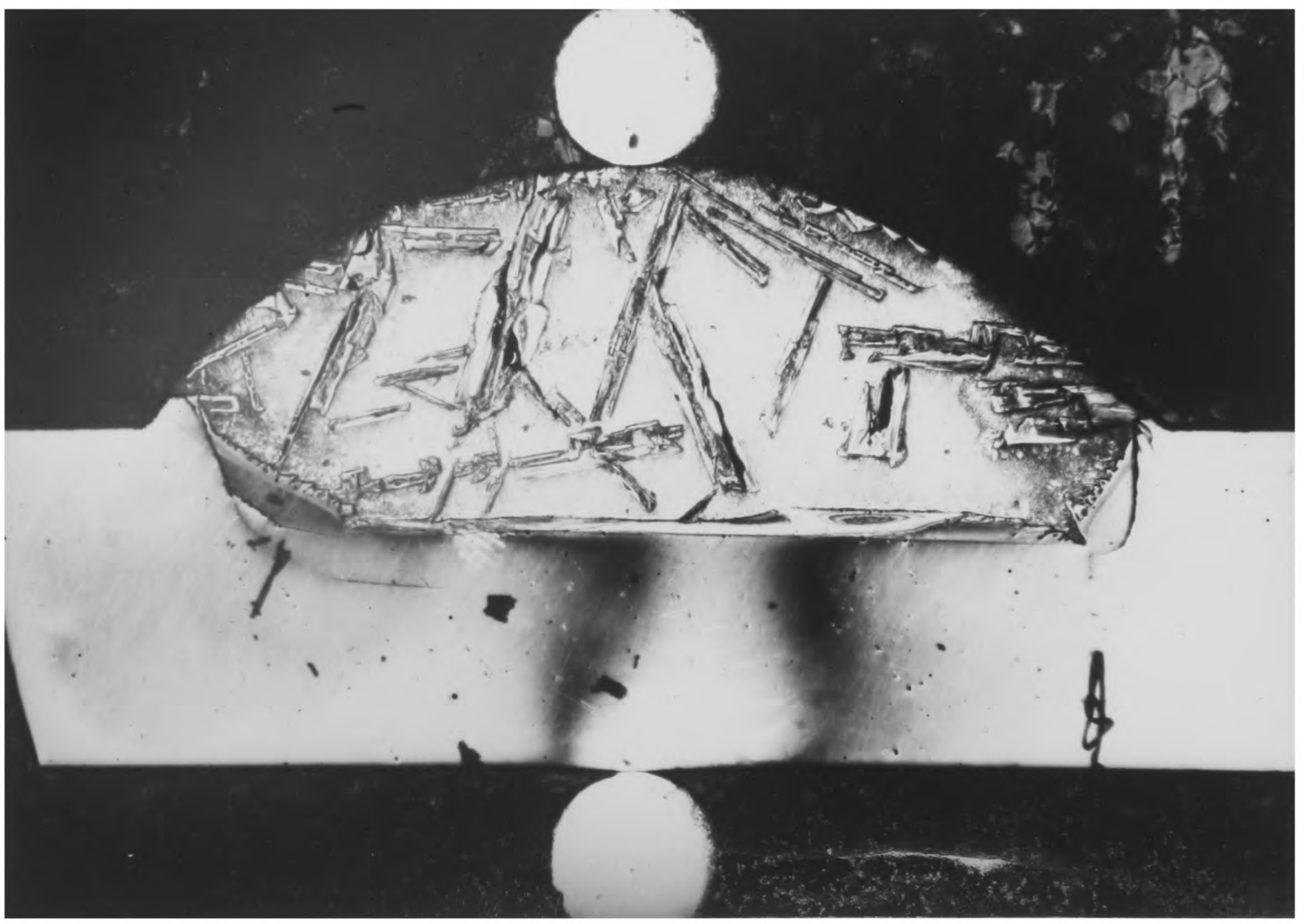

Plate 29

Small droplet. Cooling rate 0.6°C/S. Unmodified x 700. Taper section.

Plate 30

Small droplet. Cooling rate 15°C/S. Strontium modified. x 280. Taper section.

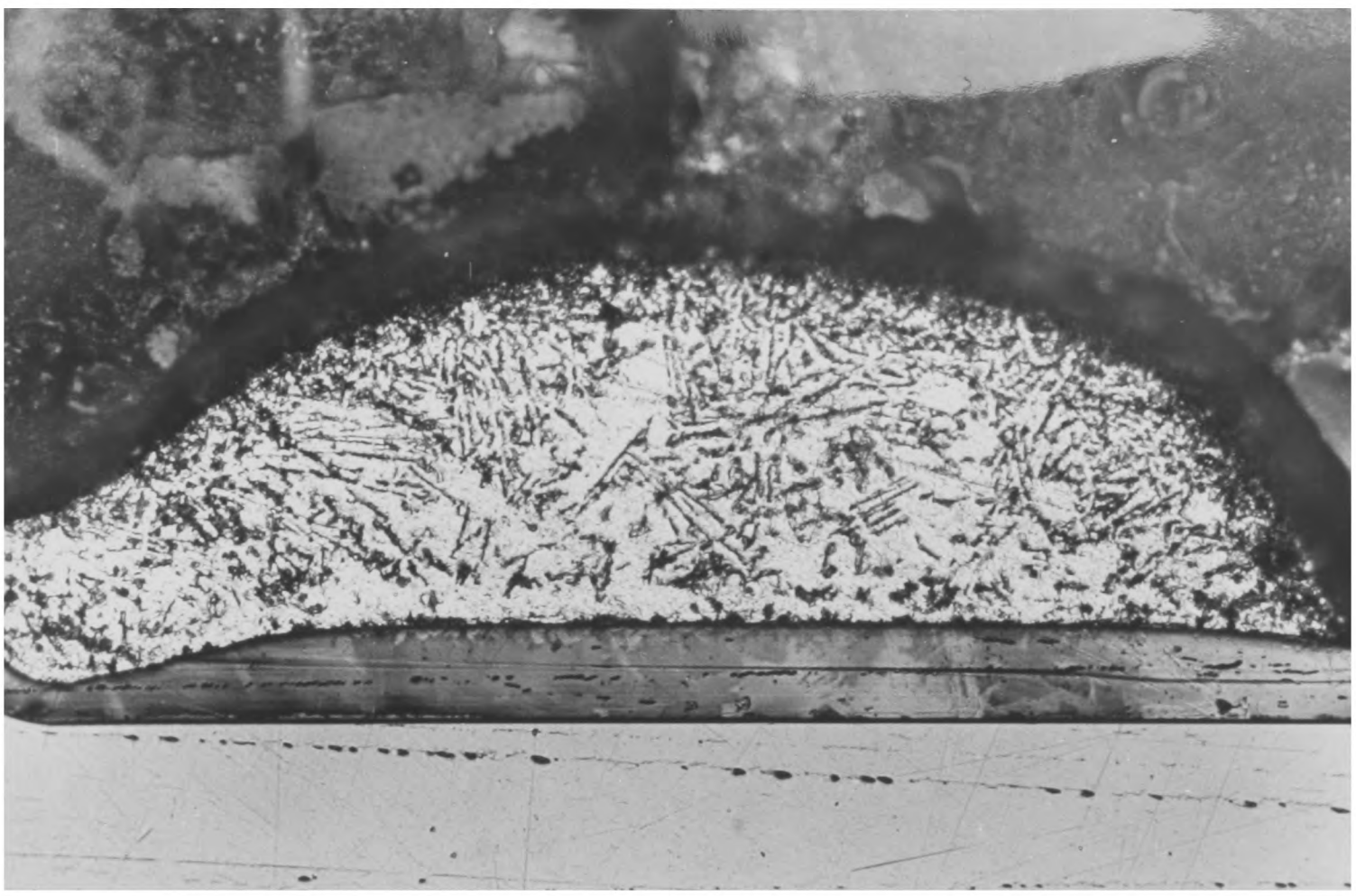

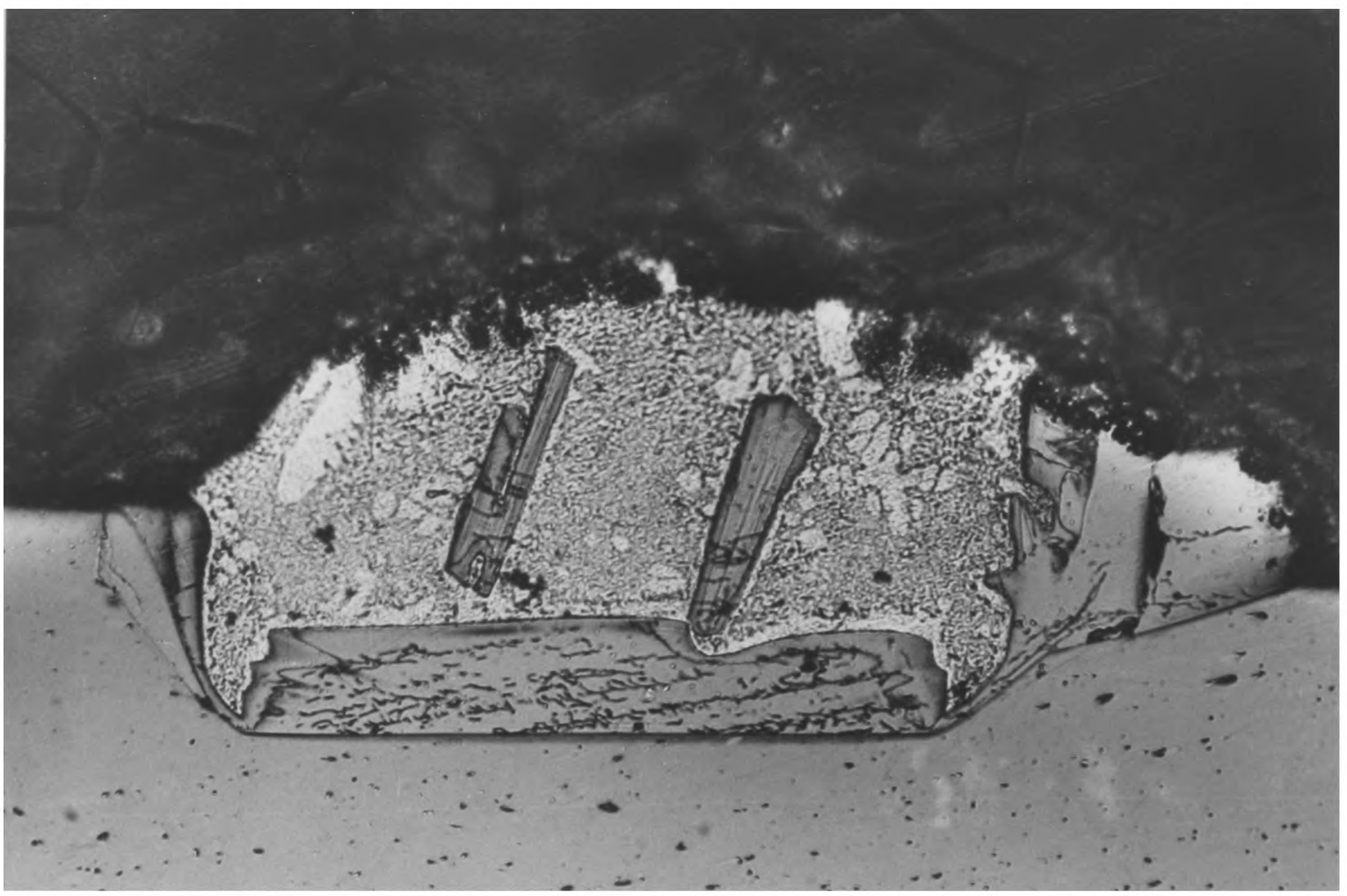

Plate 31 Twinned primary silicon crystal in slow cooled large droplet. X 700. (Etched).

Plate 32 Growth layer in slow cooled large droplet Etched. X 700.

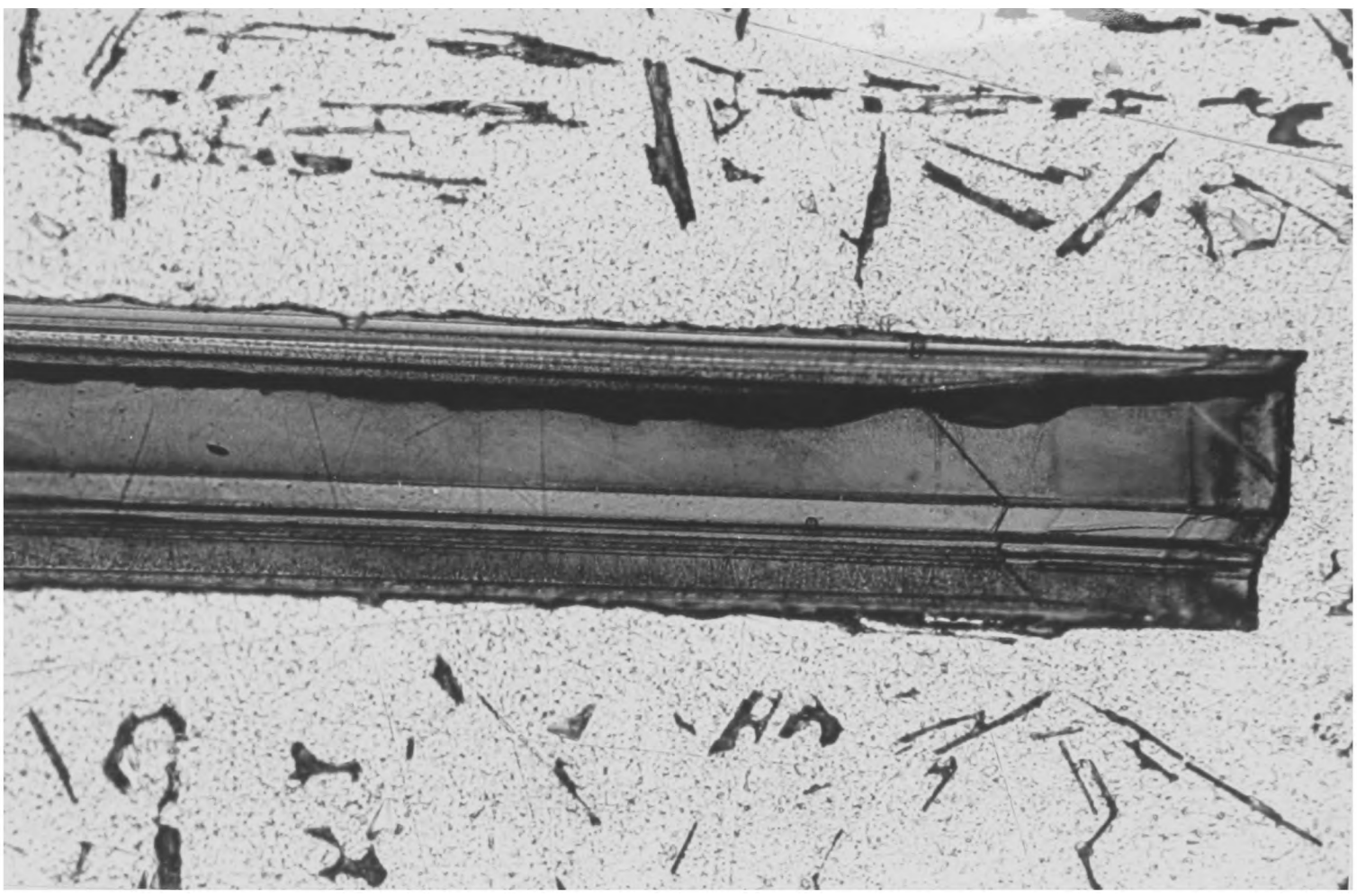

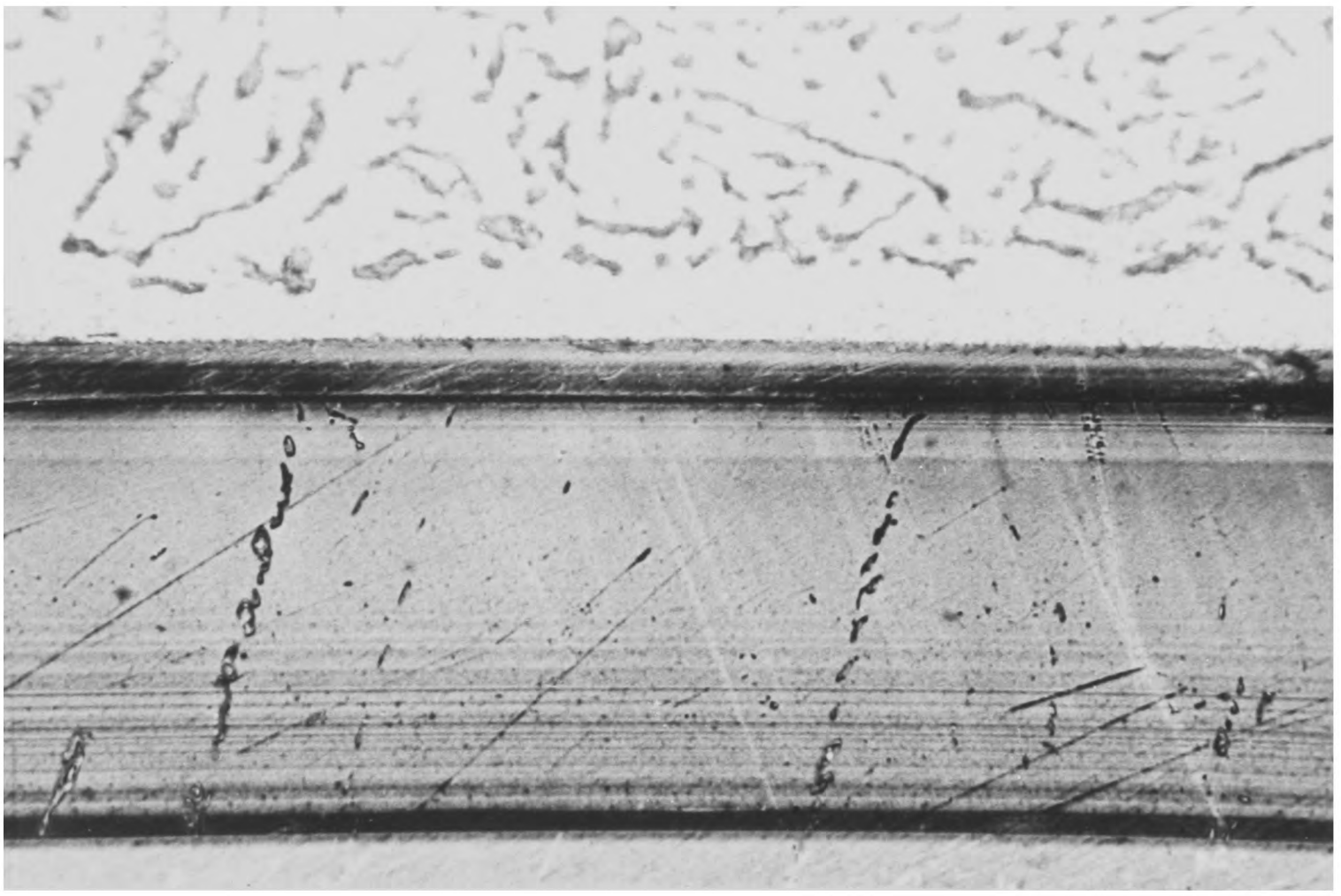

Plate 33 Primary silicon crystal projecting from the growth layer in large droplet, unmodified, cooling rate 15°C/S.

X280

Plate 34 Dark field micrograph corresponding to plate 33.

X280

Plate 35 Primary silicon crystal projecting from the growth layer in large droplet, unmodified, cooling rate 15°C/S.

X280

Plate 36 Dark field micrograph corresponding to plate 35.

X280

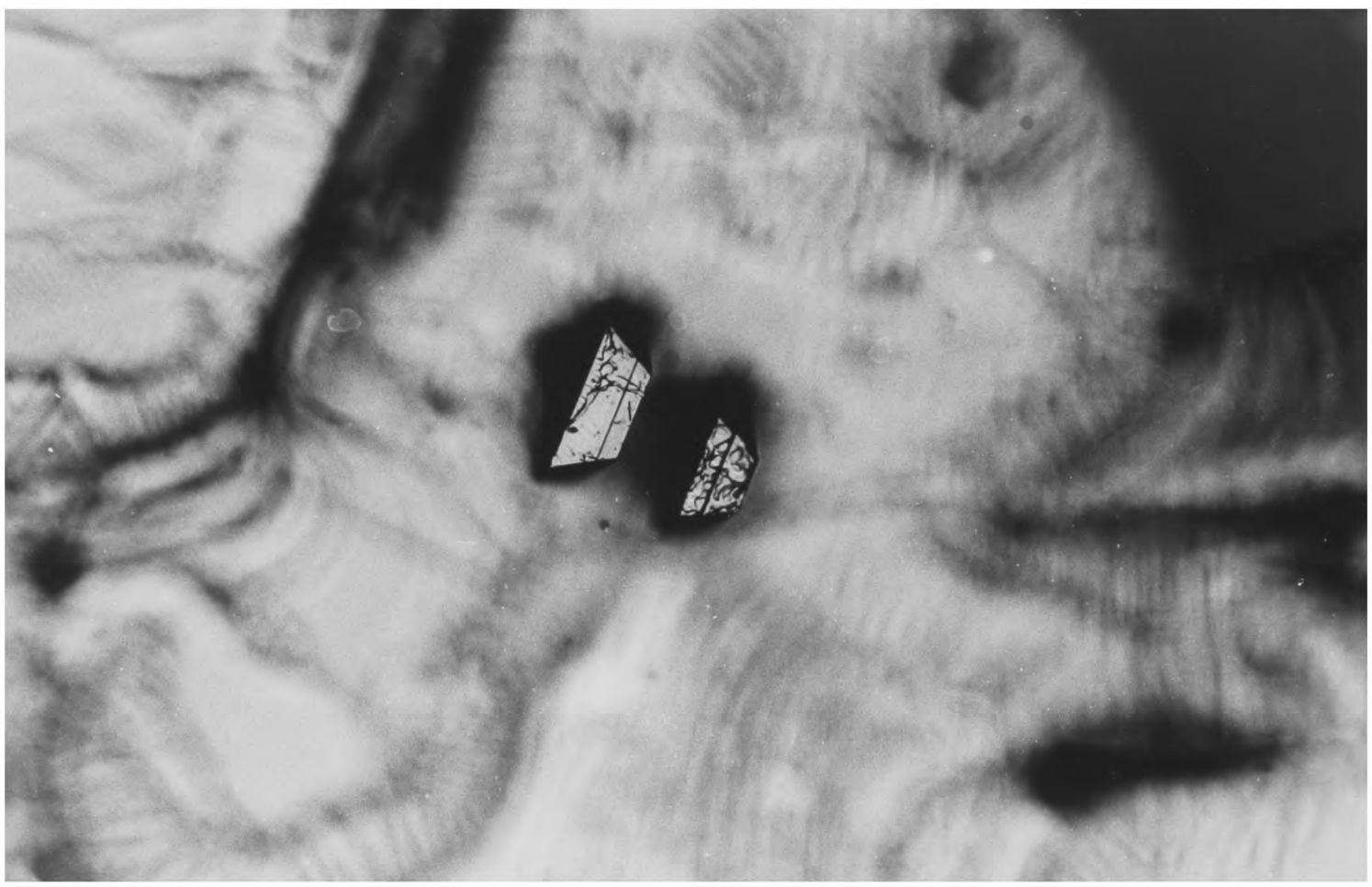

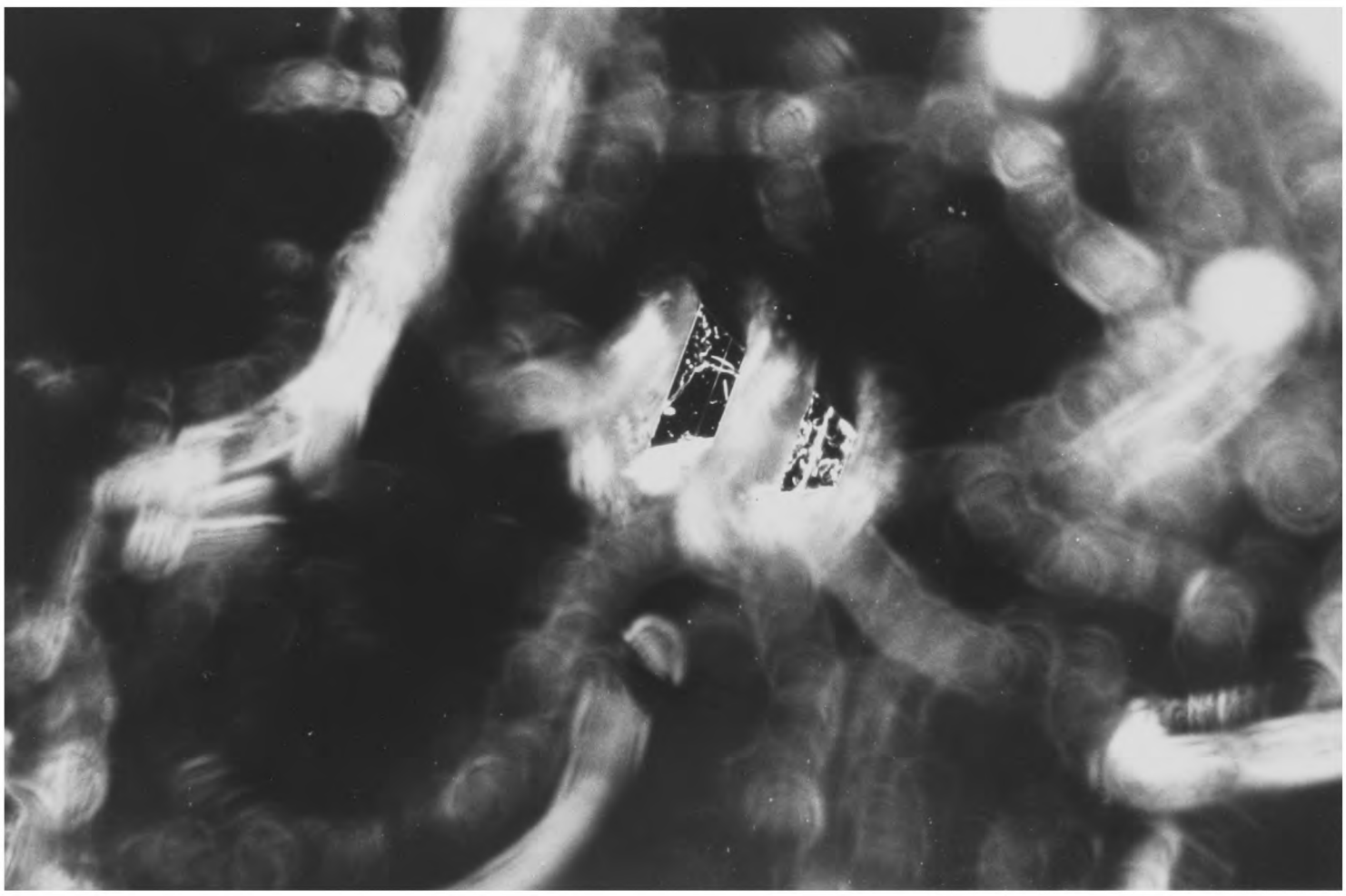

Illustrating the appearance of the surface of the growth layer.

Plate 37 (a) Large droplet cooled at 15°C/S
unmodified ×140

(b) Small droplet cooled at 15°C/S
unmodified ×280

[The imprint of an aluminium dendrite indicates that the 'rivulet' markings are a relief effect.]

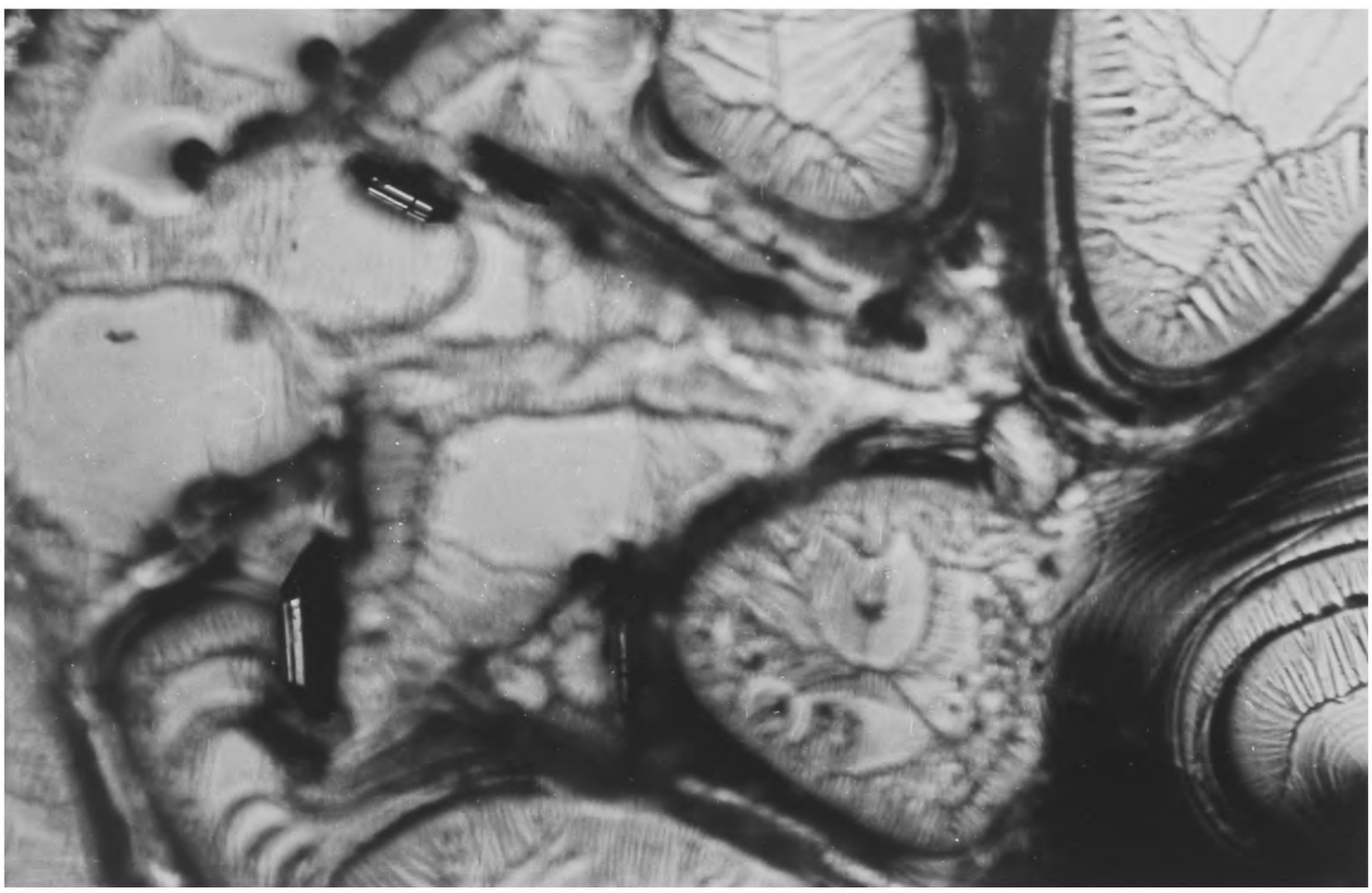

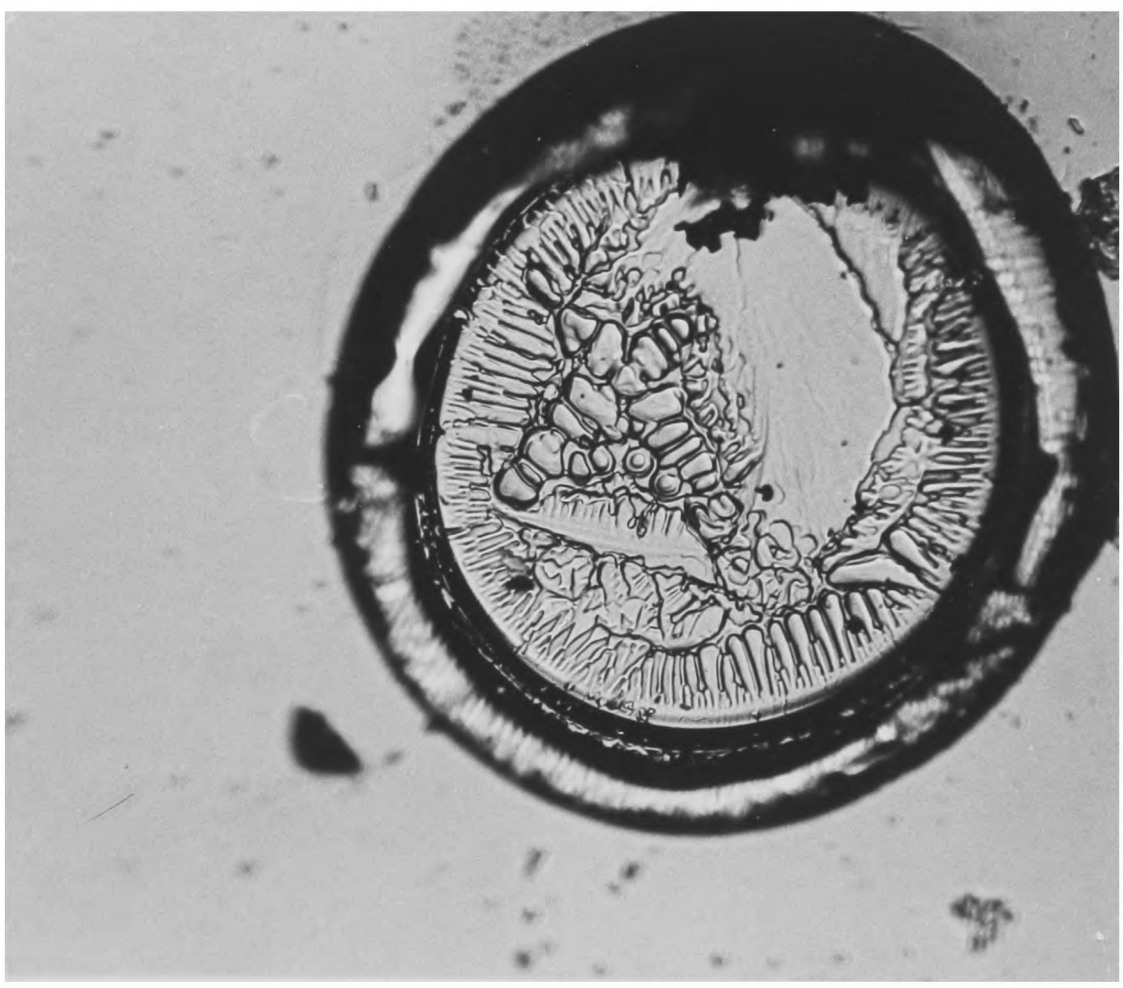

VII Thermal analysis

1) Introduction

In the review of previous work on the aluminium-silicon system, it was seen that a large number of elements are claimed to modify the eutectic. Generally the criteria used to determine whether or not modification had occurred were either not defined or else rather obscure, Kim and Heine's reference to '% modification' being an example. It was decided to compare the effects of small quantities of various impurities on the structure of the eutectic by optical and electron microscopy of small castings remelted and cooled at various rates.

2) Experimental techniques

Ingots of aluminium-silicon alloy of eutectic and hyper-eutectic composition were made up as described in ch V, 1. Impurities were added either as the pure element or else as components of fluoride or chloride fluxes.

Two rigs were used for thermal analysis, one giving a slow, and the other a relatively fast cooling rate. In both cases about 7g of alloy was loaded into a recrystallised alumina crucible 20 mm diameter and 30 mm high.

a) Slow-cooling rig - fig (29) -.

In this rig, the crucible containing the alloy was placed inside a close fitting copper pot, the lid of which contained a hole through which a thermocouple sheath could be inserted into the melt. The copper pot was supported on alumina tubing inside a silica tube, and wound with asbestos rope so that it was a fairly tight fit inside the silica tube. The open end of this tube was sealed onto a brass end cap (water cooled) by black wax, and the tube could be evacuated through the end cap by a

rotary pump. The vacuum system contained an inlet so that melting could be carried out under an argon atmosphere. The end cap contained an axial hole through which, using an 'O' ring seal, a thermocouple sheath (3 mm o.d.) could be inserted. The silica tube fitted into a platinum resistance furnace, the temperature of which was controlled by varying the output of a variac transformer. The rig was calibrated by noting the variac settings required to give two temperatures, above and below the eutectic point, and consistent cooling rates were obtained by allowing the temperature to equilibriate at the upper setting, and then turning the variac down to the lower setting.

Temperatures were recorded using a Kipp and Zonen B.D.6 chart recorder. The output from the thermocouple was balanced against a constant resistance potentiometer in series with the recorder so that a sensitive scale, 0 - 0.5 mV, could be used. The recorder specification quotes an accuracy of better than 0.5% full scale deflection, a response time of 0.7s for f.s.d. and zero drift with temperature of less than 0.02 μV per ^{o}C. Using a full scale deflection of 0.5 mV this gives an accuracy of 0.25^{o}C,

The thermocouple cold junctions were soldered and contained in glass test tubes, filled with oil to improve thermal contact with the ice-water mixture in which the tubes were immersed. Since this work was concerned with measuring undercoolings, which involved comparing heating and cooling curves for the same specimen, it was not necessary to measure absolute temperatures precisely.

Samples were cooled from about 800°C, using a cooling rate of 2.3°C/min and a chart speed of 5 mm/min. In order to obtain the most horizontal arrests it was found best to raise the thermocouple sheath slightly off the base of the crucible. After initial cooling, the variac setting was turned up and the heating arrest recorded. This was followed by another cooling curve and this time the sample was allowed to cool to room temperature. The sample was then sectioned and prepared for examination by optical and electron microscopy as described in ch V 6, while the heating and final cooling curves corresponding to the given specimen were recorded.

Methods of adding impurities varied. Non-volatile elements were melted up with the eutectic, while volatile elements were added to the molten alloy shortly before cooling. In the latter case the element was wrapped in aluminium foil and fitted into the open end of an alumina sheath, which was fitted through a second 'O' ring seal in the end plate. During melting up, the impurity was held in the cold zone of the furnace near the brass end cap, and addition was made by plunging the sheath down into the melt. After some stirring, the sheath was withdrawn and the thermocouple sheath, supporting the copper crucible lid was lowered into the melt to allow recording of the cooling curve.

b) Fast cooling rig - fig (30) -.

In order to obtain rapid cooling rates, induction heating was employed, using the bell jar furnace in which alloy ingots were originally melted up. Additions were made as described for the slow cooling rig, while some specimens were modified by melting under chloride - fluoride fluxes. Experiments were carried out under about half an atmosphere of argon. So as to minimise the thermal inertia of the system, the copper pot was

dispensed with, as it was found that reasonably horizontal arrests were still obtained, and it was found that this arrangement gave a cooling rate of 1.5°C/S on turning off the generator while the sample was molten. By switching the R.F. generator on and off during the eutectic arrest, it was found that there was no pickup on the chart recorder from the generator, so heating curves could be recorded satisfactorily.

3) Results

These are summarised in the table below:

Impurity Element	Form of addition	Cooling rate $^{o}C/min$	Growth Under-cooling ^{o}C	Comments
None	-	2.3	1.6	
		90	1.8	
Lithium	0.2 wt% metal	2.3	2.2	Unmodified
		90	6.0	Modified
Sodium	metal	2.3	6.5	Overmodified
	flux	90	8.5	Overmodified
Potassium	flux	90	5.6	Modified
Calcium	0.2 wt% metal	2.3	2.2	Unmodified
		90	3.0	Partly Modified
Strontium	0.2 wt% metal	2.3	3.0	Modified
		90	5.0	Modified
Barium	0.2 wt% metal	2.3	2.4	Unmodified
Phosphorous	element	90	1.9	Primary modified
Arsenic	0.2 wt% metal	90	1.7	Unmodified
Antimony	0.2 wt% metal	90	1.7	Unmodified
Bismuth	0.2 wt% metal	90	1.6	Unmodified

Examination of the cast ingots showed a variety of microstructures, depending on the impurity added and the cooling rate employed. Thermal analysis curves corresponding to different types are shown in figs (31 to 34), these showing melting and freezing curves superimposed. Optical and scanning electron micrographs are shown in plates (38 to 53).

The unmodified eutectics

The cooling curve and microstructures shown in fig (31) and plates (38, 39) are characteristic of specimens in which the eutectic was unmodified. The undercooling for growth was between 1.5 and 2.0°C both in the case of the pure eutectic and with the addition of the group V elements. Barium gave a slightly larger undercooling, but the eutectic silicon remained unmodified even with the addition of enough barium to form a barium rich phase. Similarly at a cooling rate of 2.3°C/min, even specimens containing 1% calcium showed no eutectic modification.

The modified and overmodified eutectic

Samples containing sodium, potassium and strontium, contained modified eutectic throughout. Representative micrographs and a thermal analysis curve are shown in plates (40, 41) and fig (32). Growth undercoolings were between 5.0 and 8.5°C. Both sodium modified specimens contained overmodification bands - plates (42, 43) -, but their cooling curves did not show any additional features compared with those of potassium and strontium. The sample containing 0.2% strontium and slow cooled showed modification throughout, but the microstructure - plates (44, 45) - was coarser than that of the other modified samples. The corresponding growth undercooling was 3°C, and the same undercooling was obtained with a sample containing 2% strontium, indicating that this small undercooling was not due to an

insufficient quantity of impurity being present.

The 'partially modified' eutectic

An ingot cooled at 90°C/min containing 0.2% calcium had a microstructure - plate 46 - which was mostly coarse flake with small regions of fine fibrous eutectic. The cooling curve - fig (33) - shows a growth undercooling of about 3°C with a marked recalescence following a further undercooling for nucleation of 3°C. Thus it seems possible that regions of fibrous eutectic present in this specimen correspond to growth directly following nucleation. Latent heat is evolved and the growth temperature rises to a steady state value, corresponding to formation of the unmodified eutectic.

The lithium modified samples

The lithium doped sample cooled at 90°C/min showed a microstructure - plates (47, 48) - which differed morphologically from both the unmodified irregular flake structure and the usual fibrous modified structure. The cooling curve - fig (34) - shows a growth undercooling of 6°C. The scanning election micrograph shows the silicon crystals to be straight and angular with a mixture of flakes and fibres being present, while on the optical micrograph the morphology appears to be mainly flaky, although much finer and more regular than the unmodified eutectic.

The slowly cooled sample also showed an anomalous microstructure - plates 49, 50 -, the silicon crystals appearing coarse and 'granular'. The growth undercooling was 2.2°C.

Primary modification

This work was concerned principally with eutectic modification, but some samples containing 15%wt silicon were examined. It was found that phosphorous modified the primary from the usual massive crystals - plate (51) - to smaller, more

equiaxed ones - plate 52 -. Sections through many of these crystals showed small crystallographic particles near the centre of the crystal. Each phase was scanned, using microprobe analysis, for phosphorous, and it was found that phosphorous was present in measurable quantities only in these small crystallographic particles. They also contained aluminium, but the quantity of silicon registered was small and variable, and it was thought that this was due to the silicon crystal in which the particle was embedded. Thus it is thought that the particles consist of a compound of phosphorous and aluminium.

One specimen containing 20%wt silicon was frozen under a potassium flux, and this showed well developed silicon dendrites - plate 53 -. The modified 15%wt silicon samples did not contain massive silicon crystals, since at undercoolings of about 6°C, the coupled region is shifted sufficiently to give coupled growth at this composition.

The solidification time for samples frozen at each rate was the same for both modified and unmodified specimens. If growth rate is estimated by dividing the ingot radius by the solidification time (i.e. assuming radial growth) rates of 0.01 mm/s (2.3°C/min) and 0.1 mm/s (90°C/min) are obtained. However according to the undercooling vs growth rate plot in ch V, undercooling increases rapidly at rates above 0.01 mm/s, so it is concluded that growth is not radial.

4) Discussion

From the results it can be seen that the unmodified eutectic corresponds to growth undercoolings of between 1.5 and 3°C, and the modified eutectic to undercoolings above 3°C. The variation in microstructure of the slow cooled strontium doped specimen is interpreted as showing that this sample was growing at an

undercooling close to that at which the eutectic morphology changes from unmodified to modified. Thus it appears that the transition due to impurity doping takes place at a growth undercooling of about 3°C.

Morphologically the modified silicon crystals produced by additions of strontium, sodium and potassium appear the same. The variations in undercoolings indicate that sodium is the most efficient modifier, followed by potassium and strontium, that is it will produce modification at lower cooling (i.e. growth) rates. The variations in undercooling with cooling rate indicate that for each modifying element there is a growth rate below which it will not produce modification, independent of the concentrations of impurity.

Doping with lithium, as described above, produces a different eutectic morphology. The crystals formed at the fast cooling rate resembled some of those found in pure eutectic specimens frozen sufficiently rapidly to modify the eutectic - plate 54 -, so it is possible that this morphology is intermediate between the unmodified and fully modified ones. However the growth undercooling, at 6°C, is greater than that for the fully modified strontium and potassium doped specimens, so it seems more likely that lithium modification is qualitatively different, and the fact that the slow cooled sample did not grow with the usual lamellar flake structure supports this.

None of the group V elements were effective in modifying the eutectic in the sense of producing a flake to fibre transition, although it has been reported that arsenic (39) and bismuth (41) produce 'some modification'. As cooling and growth rates were not given it is not possible to compare these results directly with the present experiments. It is possible

thus that these elements may produce modification at higher growth rates. Kim and Heine (39) reported that addition of phosphorous modified firstly the primary silicon, repeated additions being necessary to modify the eutectic to a 'granular' flake structure. In the present work modification of the eutectic was not observed, probably because the volatility of the phosphorous addition meant that only enough went into the alloy to modify the primary.

Fig 29

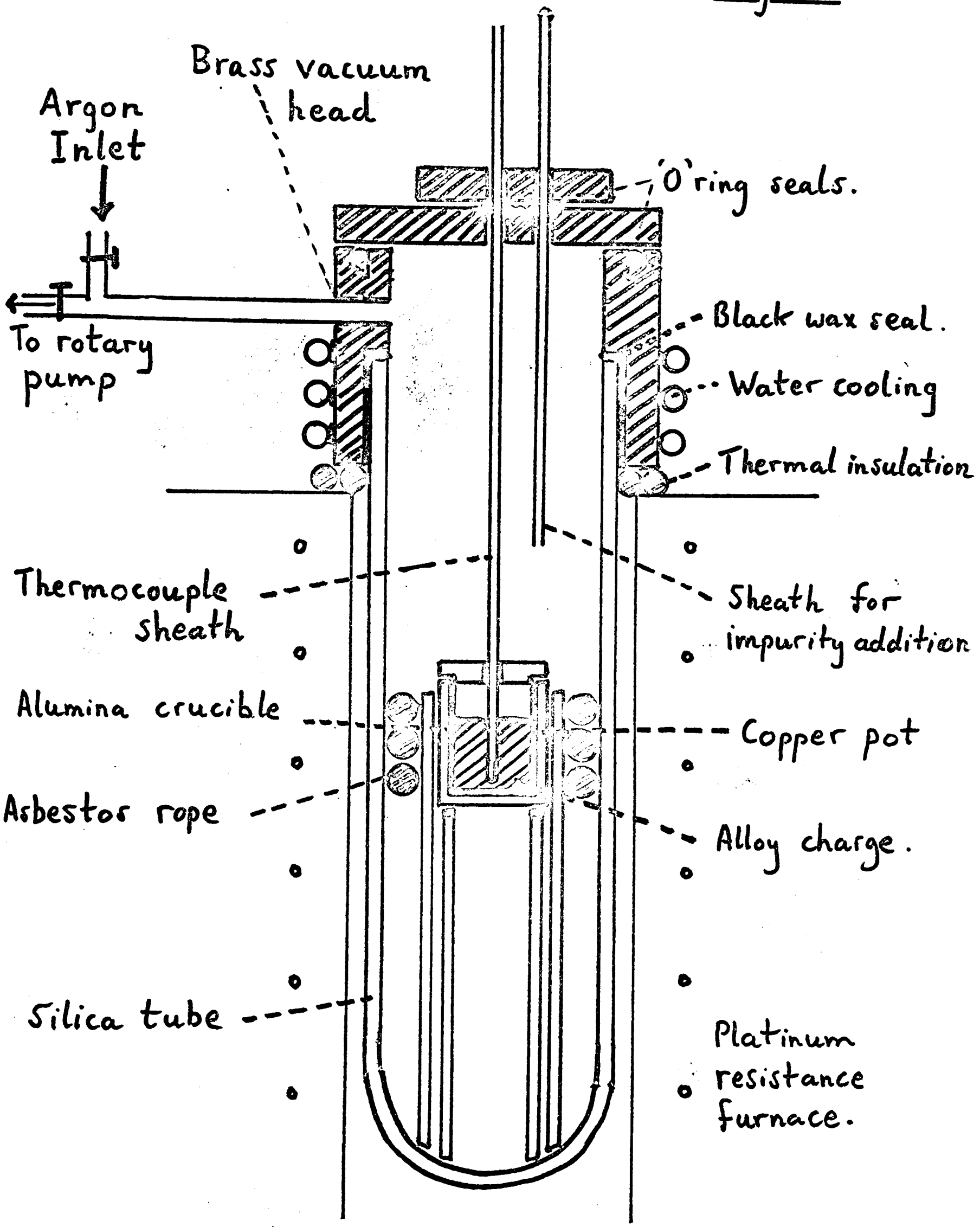

Slow cooling rig for thermal analysis.

(Section)

Fig 30

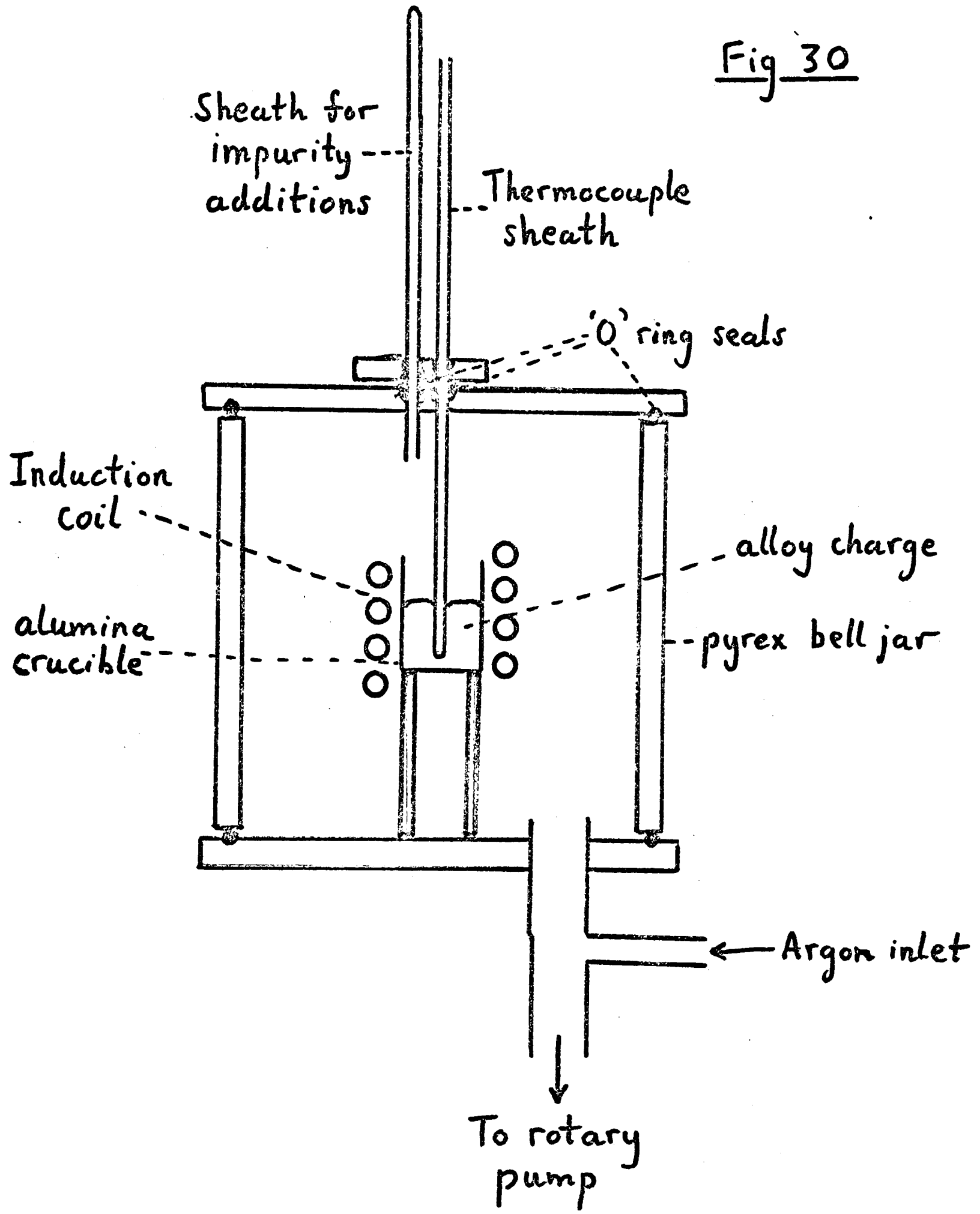

Fast cooling rig for thermal analysis.

(section)

Fig 31

Unmodified eutectic, slow cooled.

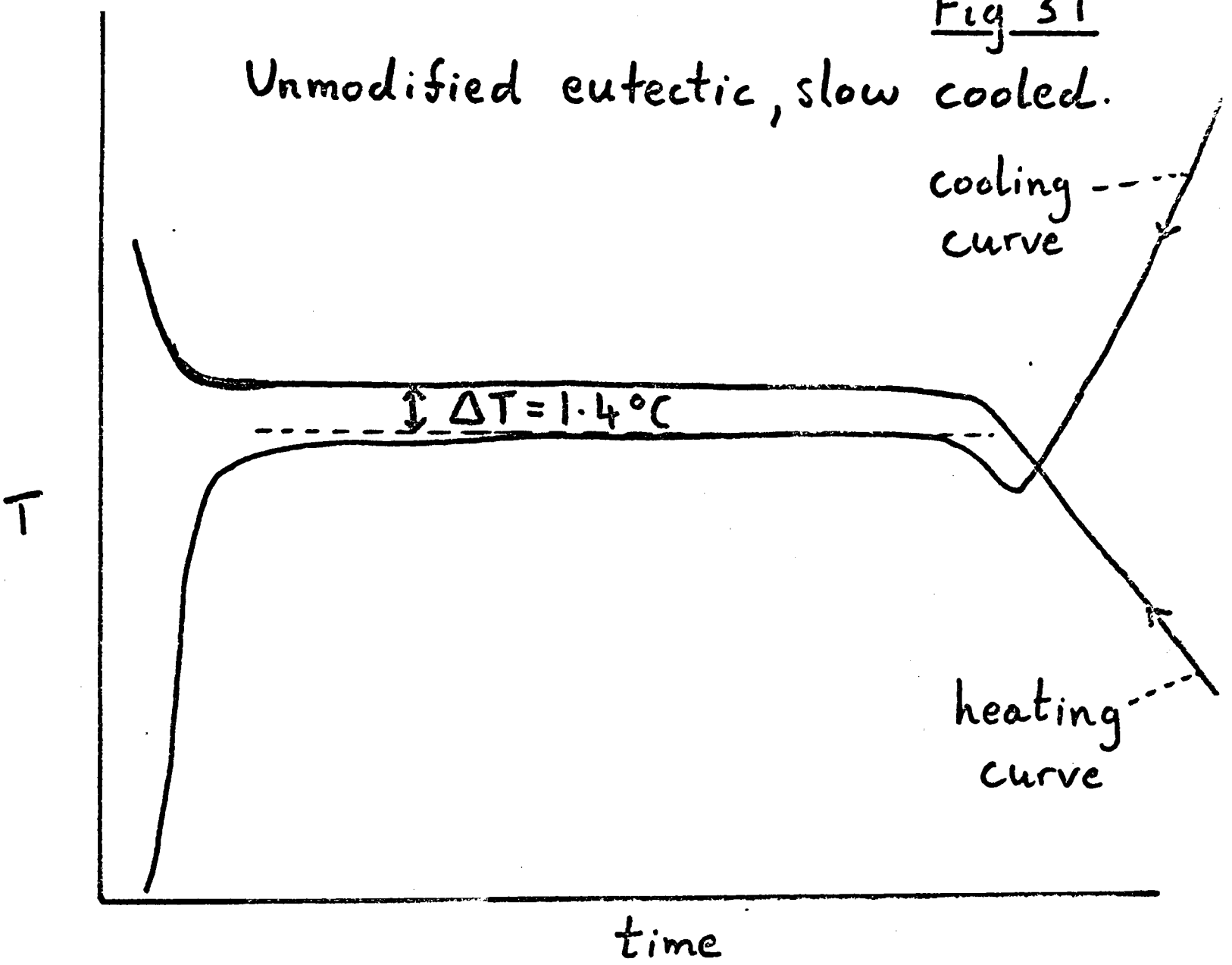

Fig 32

Strontium modified eutectic, fast cooled.

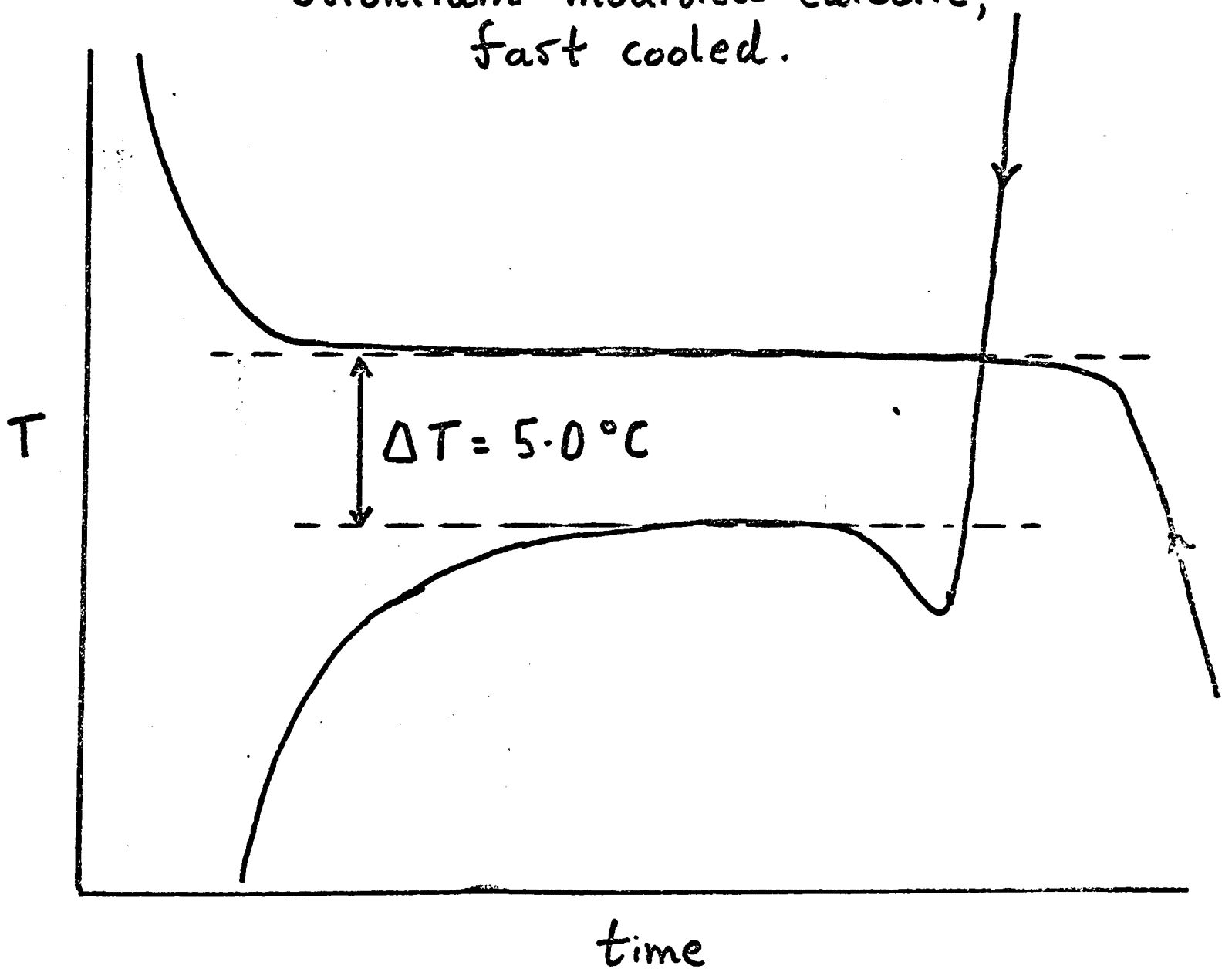

Fig 33

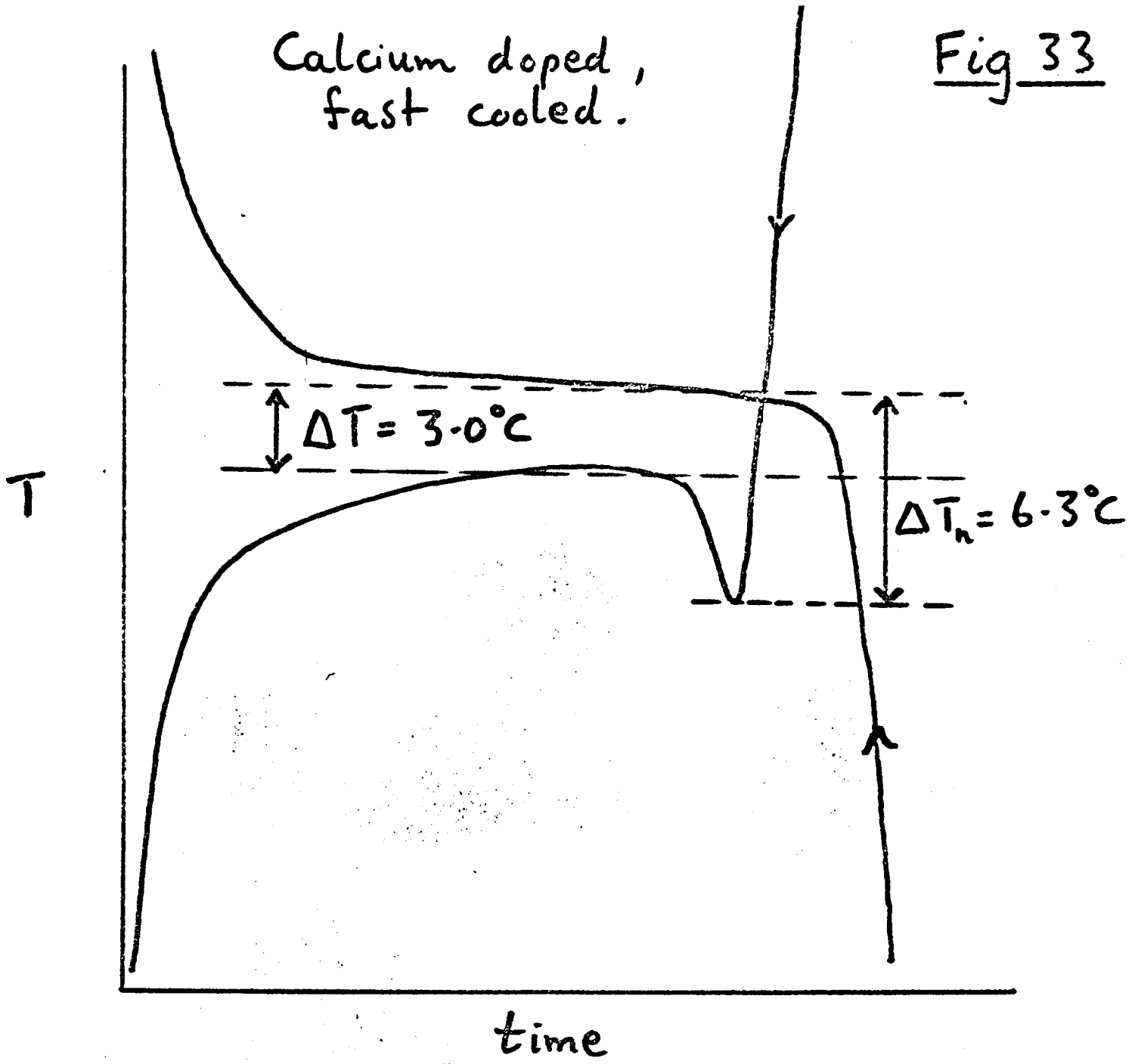
Calcium doped, fast cooled.
T
ΔT = 3·0°C
ΔT_n = 6·3°C
time

Fig 34

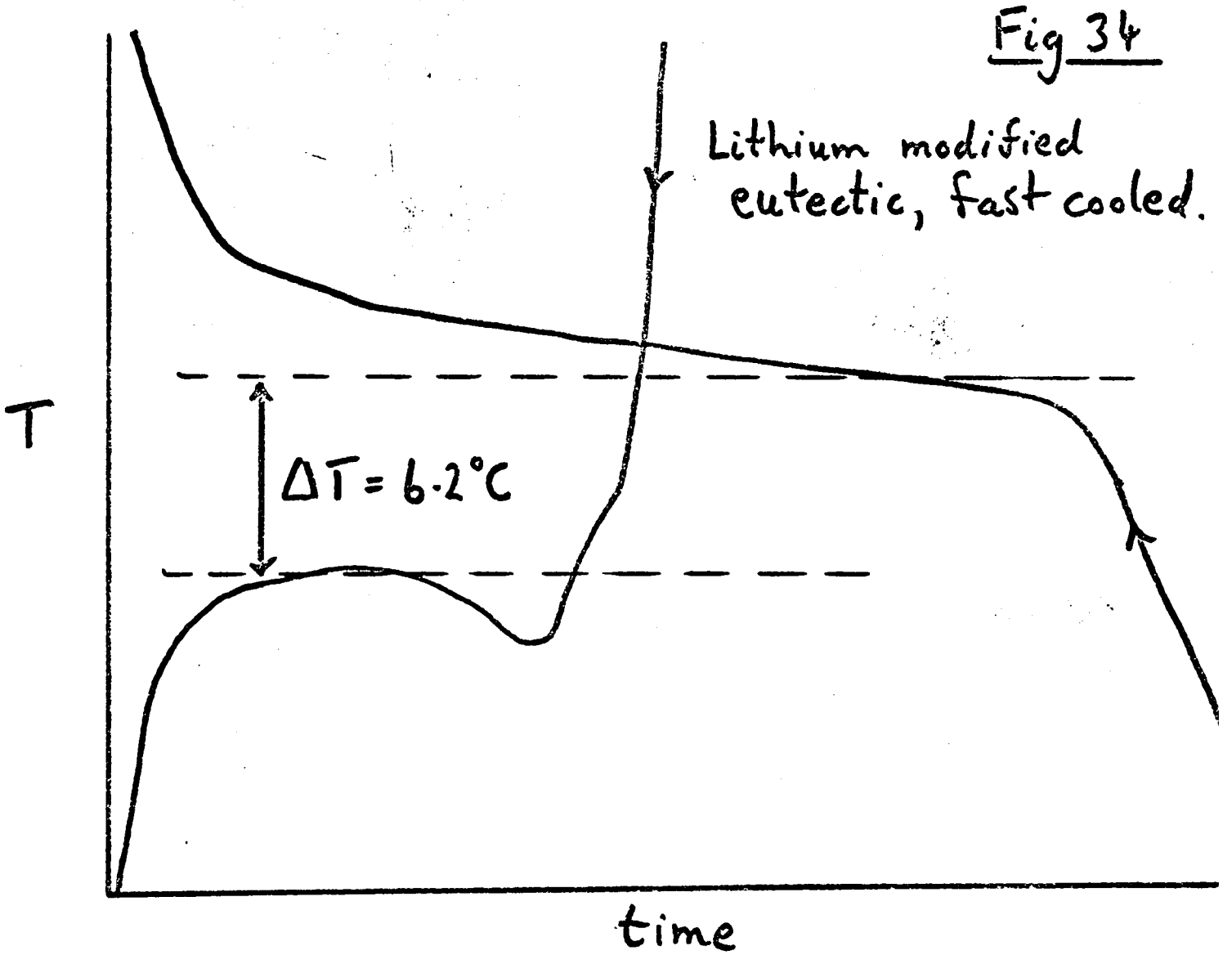
Lithium modified eutectic, fast cooled.
T
ΔT = 6·2°C
time

Unmodified eutectic.

Plate 38 Cooling rate 1.5°C/S

X 280

As above.

Plate 39 Scanning electron micrograph.

X 550

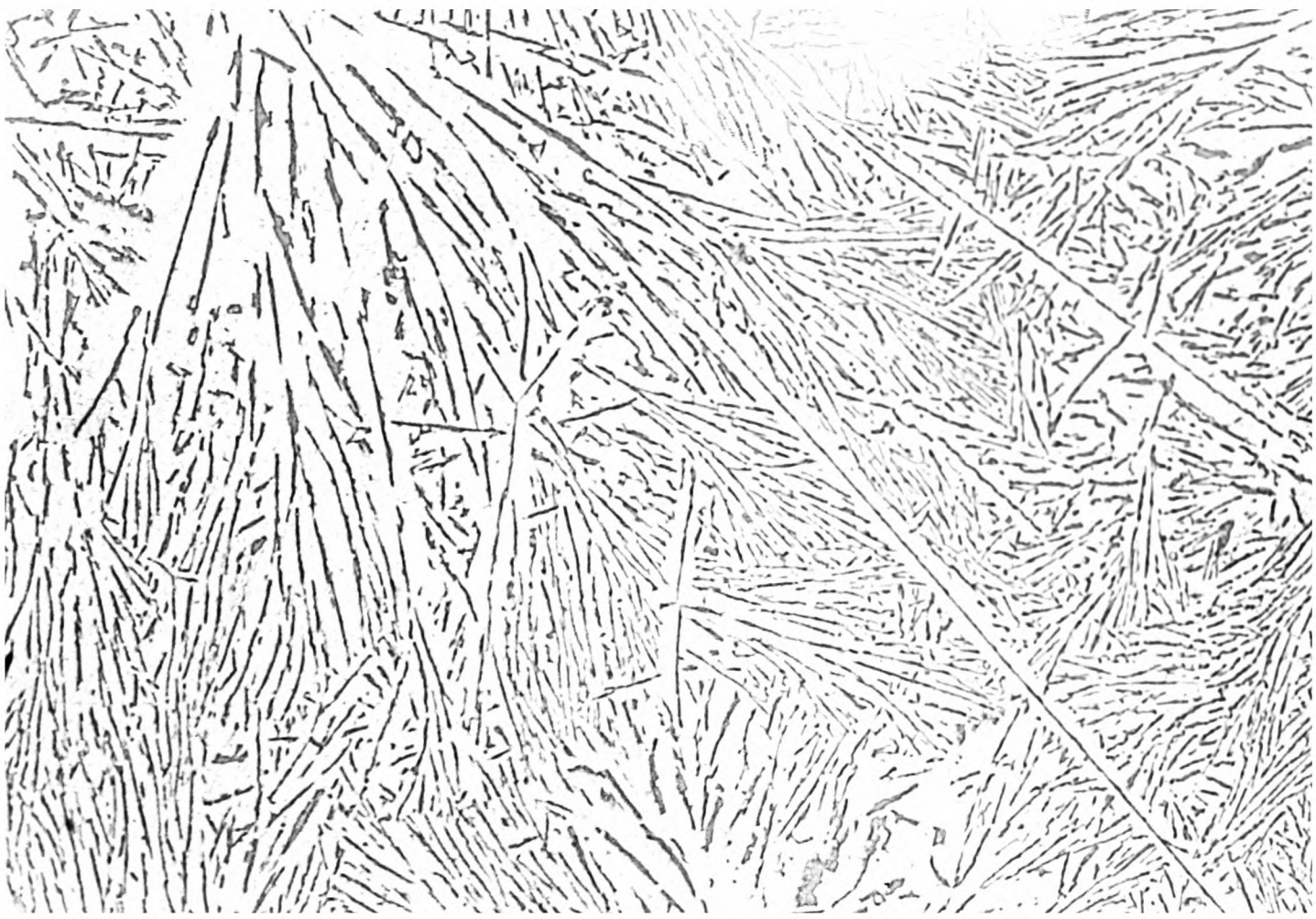

Strontium modified eutectic.

Plate 40 Cooling rate 1.5°C/S.

X 280.

Plate 41 As above

Scanning electron micrograph x 2000.

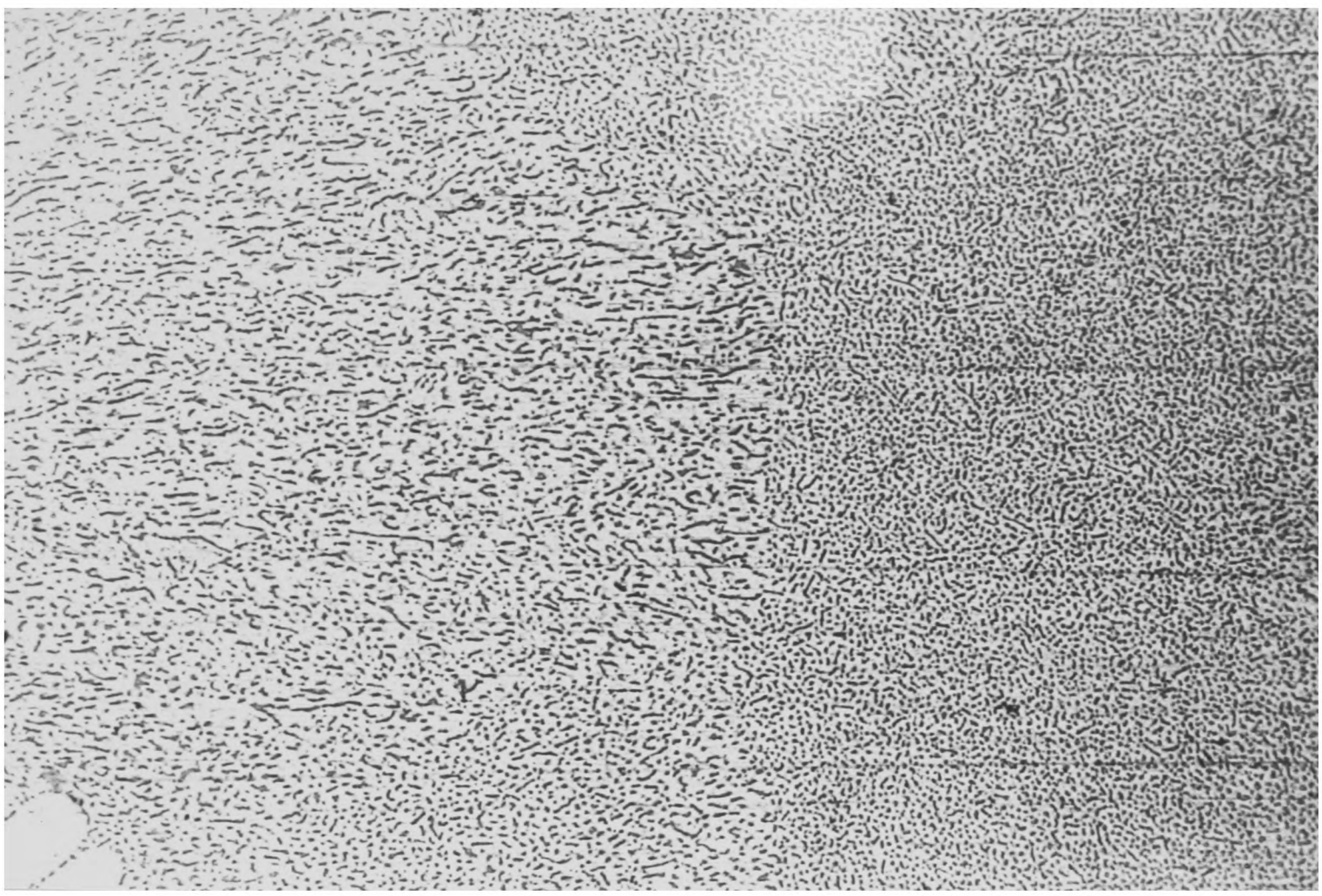

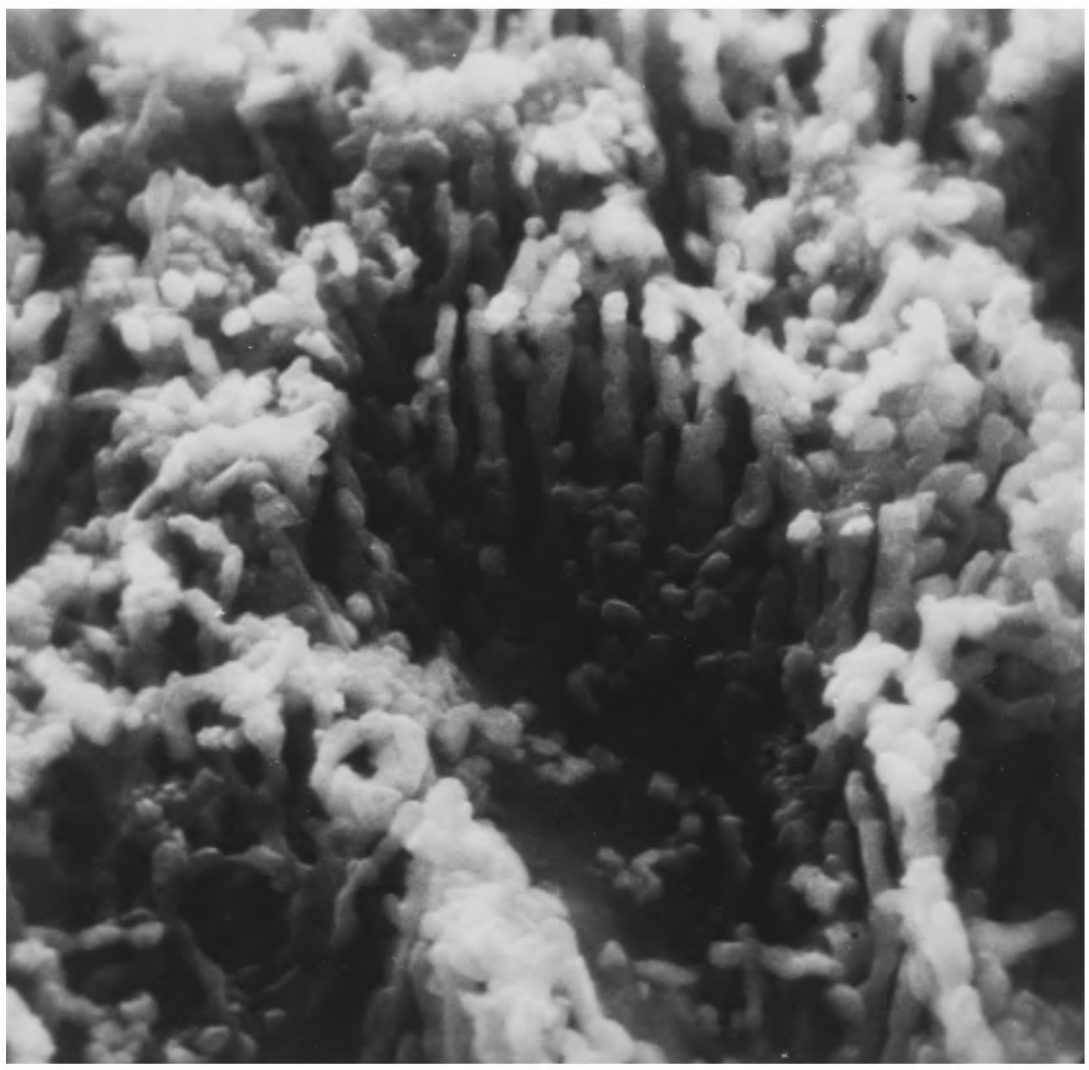

Overmodification bands in sodium modified

Plate 42 specimen cooled at 1.5°C/s.

X 280

As above.

Plate 43 Scanning electron micrograph.

X 1000

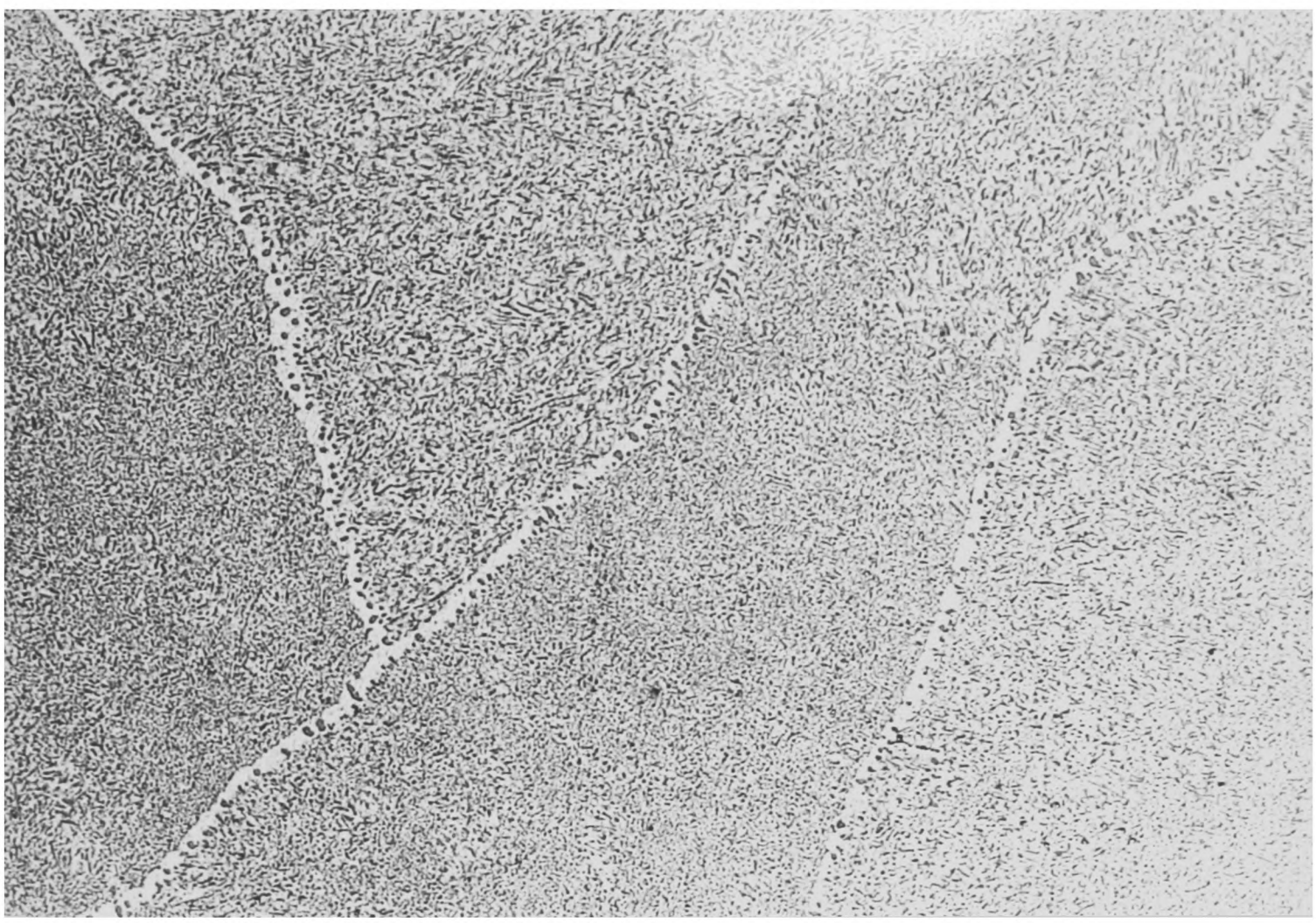

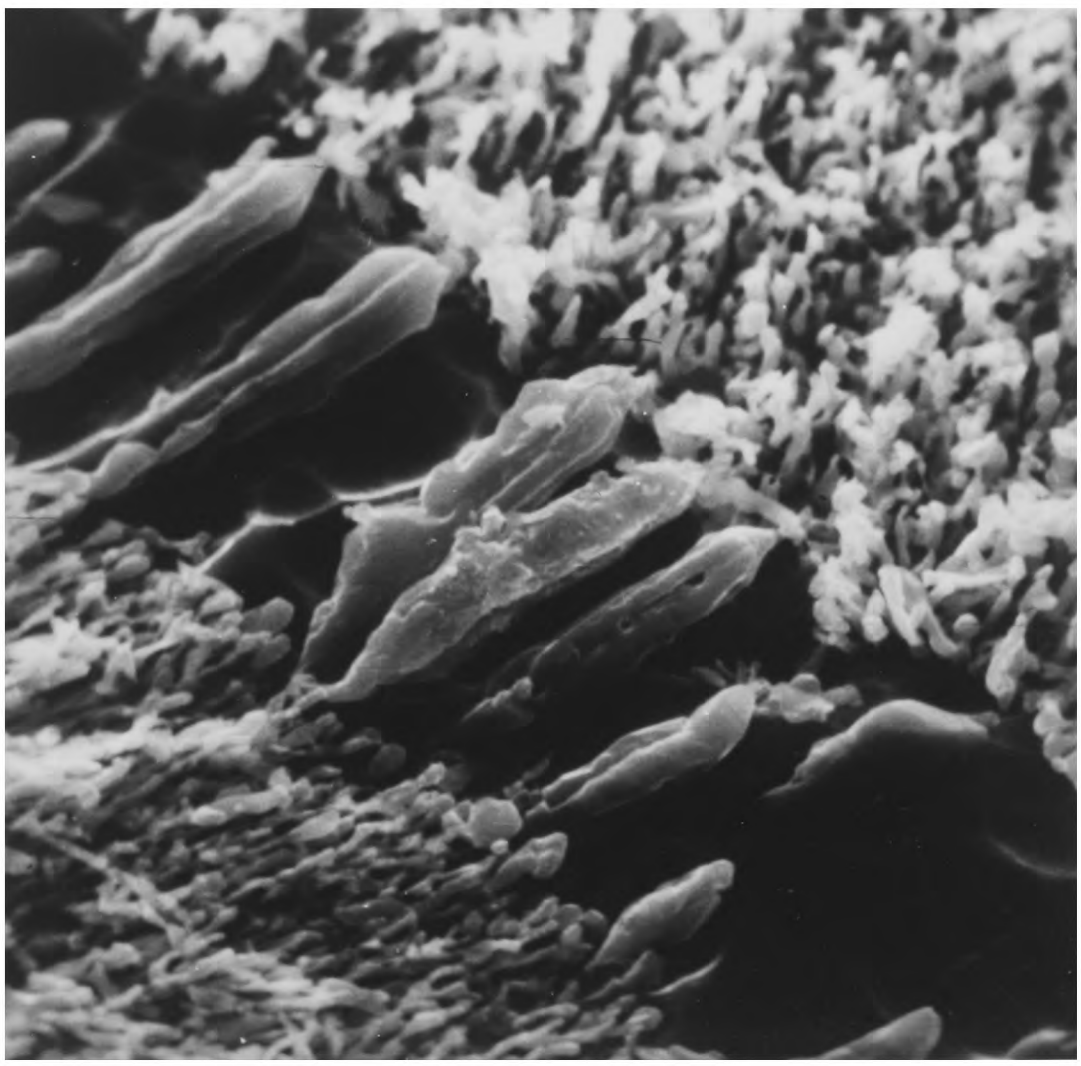

Strontium modified eutectic cooled at

Plate 44 $2.3^{o}C/min.$

X 140

As above.

Plate 45 Scanning electron micrograph.

X 1000

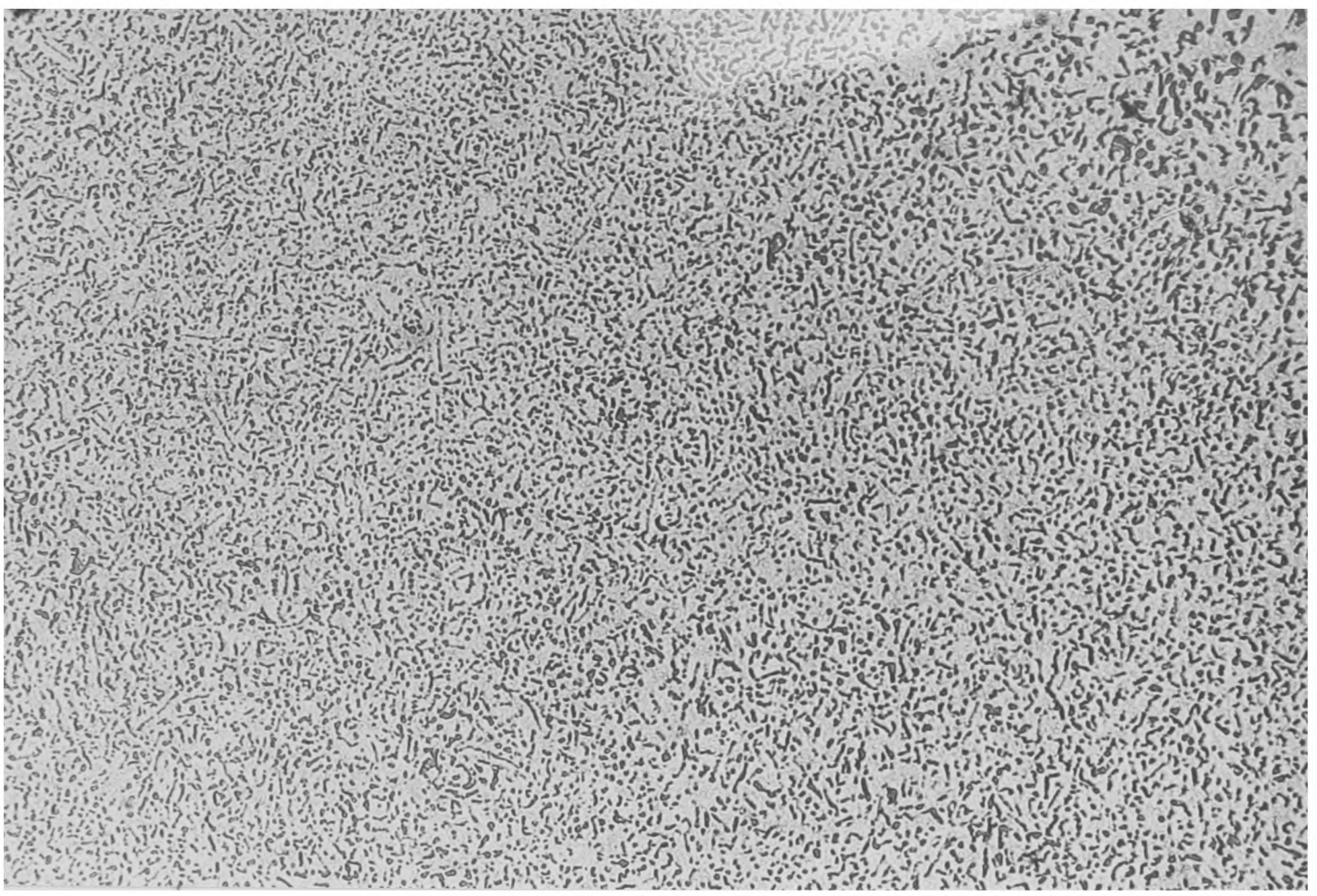

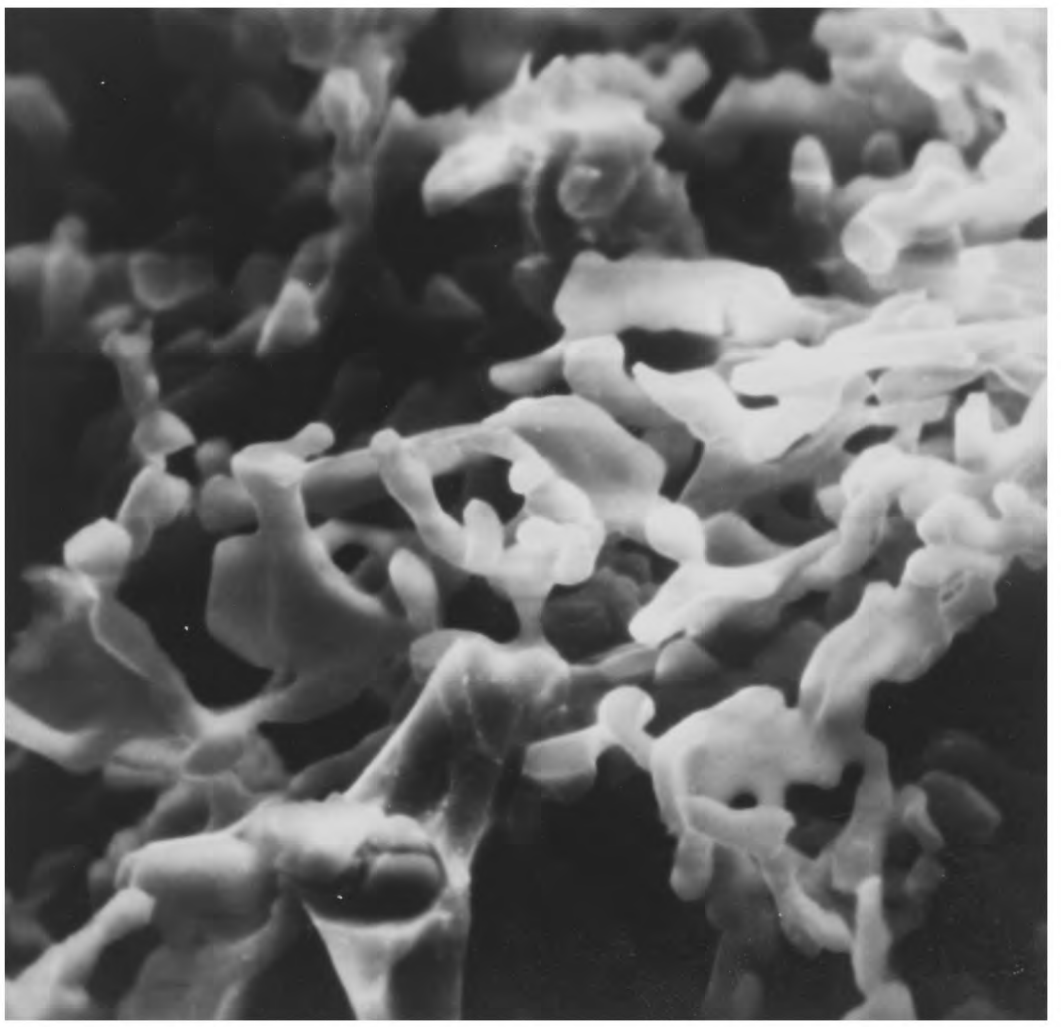

Plate 46

Calcium 'modified' eutectic cooled at 1.5°C/S

X 280

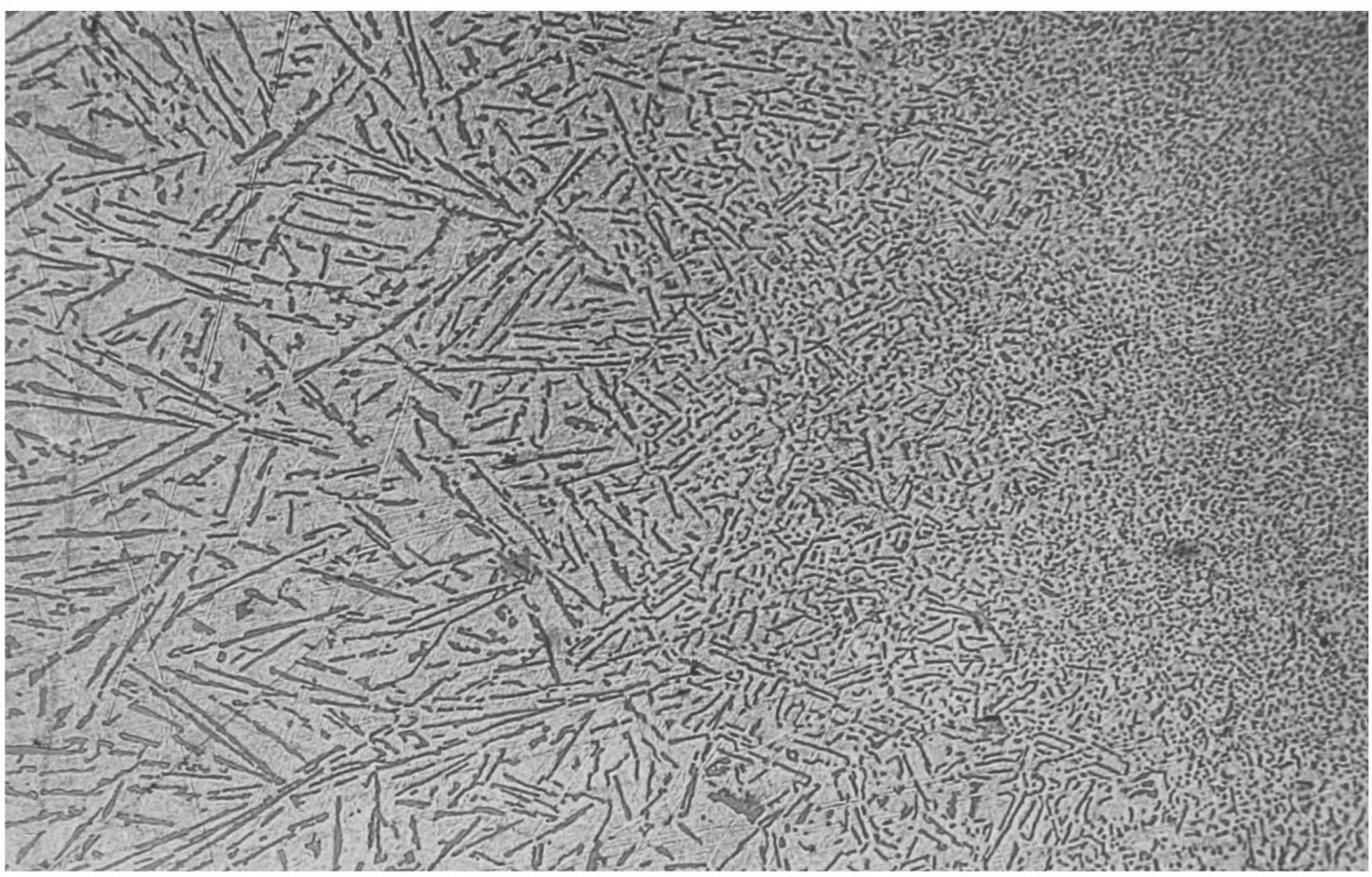

Plate 47 Lithium modified eutectic cooled at 1.5°C/S

X 140

Plate 48 As above.

Scanning electron micrograph.

X 2300

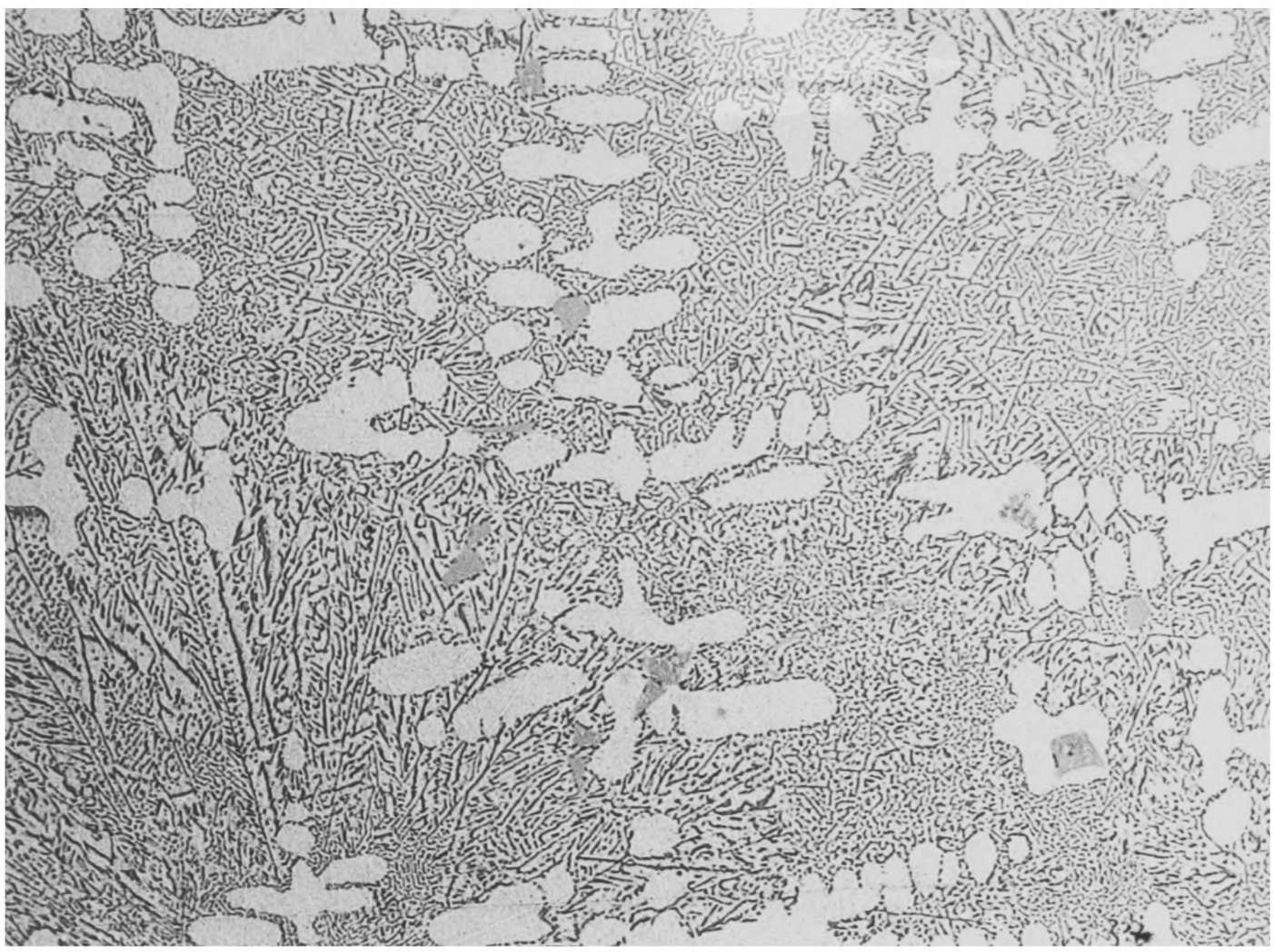

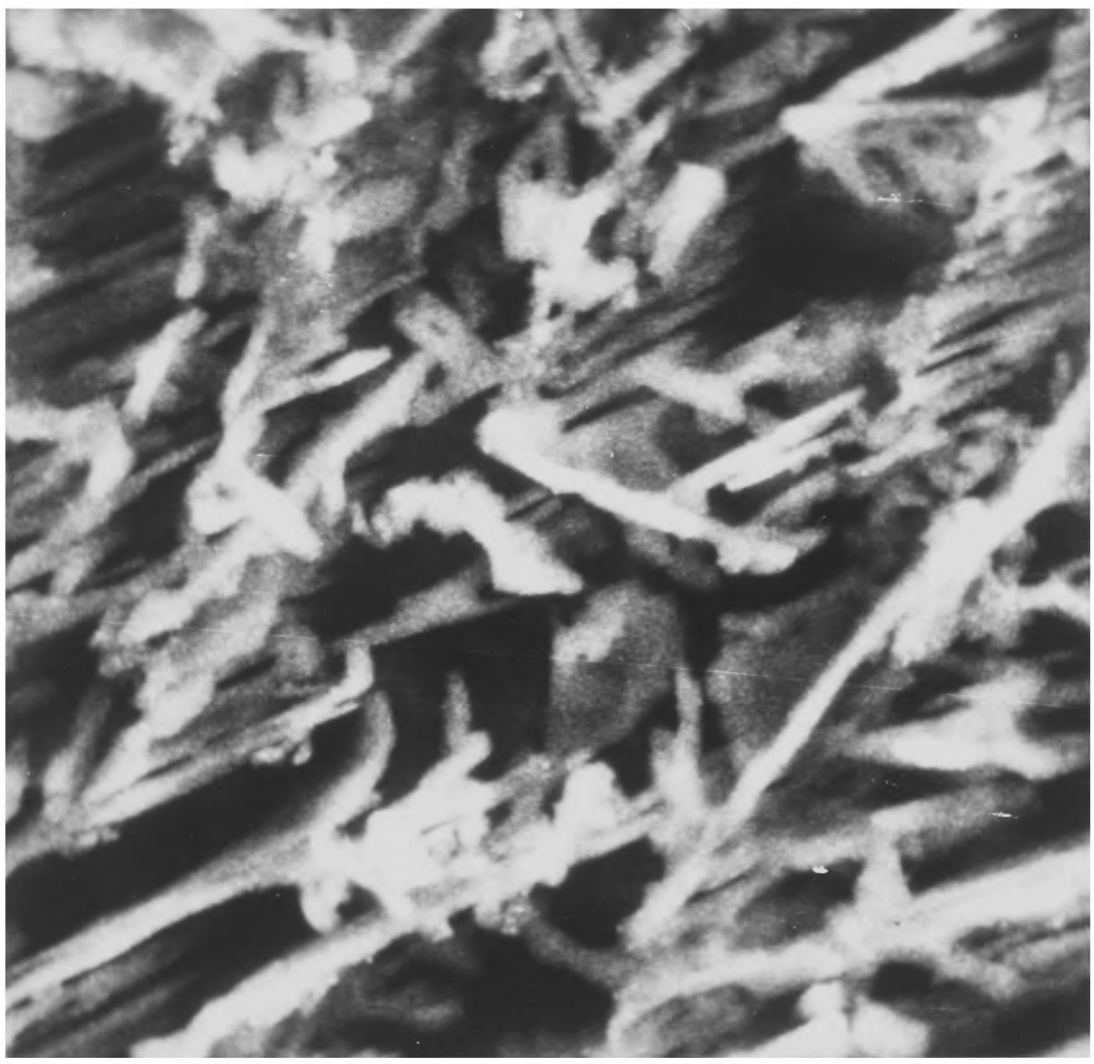

Plate 49

Lithium modified eutectic cooled at 2.3°C/min

X 140

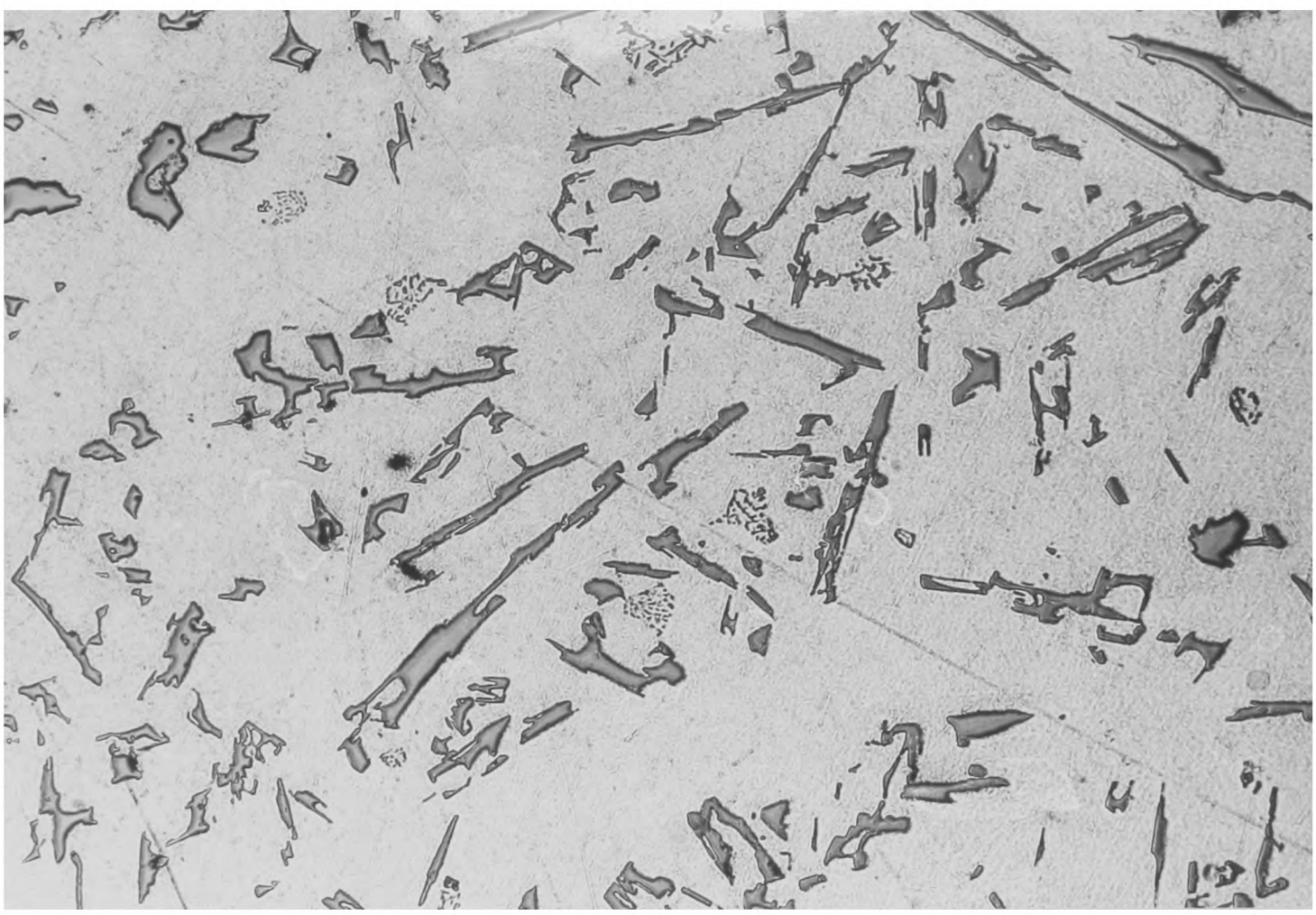

Plate 51

Unmodified primary crystals of silicon

Cooling rate 1.5°C/S

X 140

Plate 52

Phosphorous modified primary silicon

Cooling rate 1.5°C/S

(a) X 140

(b) X 700

(ข)

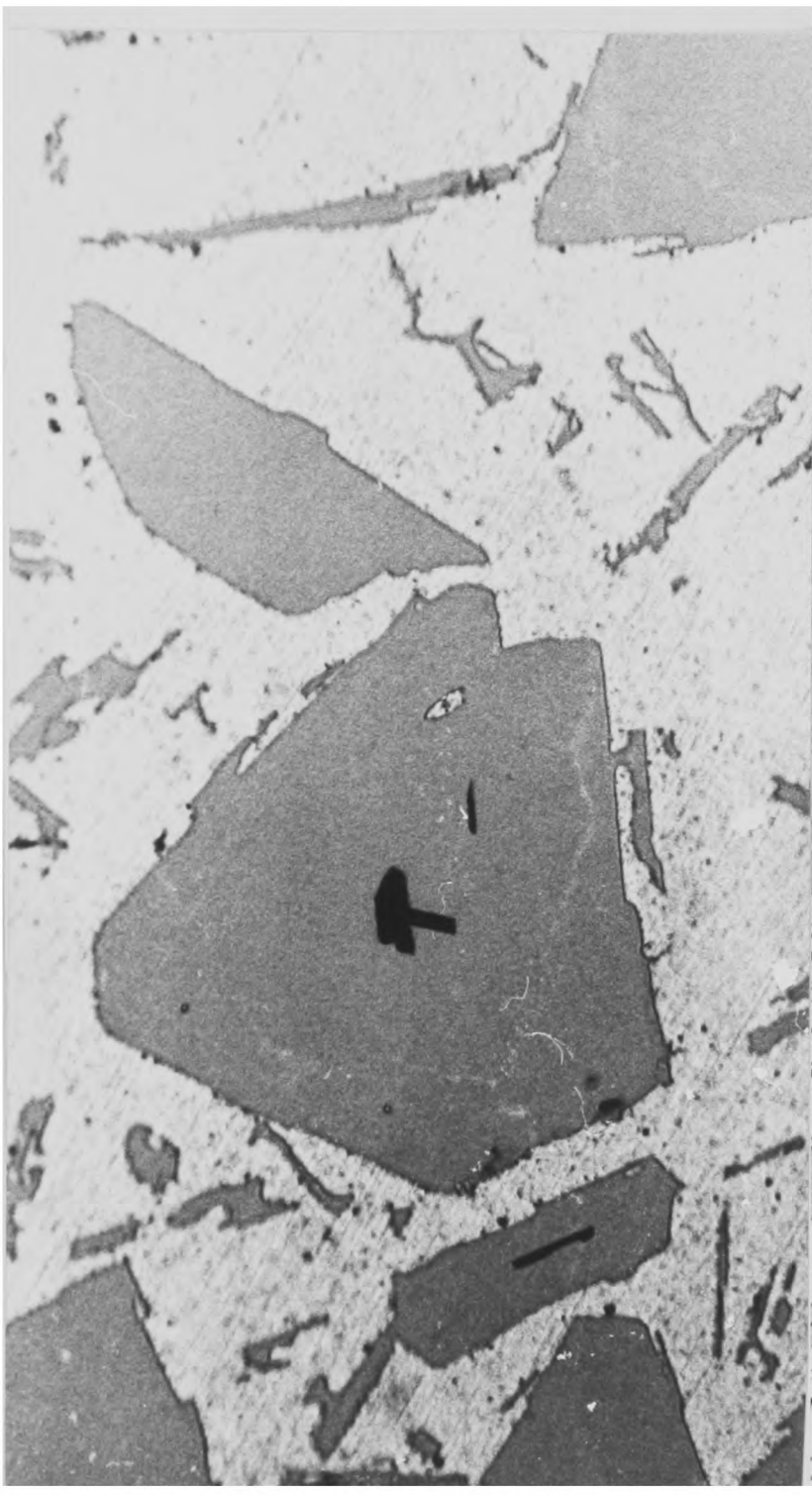

(ค)

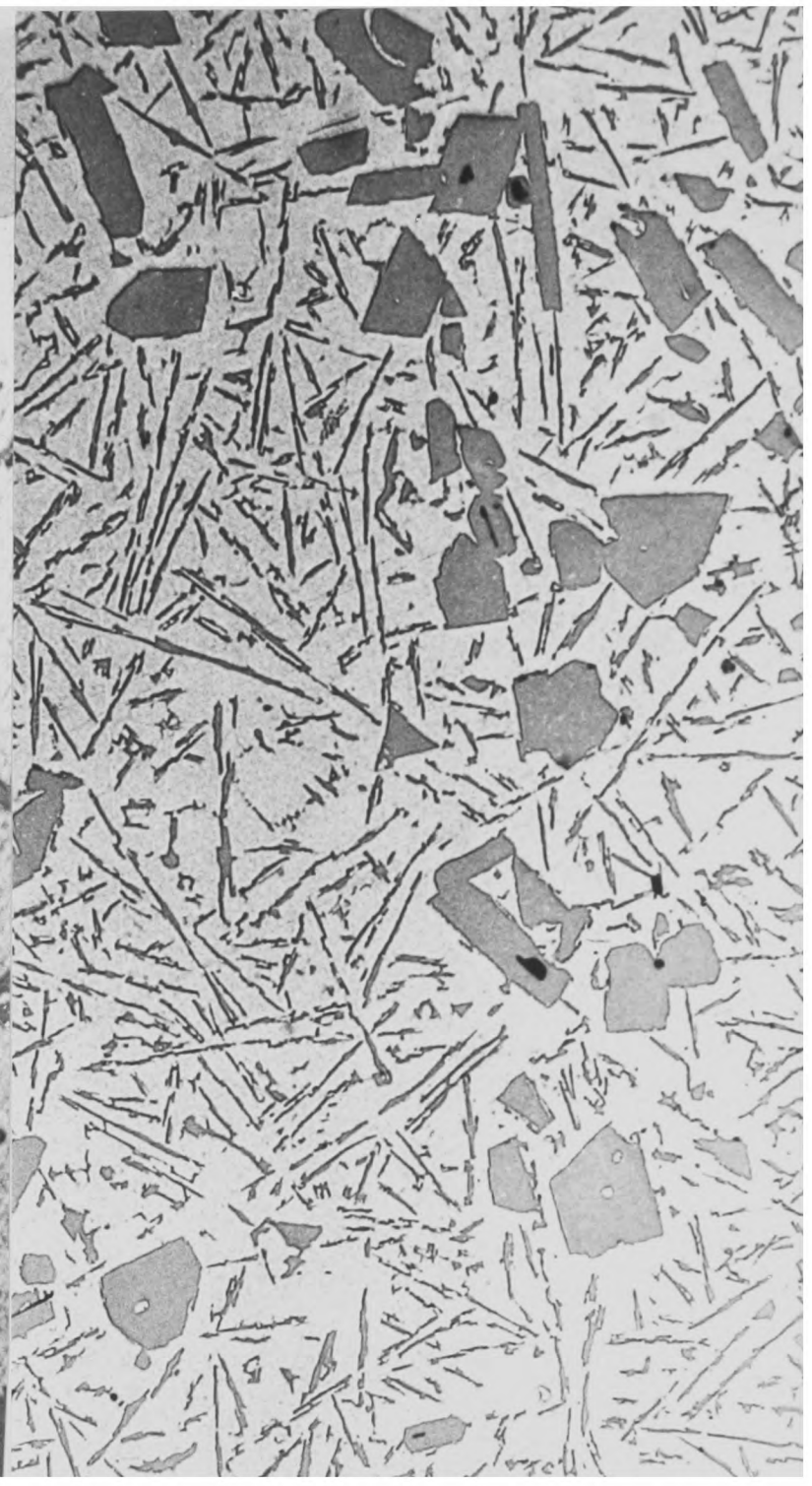

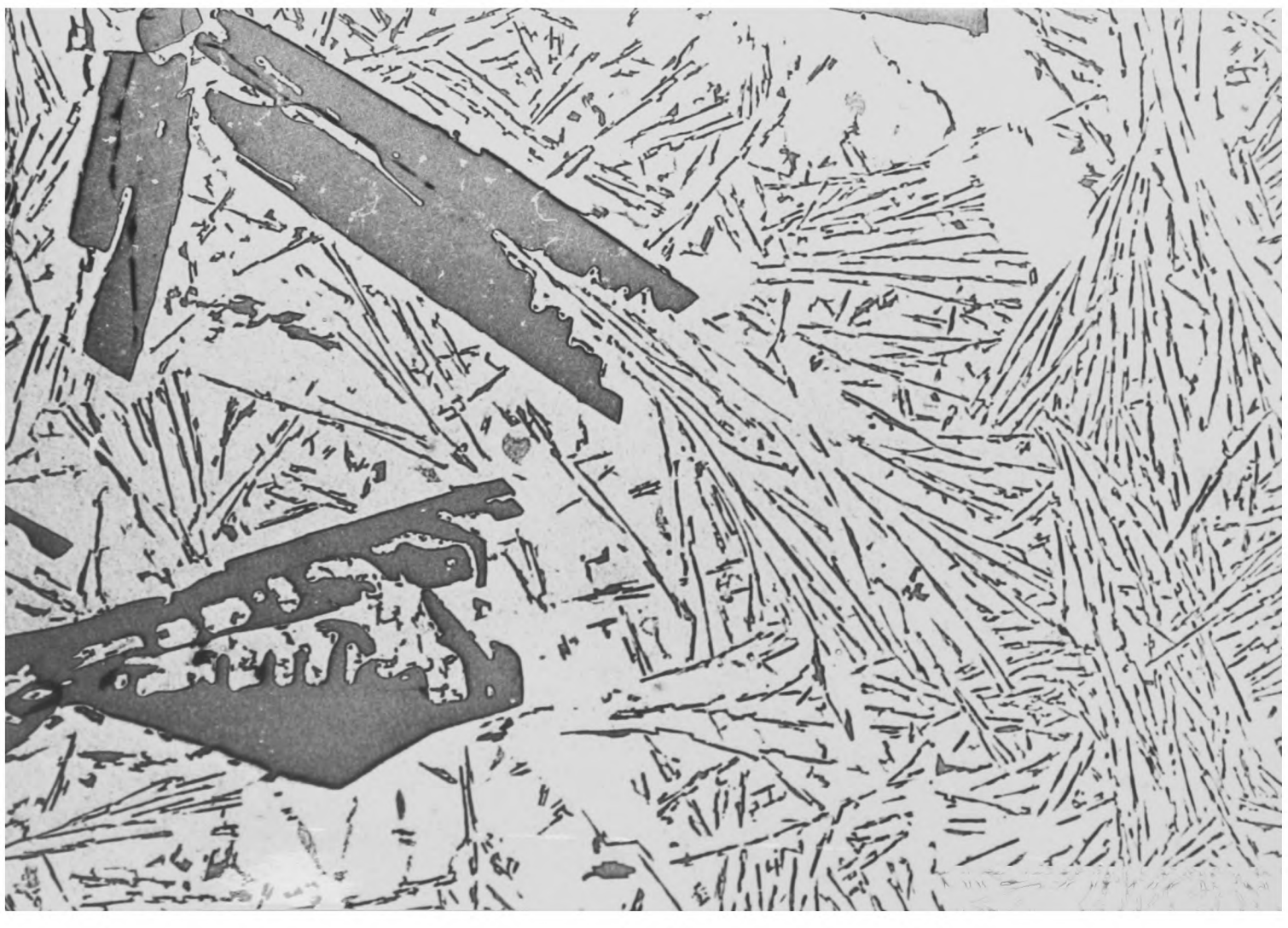

Silicon dendrites in potassium flux modified specimen cooled at 1.5°C/S.

Plate 53

X 280

V = 0.96 mm/s G = 10°C/mm

Plate 54

X 9000

Transmission electron micrograph

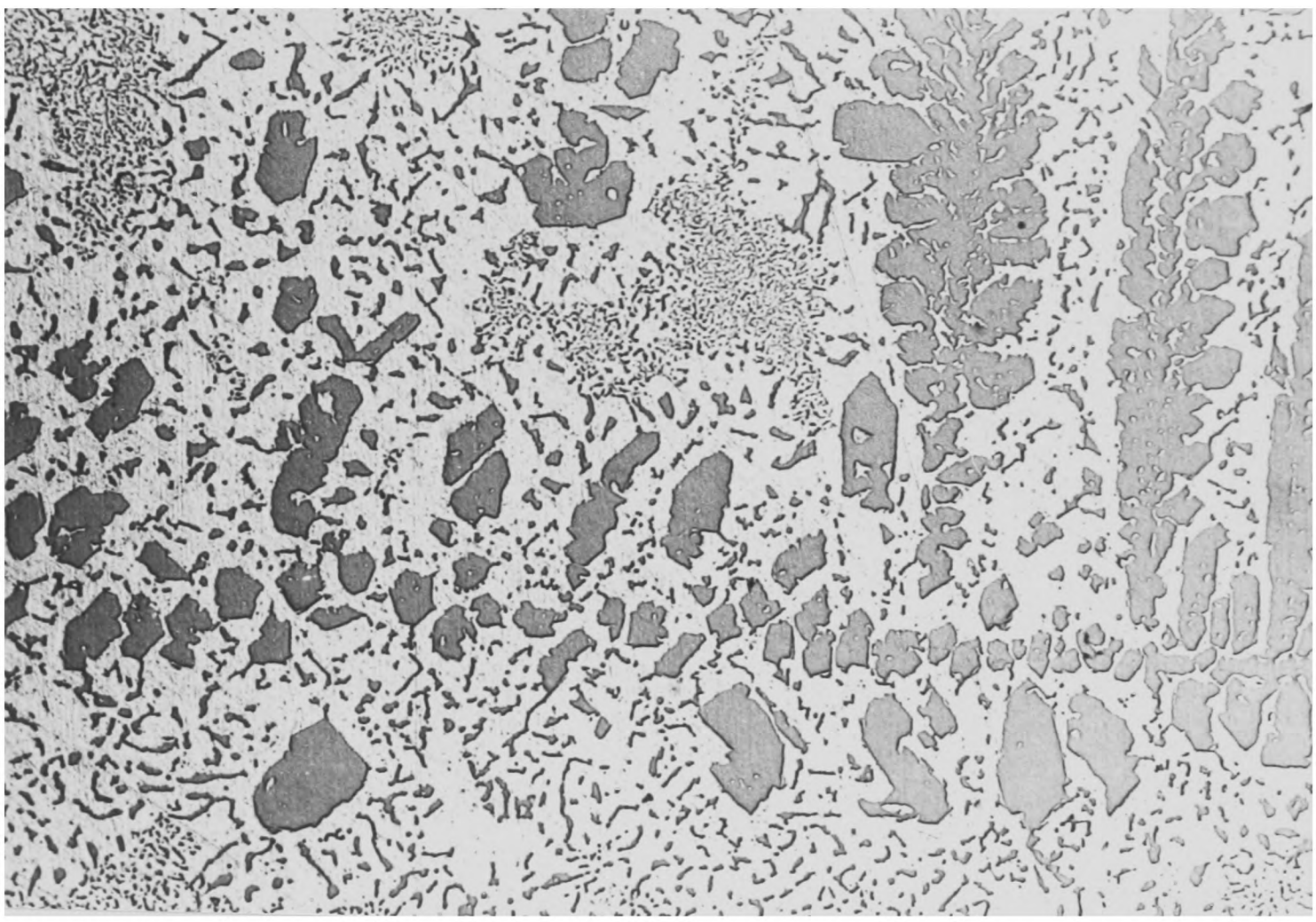

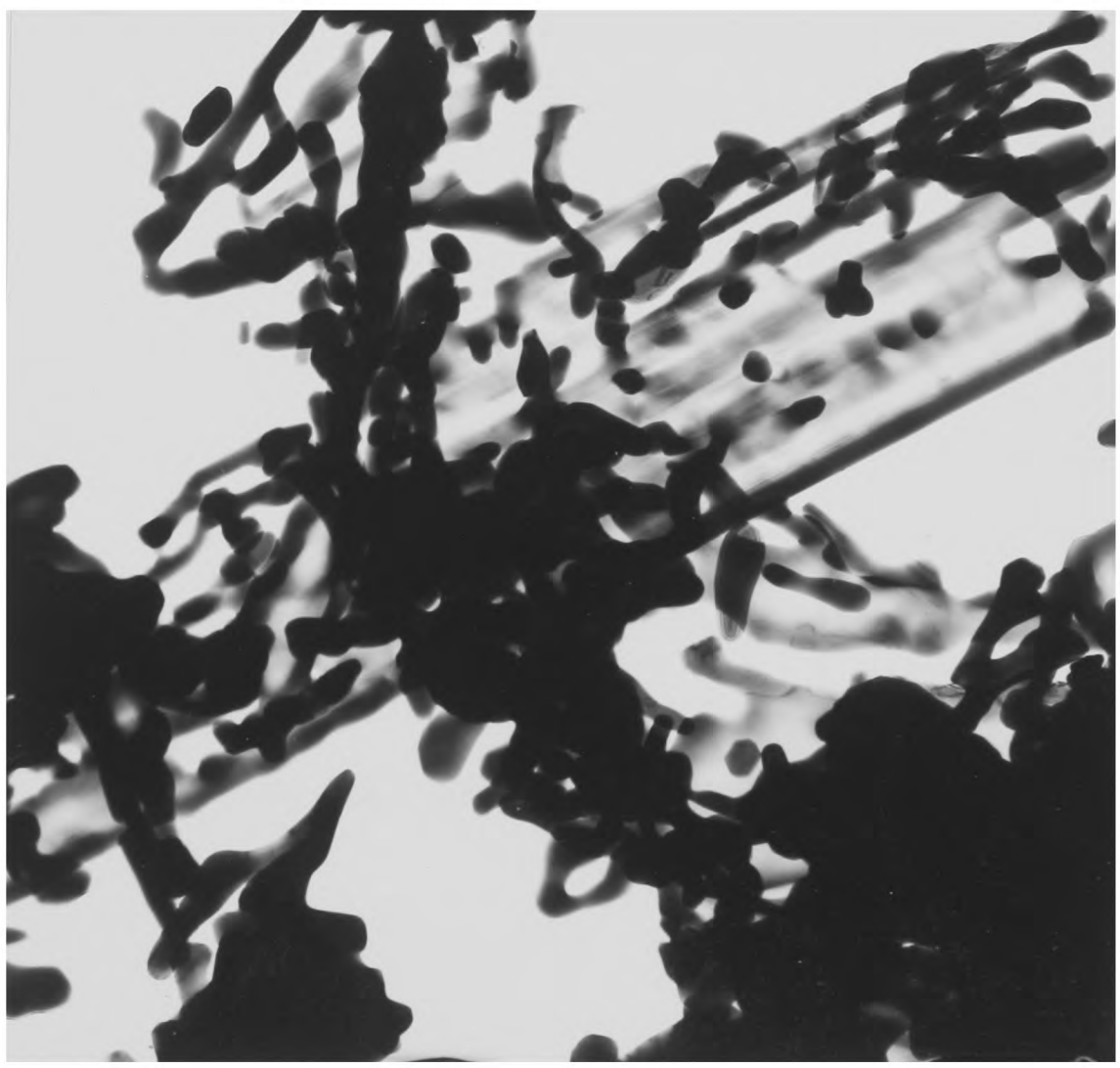

VIII General discussion

It is proposed here that the morphology of the eutectic silicon phase can be related to the imposed growth conditions of velocity and temperature gradient, and to the presence of a modifying agent, by consideration of the effect of the difference between the kinetic undercoolings of the two phases on the total growth undercooling of the eutectic.

In the discussion on layer growth, an approximate expression was derived for the kinetic undercooling of a growing {111} face in silicon:

$$\Delta T \simeq 0.1V \quad , V \text{ in mm/s}$$

The same calculation carried out for aluminium, assuming a rough interface gives:

$$\Delta T \simeq V \quad , V \text{ in mm/s}$$

Thus when silicon advances by layer growth, its kinetic undercooling is about 10X that for aluminium. It was seen that the presence of twins allowed more rapid growth, in other words reduced the kinetic undercooling of silicon. Thus, assuming similar solute and curvature undercoolings, silicon will grow behind aluminium by a distance which increases with increasing growth velocity V and decreasing temperature gradient G, i.e. with decreasing G/V. If it is assumed that increasing the lag/lead distance increases the total undercooling, possibly because solute rejection becomes less efficient, it would be expected that morphologies where the silicon phase lags behind the aluminium would be stabilised by increasing G.

The transitions in eutectic morphology were discussed by Day (2) - see p. 14-15 of this thesis -. At high G/V, kinetic undercoolings and lag/lead distances are very small, so the ⟨100⟩ fibrous silicon growing at a nearly iso thermal front is

stable. With decreasing G/V the lag/lead distance increases, and the eutectic can grow at a lower total undercooling with the silicon phase in the form of twinned {111} flakes leading the aluminium, which allows more efficient solute rejection. Hence the transition from <100> fibres to {111} flakes with decreasing G/V. There is a further transition from {111} flakes to fibres when the increased efficiency of solute redistribution (lower solute undercooling) is no longer sufficient to compensate for the rapidly increasing kinetic undercooling of the silicon, and the eutectic can grow at a lower total undercooling with aluminium leading the silicon phase. It is proposed that as the silicon drops back behind the aluminium, the aluminium/silicon/liquid triple junction becomes unstable, aluminium tending to overgrow the silicon so that {111} flakes can no longer grow, and there is a transition to a fibrous morphology. The instability of the triple junction can then account for the rippled appearance of fibres on electron micrographs.

In conclusion, the kinetic undercooling of silicon is small, but has a large effect on the total undercooling in this system, by preventing isothermal growth and inducing a large solute undercooling. Thus the total undercooling for a given eutectic morphology is sensitive to the difference between the kinetic undercoolings of the two phases. Since the morphology which occurs is that which grows at the smallest total undercooling under given conditions of V, G, and impurity content, it follows that the morphology present depends on the difference between the kinetic undercoolings of aluminium and silicon under those conditions. This is why fibrous eutectic can be grown at 3°C undercooling in the presence of a modifying agent, while a much higher undercooling is needed in the pure alloy before the fibrous

morphology can occur.

The situation is illustrated qualitatively in fig 35 in which total undercooling ΔT is plotted against growth velocity V for the flaky and fibrous morphologies both with and without the presence of a modifying agent. In the undoped alloy the flake-fibre transition takes place at ΔT_2 and V_2, and in the doped alloy at ΔT_1 and V_1. ΔT_2 and V_2 depend on the nature and concentration of the impurity element. Fig 35 implies a change in the ΔT-V slopes and relationship at the transition, which might be expected in view of the change in solid/liquid profile and in interphase spacing, while the undercooling measurements in ch V - 10-do indicate a change in the ΔT-V relationship at rates near to those over which the transition occurs.

Fig 35

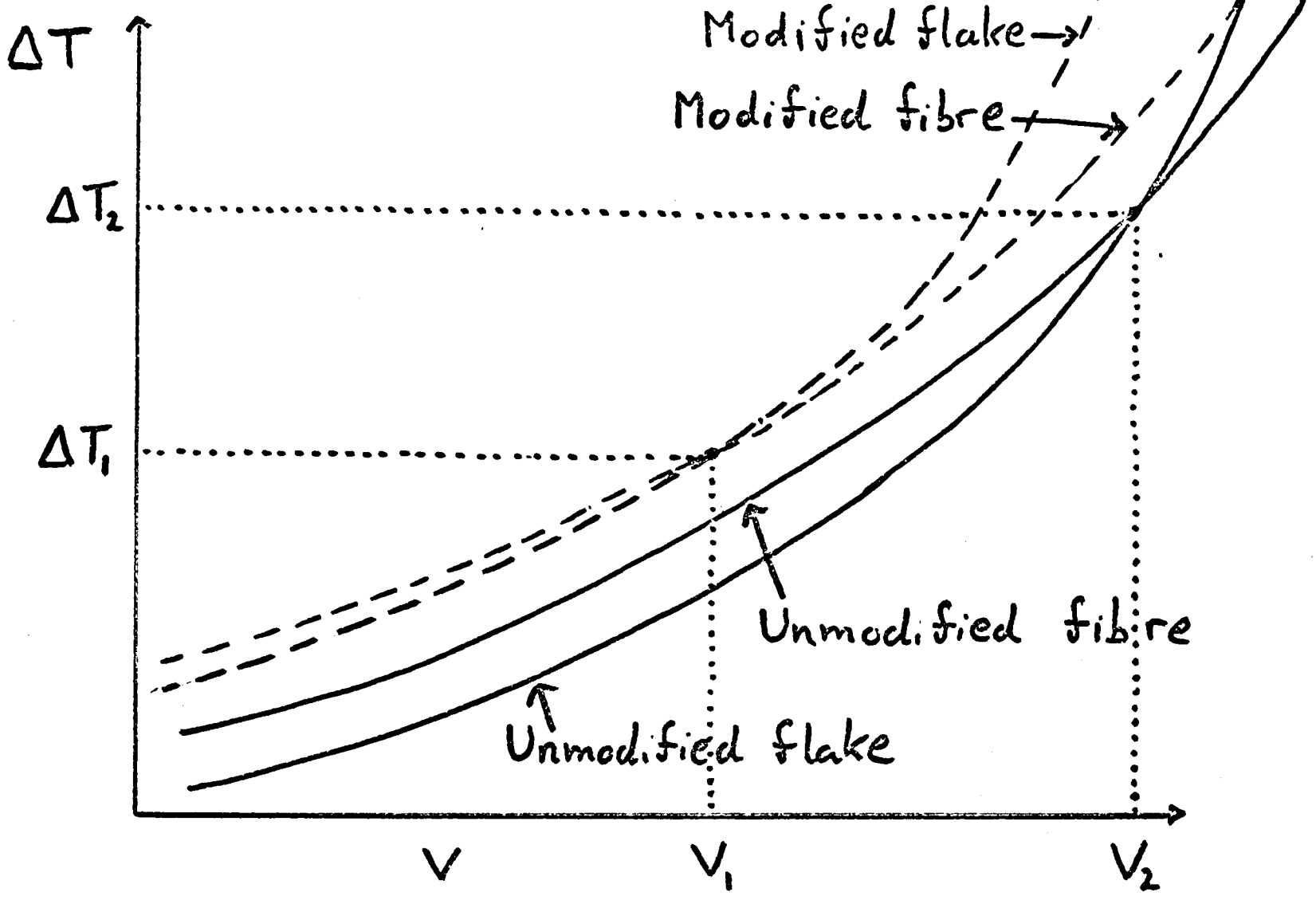

Schematic ΔT – V plot with curves for flake and fibre morphologies both with and without modifying elements being present.

REFERENCES

1) W.A. Tiller. Liquid metals and solidification. A.S.M. 1958.

2) M.G. Day. D.Phil. Thesis. Oxford 1967.

3) J.D. Hunt and K.A. Jackson. Trans Met Soc AIME vol 236, 1966, p. 843.

4) K.A. Jackson. Liquid metals and solidification. ASM 1958.

5) D.J.S. Cooksey, D. Munson, M.P. Wilkinson and A. Hellawell. Phil Mag vol 10, 1964, p. 745.

6) R.M. Jordan. D.Phil. Thesis. Oxford 1970.

7) G.A. Chadwick. Proceedings of a symposium on liquids Michigan 1963, p. 326.

8) K.A. Jackson. Proceedings of an international conference on crystal growth, Boston, p. 17.

9) F.C. Frank. Disc Faraday Soc. vol 5, 1949, p. 48.

10) R.S. Wagner. Acta Met. vol 8, 1960, p. 57.

11) K.F. Hulme and J.B. Mullin. J Phys Chem Solids, vol 17, 1960, p. 1.

12) R.M. Sharp and A. Hellawell. J Crystal Growth, vol 6, 1970, p. 253.

13) F.R. Mollard and M.C. Flemings. Trans Met Soc AIME, vol 239, 1967, p. 1526.

14) J.D. Hunt and K.A. Jackson. Trans Met Soc AIME, vol 239, 1967, p. 864.

15) A.G.C. Gwyer and H.C. Phillips. J Inst Met, vol 36 no. 2, 1926, p. 283.

16) L.A. Willey. Trans AIME vol 206, 1956, p. 263.

17) M. Hansen. The constituion of binary alloys, 1956.

18) R.P. Elliott. Supplement to (17). 1965.

19) A. Pacz. U.S. Patent No. 1,387,900. 1920.

20) M. Gayler. J Inst Met, vol 38, 1927, p. 157.

21) M. Straumanis and N. Brakss. Z Phys Chem, vol B38, 1937, p. 140.

22) B. Thall and B. Chalmers. J Inst Met, vol 77, 1950, p. 79.

23) R.C. Plumb and J. Lewis. J Inst Met, vol 86, 1958, p. 393.

24) R.A. Meussner. U.S. Naval research lab NRL reports 5331, 5341 and 5346.

25) S. Ghosh and V. Kondic. Modern Castings, vol 43 no. 2, 1963, p. 17.

26) G.A. Chadwick. Prog Mat Sci, vol 12, 1965, p. 99.

27) M.G. Day. Nature, vol 219, 1968, p. 1357.

28) J.A. Bell and W.C. Winegard. Nature, vol 208, p. 176.

29) M.G. Day and A. Hellawell. J. Inst Met, vol 95, 1967, p. 377.

30) M.G. Day and A. Hellawell. Proc Roy Soc A, vol 305, 1968, p. 473.

31) A. Rosenberg and W.C. Winegard. Acta Met, vol 2, 1954, p. 342.

32) H.A.H. Steen. Part II thesis. Oxford 1970.

33) M.F.X. Gigliotti and G.A. Colligan. Met Trans, vol 3, 1972, p. 933.

34) M. Hillert and N. Lange. Swedish Council for Applied Research Report 4601, 1968.

35) M. Hillert, H. Fredriksson and N. Lange. To be published.

36) M. Sundquist and L. Mondolfo. Trans Met Soc AIME, vol 221, 1961, p. 157.

37) P.B. Crosley and L. Mondolfo. Modern Castings, vol 49, 1966, p. 63.

38) J.D. Edwards, F.C. Frary and H.V. Churchill. U.S. Patent No. 1,410,461, 1920.

39) C.B. Kim and R.W. Heine. J Inst Met, vol 92, 1963, p. 367.

40) G. Gurtler. Z Metallk, vol 44, 1953, p. 503.

41) Videl Davies and J.M. West. J Inst Met, vol 92, 1963, p. 175.

42) Videl Davies and J.M. West. J Inst Met, vol 92, 1963, p. 208.

43) A. Guillet. Revue Metall, vol 19, 1922, p. 303.

44) Z. Jeffries. Chem Metall Eng, vol 26, 1922, p. 750.

45) C.E. Ransley and H. Neufeld. J Inst Met, vol 78, 1950, p. 25.

46) J.D. Edwards and R.S. Archer. Chem Metall Eng, vol 31, 1924, p. 504.

47) R.S. Archer and L.W. Kempf. Trans Met Soc AIME, vol 73, 1926, p. 581.

48) Z. Obinata and N. Komatsu. Sci Rep Res Inst Tohoku Univ vol A9, 1957, p. 107.

49) M.H. Buden. D.Phil. Thesis. Oxford 1973.

50) J.H. Wernick. Trans AIME, vol 209, 1957, p. 1169.

51) W.A. Tiller. J. Appl Phys, vol 34, 1963, p. 2757.

52) H.E. Cline and T.R. Anthony. Phil Mag, vol 22, 1970, p. 893.

53) W.A. Tiller. J Crystal Growth, vol 6, 1969, p. 77.

54) H.E. Cline and T.R. Anthony. General Electric Company report No. 70 - C - 341.

55) L.M. Hogan, A.J. McLeod, C. McLAdam and D.C. Jenkinson. To be published.

56) R.M. Sharp. D. Phil. Thesis, Oxford 1971.

57) P.B. Hirsch et al. Electron Microscopy of Thin Crystals, 1965.

58) W.A. Tiller, KA. Jackson, J.W. Rutter and B. Chalmers, Acta Met, vol 1, 1953, p. 428.

59) J. D. Hunt. Private communication.